

Fall 2004

The Venetian blind effect: Contrast disparity modulation in irradiation stereoscopy

Eugene T. Filley

University of New Hampshire, Durham

Follow this and additional works at: <https://scholars.unh.edu/dissertation>

Recommended Citation

Filley, Eugene T., "The Venetian blind effect: Contrast disparity modulation in irradiation stereoscopy" (2004). *Doctoral Dissertations*. 227.

<https://scholars.unh.edu/dissertation/227>

This Dissertation is brought to you for free and open access by the Student Scholarship at University of New Hampshire Scholars' Repository. It has been accepted for inclusion in Doctoral Dissertations by an authorized administrator of University of New Hampshire Scholars' Repository. For more information, please contact nicole.hentz@unh.edu.

THE VENETIAN BLIND EFFECT:
CONTRAST DISPARITY MODULATION IN IRRADIATION
STEREOSCOPY

BY

EUGENE T. FILLEY

B.A., University of New Hampshire, 1993

M.A., University of New Hampshire, 1998

Submitted to the University of New Hampshire
in Partial Fulfillment of
the Requirements for the Degree of

Doctor of Philosophy

in

Psychology

September, 2004

UMI Number: 3144745

Copyright 2004 by
Filley, Eugene T.

All rights reserved.

INFORMATION TO USERS

The quality of this reproduction is dependent upon the quality of the copy submitted. Broken or indistinct print, colored or poor quality illustrations and photographs, print bleed-through, substandard margins, and improper alignment can adversely affect reproduction.

In the unlikely event that the author did not send a complete manuscript and there are missing pages, these will be noted. Also, if unauthorized copyright material had to be removed, a note will indicate the deletion.

UMI[®]

UMI Microform 3144745

Copyright 2004 by ProQuest Information and Learning Company.

All rights reserved. This microform edition is protected against unauthorized copying under Title 17, United States Code.

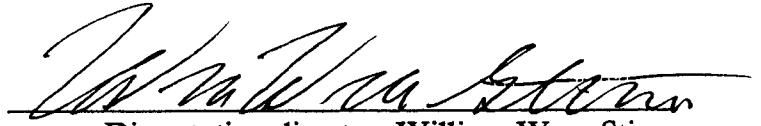
ProQuest Information and Learning Company
300 North Zeeb Road
P.O. Box 1346
Ann Arbor, MI 48106-1346

ALL RIGHTS RESERVED

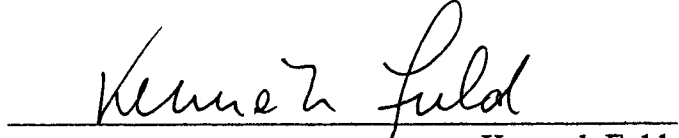
© 2004

Eugene T. Filley

This dissertation has been examined and approved.



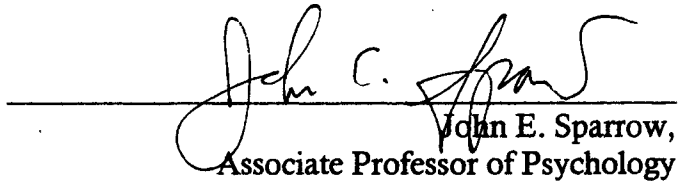
Dissertation director, William Wren Stine,
Associate Professor of Psychology



Kenneth Fuld,
Professor of Psychology



Robert Drugan,
Associate Professor of Psychology



John E. Sparrow,
Associate Professor of Psychology



Dan J. Swift,
Associate Professor of Psychology

7/23/04
Date

In loving memory of my mother, Edna H. Christie

ACKNOWLEDGMENTS

A project like this cannot be completed without the help of many people. I want to thank my committee chair, Bill Stine, for his continued insight and support throughout the project. I would also like to thank the members of my dissertation committee for their insightful comments and ideas. A special thanks goes to JMS and WWS for their many hours spent as experimental subjects.

A number of individuals supported me in absolutely essential ways, for which I am deeply grateful. Janice Chadwick somehow always found teaching work and other forms of support for me when I most needed it. Thank you Janice. Robin, Anne and Donna cheerfully made a big difference.

Good friends outside UNH also kept me going. Rick, Brad, Linda. Thank you.

I am forever grateful to my family, starting with my grandparents, both gone now. Grampa put magic into our childhoods. Grammy was like a sweet little bird. My brother, Ralph, and his wife Diane, showered love and support on me throughout this project. My sister, Viola, always knew when to call and what to say. My sister, Charlene, continually demonstrated the meaning of the word "spirited." Sadly, my sister, Laura, passed away at the age of 44 on March 7, 2001. She was very special to us and we all miss her. My mother, Edna, passed away on August 11, 1996. She was the heart of the family, the most loving, generous, patient person I ever knew. She remains in our memories.

TABLE OF CONTENTS

DEDICATION	iv
ACKNOWLEDGMENTS	v
TABLE OF CONTENTS	vi
LIST OF FIGURES	ix
ABSTRACT	xiii
INTRODUCTION	1
GENERAL METHOD	17
Subjects	17
Apparatus	17
Stimuli	18
Task and procedure	20
EXPERIMENT 1	23
Introduction	23
Methods	23
Subjects	23
Apparatus	23
Stimuli	23
Procedure	24
Results	25
ETF	26
JMS	26
WWS	27

Discussion	27
EXPERIMENT 2	32
Introduction	32
Methods	32
Subjects	32
Apparatus	32
Stimuli	33
Procedure	34
Results	34
ETF	34
JMS	35
WWS	35
Discussion	36
EXPERIMENT 3	41
Introduction	41
Methods	41
Subjects	41
Apparatus	41
Stimuli	41
Procedure	42
Results	43
ETF	43
JMS	43

WWS	44
Discussion	44
GENERAL DISCUSSION	49
REFERENCES	64
APPENDICES	67
Appendix 1. Exp. 1 Sample Stimuli, Luminance Plots, Fouriers	68
Appendix 2. Exp. 2 Sample Stimuli, Luminance Plots, Fouriers	73
Appendix 3. Exp. 3 Sample Stimuli, Luminance Plots, Fouriers	78
Appendix 4. Exp. 1 Fourier Plots at Threshold	83
Appendix 5. Exp. 2 Fourier Plots at Threshold	87
Appendix 6. Exp. 3 Fourier Plots at Threshold	91
Appendix 7. 1-Parameter Model Results	95
Appendix 8. 2-Parameter Model Results	98
Appendix 9. 3-Parameter Model Results	101
Appendix 10. False Alarm Time Series	104
Appendix 11. Contrast Disparity Modulation Scheme	106
Appendix 12. Monitor Calibration	108
Appendix 13. IRB Documentation	111

LIST OF FIGURES

Figure 1. Venetian blind effect stimulus	1
Figure 2. Cibis and Haber model	4
Figure 3. Rotation as a function of spatial frequency	5
Figure 4 Fiorentini and Maffei high contrast edge	9
Figure 5. Filley & Stine (1998) results	11
Figure 6. Stereogram containing an unmodulated carrier square-wave	14
Figure 7. Stereogram with contrast disparity modulation	15
Figure 8. Experiment 1, condition 1 stimulus	18
Figure 9. Experiment 1 stimuli	24
Figure 10. ETF, Experiment 1 contrast disparity thresholds	28
Figure 11. JMS, Experiment 1 contrast disparity thresholds	29
Figure 12. WWS, Experiment 1 contrast disparity thresholds	30
Figure 13. Experiment 1 session matched median contrast disparity thresholds	31
Figure 14. Experiment 2 stimuli	33
Figure 15. ETF, Experiment 2 contrast disparity thresholds	37
Figure 16. JMS, Experiment 2 contrast disparity thresholds	38

Figure 17. WWS, Experiment 2 contrast disparity thresholds	39
Figure 18. Experiment 2 session matched median contrast disparity thresholds . .	40
Figure 19. Experiment 3 stimuli	42
Figure 20. ETF, Experiment 3 contrast disparity thresholds	45
Figure 21. JMS, Experiment 3 contrast disparity thresholds	46
Figure 22. WWS, Experiment 3 contrast disparity thresholds	47
Figure 23. Experiment 3 session matched median contrast disparity thresholds . .	48
Figure 24. Luminances plot	50
Figure 25. Normalized contrast sensitivity function	53
Figure 26. Fourier plot of the difference in luminances	53
Figure 27. Modulation of sine-waves	54
Figure 28. Fourier plot of modulation of sine-waves	55
Figure 29. Experiment 1, condition 1 stimulus with Fourier plot	69
Figure 30. Experiment 1, condition 2 stimulus with Fourier plot	70
Figure 31. Experiment 1, condition 3 stimulus with Fourier plot	71
Figure 32. Experiment 1, condition 4 stimulus with Fourier plot	72
Figure 33. Experiment 2, condition 1 stimulus with Fourier plot	74

Figure 34. Experiment 2, condition 2 stimulus with Fourier plot	75
Figure 35. Experiment 2, condition 3 stimulus with Fourier plot	76
Figure 36. Experiment 2, condition 4 stimulus with Fourier plot	77
Figure 37. Experiment 3, condition 1 stimulus with Fourier plot	79
Figure 38. Experiment 3, condition 2 stimulus with Fourier plot	80
Figure 39. Experiment 3, condition 3 stimulus with Fourier plot	81
Figure 40. Experiment 3, condition 4 stimulus with Fourier plot	82
Figure 41. ETF, Experiment 1 Fourier plots	84
Figure 42. JMS, Experiment 1 Fourier plots	85
Figure 43. WWS, Experiment 1 Fourier plots	86
Figure 44. ETF, Experiment 2 Fourier plots	88
Figure 45. JMS, Experiment 2 Fourier plots	89
Figure 46. WWS, Experiment 2 Fourier plots	90
Figure 47. ETF, Experiment 3 Fourier plots	92
Figure 48. JMS, Experiment 3 Fourier plots	93
Figure 49. WWS, Experiment 3 Fourier plots	94
Figure 50. Experiment 1 contrast disparity thresholds and 1-parameter model predictions	96

Figure 51. Experiment 2 contrast disparity thresholds and 1-parameter model predictions	97
Figure 52. Experiment 1 contrast disparity thresholds and 2-parameter model predictions	99
Figure 53. Experiment 2 contrast disparity thresholds and 2-parameter model predictions	100
Figure 54. Experiment 1 contrast disparity thresholds and 3-parameter model predictions	102
Figure 55. Experiment 2 contrast disparity thresholds and 3-parameter model predictions	103
Figure 56. Probability of false alarm as a function of experimental session	105
Figure 57. Contrast disparity modulation scheme	107
Figure 58. Luminance as a function of GrayLevel	109

ABSTRACT

THE VENETIAN BLIND EFFECT:
CONTRAST DISPARITY MODULATION IN IRRADIATION STEREOSCOPY

BY

EUGENE T. FILLEY

University of New Hampshire, September, 2004

In Experiment 1 we measured contrast disparity thresholds for the perception of slant in the venetian blind effect for a square-wave carrier spatial frequency of 3.14 c/deg and square-wave modulation spatial frequencies of 0.26, 0.39, 0.79, and 1.57 c/deg.

In Experiment 2 we increased the spatial frequencies. We measured contrast disparity thresholds for the perception of slant for a square-wave carrier spatial frequency of 5.24 c/deg and square-wave modulation spatial frequencies of 0.33, 0.65, 1.31, and 2.62 c/deg.

In Experiment 3 we returned to the spatial frequencies of Experiment 1 but used sine-wave modulation. We measured contrast disparity thresholds for the perception of slant for a square-wave carrier spatial frequency of 3.14 c/deg and sine-wave modulation spatial frequencies of 0.26, 0.39, 0.79, and 1.57 c/deg.

Fourier analyses were performed on the luminance differences of left and right half-images at threshold, and adjusted for the contrast sensitivity function. Sum and difference spikes, caused by phase changes between the half-images, appeared in the resulting Fourier plots. One parameter, two parameter, and three parameter models were generated to fit the Fourier results. The models predicted thresholds moderately

well for two out of three subjects (ETF, JMS) but performed poorly in predicting thresholds for the remaining subject (WWS). A systematic feature of the remaining errors is noted and some future directions in venetian blind research are discussed.

INTRODUCTION

In 1941, C. Münster reported a depth illusion, today called "the venetian blind effect." The illusion occurs when binocularly viewing a vertically oriented square-wave grating with a neutral density filter placed before one eye (see Figure 1).

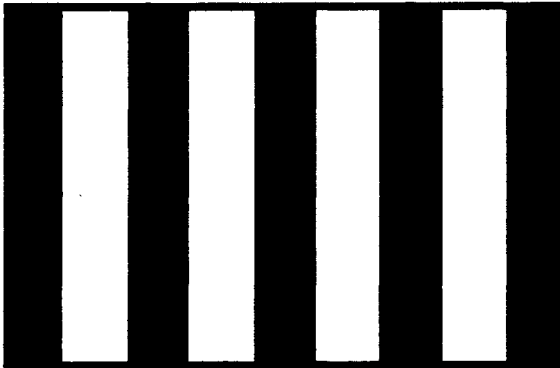


Figure 1. An image suitable for producing the venetian blind effect when viewed binocularly with a neutral density filter placed before one eye

Typically, each of the light bars of the grating appears to be rotated about its own vertical axis, like a partly opened venetian blind.¹ With the neutral density filter placed over the left eye, each bar appears to slant so that its left edge is closer than its right edge. With

the neutral density filter placed over the right eye, the sense of rotation reverses.²

Howard and Rogers (1995a, p. 310) summarize a number of findings for the venetian blind effect.

Cibis and Haber (1951) independently rediscovered the venetian blind effect.

They considered it to be one of a large number of "anisopic stereo-effects," distortions

¹ The perceived slant in the venetian blind effect is "multi-axis" rotation, not "single-axis" rotation. In multi-axis rotation about vertical axes, individual elements of the stimulus (bars, in this case) rotate or appear to rotate about their own independent vertical axes. In single-axis rotation, an entire stimulus rotates or appears to rotate around a single axis.

² Occasionally, the dark bars may appear to rotate instead of the light bars but in the opposite direction, or a corrugation of alternating dark and light bars may be seen, depending on figure-ground organization.

of visual space caused by "unequal imagery" in the eyes (p. 676).³ Cibis and Haber produced apparent slant in several ways — artificial pupils (unspecified diameters) that differed in size in the two eyes, spherical or cylindrical lenses (up to ± 1.5 diopters over one eye), retinal bleaching (about 3200 lx to the right eye for 10 minutes), and neutral density filters (0.1 log units to 3.0 log units) placed over one eye.⁴

In a series of nulling-method experiments⁵ using a neutral density filter in front of one eye, Cibis and Haber asked subjects to view binocularly two white squares (each with retinal angles of $2.44^\circ \times 2.44^\circ$) placed in the fronto-parallel plane with a very dark background (black felt). The squares were yoked together so that subjects could rotate them simultaneously about their individual vertical axes. (Cibis and Haber do not specify the distance between the vertical axes). The subjects' task was to rotate the bars back into the perceived fronto-parallel plane, nulling the apparent slant. Cibis and Haber then measured the actual angle of rotation of the squares away from the fronto-parallel plane and calculated angular disparity for the squares.

³ Ogle (1952) objects to Cibis and Haber's use of the term "anisopia" in this context on the grounds that the term has a well established clinical meaning: "an anomaly in the binocular visual processes (including corrected refractive errors) in which a difference in magnification exists between the images for the two eyes." The established meaning, says Ogle, precludes the use of the term for "differences in the size of the dioptric images on the retinas caused by special geometrical configurations and special arrangements of objects in the field of view."

⁴ Apparent slant seen using the neutral density filters was largely independent of the luminance of the targets from 0.03 cd/m^2 to 111 cd/m^2 . Cibis and Haber did not report the adaptation state of subjects and did not use artificial pupils in these neutral density filter experiments.

⁵ "Nulling-method" experiments measure the amount of one stimulus dimension required to counteract the response to the same dimension of another stimulus.

Cibis and Haber found that the sides of the squares that seemed closer to subjects were on the same side as the filtered eye and that apparent slant increased with filter density. Apparent slant increased linearly from about 5° (corresponding to 10 arc seconds of angular disparity) for filters of 0.1 log units, to 25° (corresponding to 45 arc seconds of angular disparity) for filters of 1.25 log units. Filter densities greater than 1.0 had reduced effectiveness, until saturation was reached near 2.5 log units with 35° of apparent slant (corresponding to 55 arc sec of angular disparity).

Cibis and Haber proposed that the visual system determines the width of a bar presented to an eye by using the locations at which the edges of the bar cross a retinal illuminance threshold for that eye (see Figure 2a). Because the retinal illuminance profile of a bar has only finite slopes, reducing the retinal illuminance of the bar will decrease the width of the supra-threshold part of the image (the light bar area) while increasing the width of the sub-threshold part (the dark area around the bar), provided that a retinal illuminance threshold for the visual system exists somewhere between the light area and dark area retinal illuminance levels. This amounts to a spatial duty cycle reduction for the filtered eye.⁶ When the two images are fused, one sees a rotation about the vertical axis of the bar. When several bars are viewed beside each other, one sees multi-axis rotation (see Figure 2b). According to Cibis and Haber, productions of multi-axis rotation using filters, artificial pupils, or bleaching all depend upon a spatial duty cycle reduction of the retinal image in one eye, creating an effective disparity between the two eyes.

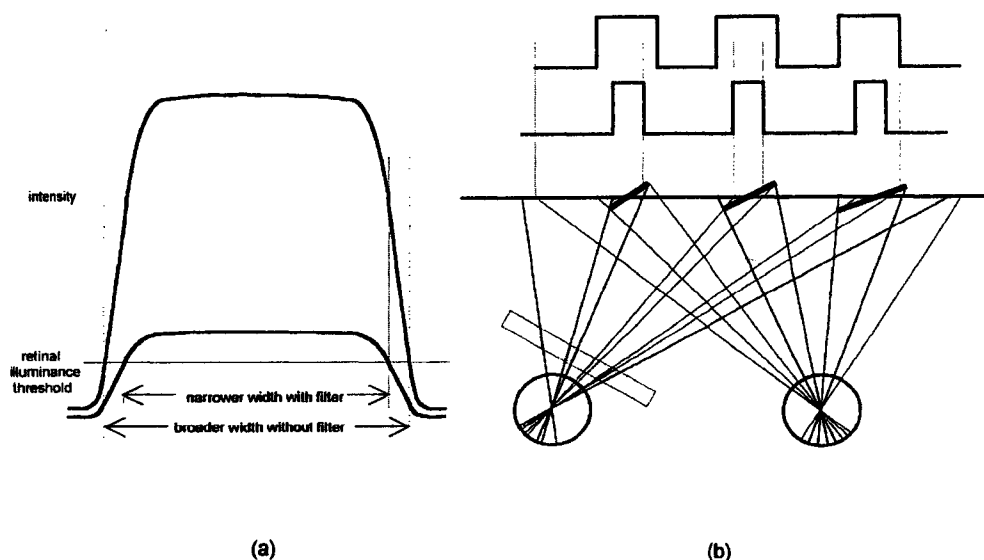


Figure 2. (a) According to Cibis and Haber (1951), placing a neutral density filter before one eye reduces the retinal illuminance for a bar stimulus, which reduces the width of that portion of the stimulus that is above threshold of retinal illuminance and increases the width of that portion of the stimulus that is below threshold. Together, these changes amount to a spatial duty cycle reduction. (b) Spatial duty cycle reduction leads to apparent multi-axis rotation.

Because supra-threshold dark bars do not provide points that cross a retinal illuminance threshold, Cibis and Haber's model does not predict multi-axis rotation for gratings with supra-threshold dark bars. Further, since their model uses a retinal illuminance threshold and not a contrast threshold, it does not predict multi-axis rotation based upon contrast disparities.⁷ Both of these effects were subsequently observed (Filley, 1998; Filley and Stine, 1998).

⁶ The spatial duty cycle for a square-wave grating is the ratio of the width of a light bar to the width of a light and dark bar taken together. A square-wave grating has a spatial duty cycle of 0.5 but a rectangular wave grating generally does not.

⁷ Cibis and Haber's model predicts multi-axis rotation for "degenerate cases" where the contrast is close to 1.0 and the dark bar illuminances are below threshold. Because Cibis and Haber do not specify the shape of the luminance profile, it is difficult to know what they might have said outside this range.

Ogle (1962), who appears to have agreed, more or less, with Cibis and Haber's proposal (although he did not explicitly mention a threshold), considered the venetian blind effect to be a "unique stereoscopic effect" and coined the term "irradiation stereoscopy" to describe it.⁸ The term highlights the point that in the venetian blind effect a difference in the level of retinal irradiance in the two retinas creates a spatial duty cycle reduction in the retinal image of the filtered retina relative to the unfiltered retina (retinal disparities). This spatial duty cycle reduction can then be used to explain the effect on a geometric basis. This differs only somewhat from the way that stereopsis may be produced for a real venetian blind: a difference in retinal viewpoints creates a spatial duty cycle reduction in the retinal image of one eye relative to the other, which can then be used to explain the effect on a geometric basis.

Von Békésy (1970) performed a series of nulling-method experiments to measure

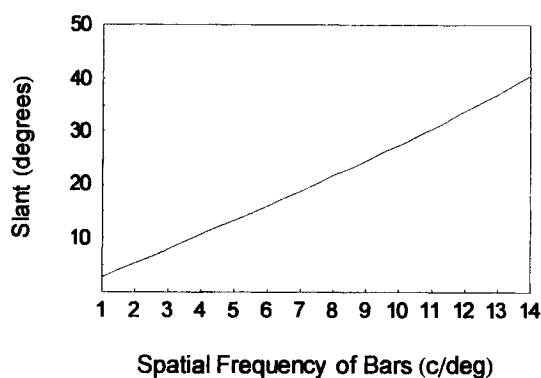


Figure 3. Rotation out of the fronto-parallel plane plotted as a function of spatial frequency for square-wave bars with retinal disparity fixed at 5 arc seconds. (Viewing distance = 100 cm, interpupil distance = 6 cm.)

effective angular disparity (i.e., the change in the angular width of a bar required to return it to the perceived fronto-parallel plane for various neutral density filters placed over one eye). In a pair of related experiments in which subjects were fitted with a chin rest and artificial pupils (size

⁸ "Illuminance" might be more to the point than "irradiance."

unreported), von Békésy used a bar luminance of 17 cd/m^2 and a viewing distance of 25 cm. One of two experiments used a bar with a retinal angle of 0.46° (2 mm wide), and the other used a bar with a retinal angle of 1.38° (6 mm wide).

Von Békésy found that bar width (0.46° , 1.38°) had little effect on the change in bar width required to bring the bar back into the perceived fronto-parallel plane. In both experiments the effective retinal disparity increased to about 50 arc sec as neutral density increased to 1.25 log units. The geometry implies that for a fixed retinal disparity, increasing the spatial frequency of the bars increases the slant (see Figure 3), so the slant detection threshold might be expected to vary as an inverse function of the ratio of spatial frequency to retinal disparity. However, Khutoryansky (2000) examined this possibility for luminance disparity (Experiment 2) and contrast disparity (Experiment 3) and found no such spatial frequency effect on thresholds for square-wave gratings with spatial frequencies up to about 4 c/deg (34.5 cd/m^2 mean luminance, 3 mm artificial pupils, statistical power ranging from 0.53 to 0.72 for detecting a partial ω^2 of 0.10).

Von Békésy (1970) also conducted a series of experiments in which he presented to subjects a number of stimuli consisting of bars or dots with varying geometries. In these experiments, von Békésy observed an interaction between stimulus geometries and combinations of perceived multi-axis or single-axis rotation, which could not be explained by irradiation effects alone. In one experiment, von Békésy investigated the effects of flanking bars on the venetian blind effect. A flanking bar is a rectangle, generally of some constant luminance, that is placed beside the venetian blind stimulus. Von Békésy generated a venetian blind stimulus in which the light bar

width was 2.5 mm, the light bar luminance was 17 cd/m^2 and the contrast was unspecified. (Viewing distance is not entirely clear from the paper but it seems to be 50 cm, which would give one cycle a retinal angle of about 0.57° and a spatial frequency of about 1.75 c/deg.) Von Békésy placed a high luminance flanking bar on one side of the venetian blind stimulus and a low luminance flanking bar (luminance not reported) on the other side. This arrangement systematically altered the response to the venetian blind stimulus when a neutral density filter (1.0 log units) was placed before one eye. Closer to the light flanking bar, the venetian blind bars appeared to be progressively more slanted. Closer to the dark flanking bar, the bars appeared progressively less slanted. The effect was stronger at low luminance levels.⁹ Von Békésy proposed that a combination of lateral inhibition and irradiation is needed to account for these results.

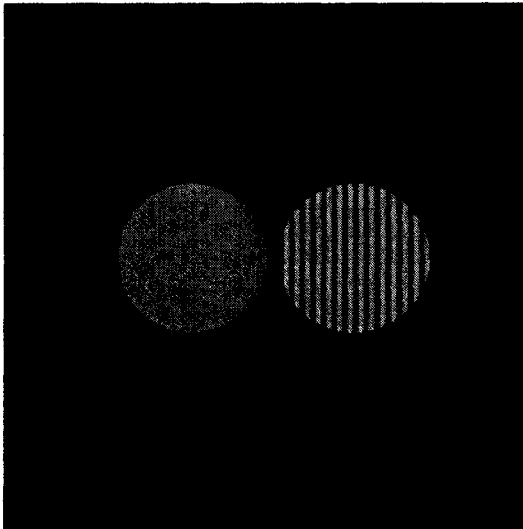
Fiorentini and Maffei were influenced by the spatial frequency approach taken in the work of Campbell and Robson (1968), Campbell, Cooper and Enroth-Cugell (1969), and Blakemore and Campbell (1969). According to that approach, the visual system uses a number of relatively independent, limited bandwidth spatial frequency channels to extract visual information from the environment. Fiorentini and Maffei (1971) suggested that the results of one of their experiments (Experiment 3) could not be interpreted in terms of edge disparities but could be understood on the basis of a

⁹ The author tried to replicate von Békésy's flanking bar finding but was unable to produce results stable enough for systematic inquiry, though one can see the effect.

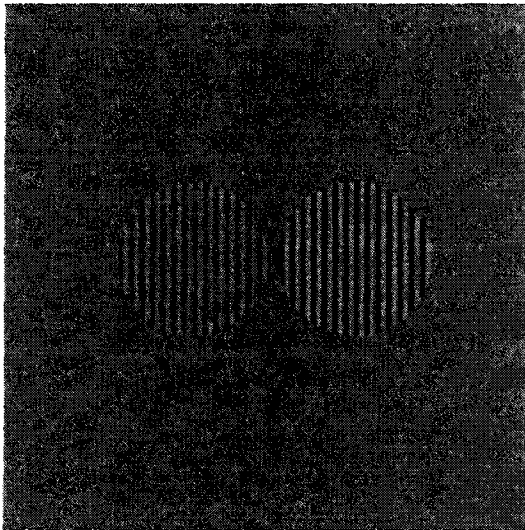
spatial frequency approach.¹⁰ In that experiment, Fiorentini and Maffei presented sine wave gratings of matched spatial frequencies but differing contrasts to each eye for fusing and asked subjects to adjust the slant of a rotatable rectangle to match the apparent slant of the fused grating image. Although the spatial frequency and mean luminance of the two gratings were identical, Fiorentini and Maffei reported apparent single-axis rotation of the entire stimulus when the contrasts differed by 0.2 log units or more.¹¹ Fiorentini and Maffei argue that these results cannot be explained in terms of edge disparities because sine-waves have no edges, regardless of their contrast. They propose that signals encoding the spatial frequencies of each image are separated into a number of spatial frequency channels and the intensities of the two images are compared at these spatial frequencies. When the spatial frequencies, mean luminance and contrast are matched, the visual system infers no slant but when the energy received at the fundamental frequency in one eye differs from the energy received at that frequency in the other eye, the visual system infers the presence of slant. Typically, this would happen because the fundamental frequencies differ between eyes but it could also be expected to happen for sine waves of matched spatial frequencies and mean luminances if the contrast differed between the eyes. The visual system would then infer single-axis rotation of the entire fused grating based on a contrast difference alone.

¹⁰ In one interpretation of the spatial frequency approach, the visual system performs Fourier analysis and synthesis on visual information. Howard and Rogers (1995) argue that this version is biologically implausible, except in a trivial sense (p.259).

¹¹ In a related control experiment, Fiorentini and Maffei temporarily paralyzed the subject's lenses to eliminate the possibility that differential accommodation could account for their results.



(a)



(b)

Figure 4 (a) Fiorentini and Maffei (1971) reported apparent single axis rotation for dichoptically presented sine wave gratings with matched spatial frequency and mean luminance but differing contrast. The high contrast edge created by the circular aperture might have produced apparent rotation. In (b) the luminance of the region outside the aperture is close to the mean luminance of the gratings. Apparent rotation may vanish. Reprinted from Stine and Filley (1998).

Two issues arise with Fiorentini and Maffei's third experiment. First, Fiorentini and Maffei placed circular black cardboard apertures around the oscilloscope screens used to present stimuli to subjects. The apertures should have produced a visible edge around the stimulus at the reported luminances, as in Figure 4a, although that is not reported. Such an edge could create an apparent single-axis rotation of the stimulus, as demonstrated by Stine and Filley (1998). When the luminance of the region outside the aperture is matched to the mean luminance of the gratings, as in Figure 4b, the apparent rotation may vanish, although a well-controlled study is needed to confirm this initial observation.

Second, Blake and Cormack (1979) tried and failed to replicate Fiorentini and Maffei's result using similar stimuli.

However, it should be noted that Blake and

Cormack presented stimuli for only 1 second, which could have been too short for apparent rotation to occur.

Filley (1998) and Filley and Stine (1998) examined the effects of contrast disparity and mean luminance disparity on slant perception for dichoptically presented vertically oriented square-wave grating stereograms. Adaptation level was controlled by placing subjects in Maxwellian view with 3 mm artificial pupils and having them adapt to a 34.5 cd/m² neutral gray field for 5 minutes before each session, as well as for 10 seconds of interstimulus interval (ISI) between each trial. Each stimulus presentation lasted 5 seconds. All stereograms consisted of 4 dark bars and 3 light bars with a spatial frequency of 1.2 c/deg. On each trial, a standard image with a mean luminance of 34.5 cd/m² and Michelson contrast¹² of 0.5 (Michelson, 1927) was displayed to one eye, while a variable image (with contrast between 0.2 and 0.8 and a mean luminance between 12 cd/m² and 57 cd/m², combined factorially) was displayed to the other eye. On each trial, selection of the eye for the standard image was randomized and the mean luminance or the contrast of the variable image was altered. Subjects were asked to indicate which side of each light bar (left or right) appeared closer. Filley and Stine produced a probability map depicting the probability that the variable stimulus side of the fused light bars would appear closer than the other side. They found a contrast disparity effect, a mean luminance disparity effect, and an interaction between the two (see Figure 5).

$$^{12} \text{Michelson contrast} = \frac{\text{maximum luminance} - \text{minimum luminance}}{\text{maximum luminance} + \text{minimum luminance}}$$

(In this document, "contrast" always refers to Michelson contrast.)

For variable images whose contrast was below that of the standard, the variable image side of the light bars appeared closer at all mean luminances. For variable images whose contrast was greater than that of the standard, the variable image side

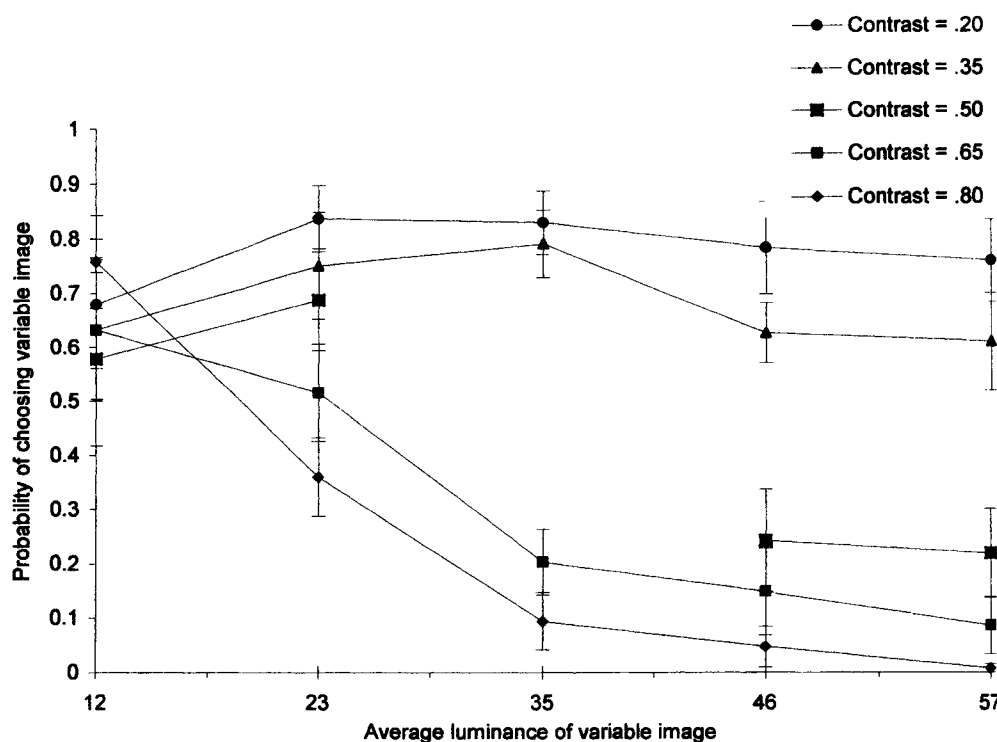


Figure 5. The probability of perceiving the variable image side of the light bars of a square-wave grating stereogram as being closer than the standard image side of the light bars, plotted as a function of mean luminance (cd/m^2) of the variable image (means for 4 subjects). Data are shown for five Michelson contrasts. The standard image had a mean luminance of $34.5 \text{ cd}/\text{m}^2$ and a Michelson contrast of 0.5 in all cases. Data from Filley & Stine (1998).

of the light bars still appeared closer at low mean luminances. However, for high contrast, high mean luminance variable images, the sense of rotation switched. In short, the variable side looked closer, except when it was high luminance high contrast.

Khutoryansky (2000) Experiment 1 examined the effects of blurring the edges of bars in venetian blind stimuli. Edges of a square-wave grating, normally

approximating a step function, were replaced with a sine-wave component: a quarter cycle of sine-wave of known spatial frequency, creating a blurred edge. Subjects were placed in Maxwellian view (3 mm artificial pupil), pre-adapted to 34.5 cd/m^2 for 5 minutes, and re-adapted to that luminance level during each subsequent ISI (8 seconds). On each trial, subjects were presented with a stereogram for 8 seconds. In each stereogram a standard image was randomly placed on the left or right side, with a variable image on the opposite side. The spatial frequency of the sine-wave component (the blurred edge) was altered from trial to trial (from 1.28 c/deg to 15.4 c/deg), while the spatial frequency of the square-wave component (i.e., the square-wave grating, itself) was held constant at 1.92 c/deg . The subject's task, in a Yes-No paradigm, was to indicate whether or not the stimulus appeared flat. An adaptive psychometric procedure, called QUEST, first suggested by Watson and Pelli (1983), was used to measure contrast disparity threshold and mean luminance disparity threshold. On each trial, QUEST computes a Bayesian estimate of the most probable threshold, assuming a Weibull psychophysical function for $\log(\text{contrast})$ or $\log(\text{luminance})$, and uses that estimate as the stimulus intensity for the next stimulus presentation.

Khutoryansky observed no spatial frequency effect of the sine-wave component on either luminance thresholds or contrast thresholds. Khutoryansky used the results of Bex and Edgar (1996), which indicate the amount of shift in the perceived edge position caused by a change in either contrast or contrast ramp width, as well as the results of Morgan et al. (1984), which showed that a non-linear luminance response prior to a zero-crossing extraction mechanism may also lead to a shift in edge

position, to calculate that the experiment had sufficient statistical power (0.88) to detect the predicted spatial frequency effects for the sine-wave component.

In Experiments 2 and 3, Khutoryansky eliminated the sine-wave component and varied the frequency of the square-wave grating from 0.855 c/deg to 3.85 c/deg while measuring contrast disparity threshold and mean luminance disparity threshold. No spatial frequency effect on thresholds was seen, although Howard and Rogers (1995b, p. 164) would lead one to expect a large fall-off in retinal disparity sensitivity in the range 0.5 c/deg to 2 c/deg.

In all of the above cases the gratings seen by each eye were always well above threshold for monocular detection, so a spatial frequency effect for slant perception in venetian blind stimuli should not be imposed by monocular bandpass limitations. Rogers and Graham (1982) report a bandpass function for disparity sensitivity over the spatial frequency range from 0.1 c/deg to 1.6 c/deg (with greatest sensitivity for corrugations around 0.3 c/deg) when detecting surface corrugation using random dot stereograms. Tyler et al. (1992) examine spatial frequencies from 0.05 c/deg to 1.5 c/deg, and report that stereo thresholds for detection of depth modulation dropped from a high at 0.05 c/deg to a low in the range of 0.5 c/deg to 1.5 c/deg (at temporal modulation frequencies around 0.1 Hz). Frisby and Mayhew (1978) report contrast sensitivity functions for detection of random-dot images presented binocularly, as well as contrast sensitivity functions for detection of depth in random-dot stereograms. Each shows a pronounced spatial frequency effect, with thresholds increasing from 2.5 c/deg to 15 c/deg, much like a monocular contrast sensitivity function. Given that the stereo system is responding as though it is seeing a retinal

edge disparity in the venetian blind effect, it is unclear what stimulus properties are actually being used by the stereo system. If a disparity mechanism is controlling the response then the venetian blind effect might be expected to show a spatial frequency effect with peak sensitivity near 0.5 c/deg and with a 50% reduction in sensitivity near 0.1 c/deg and 2 c/deg. On the other hand, if contrast sensitivity controls response, then the venetian blind effect might be expected to show a spatial frequency effect with peak sensitivity around 6 c/deg, like the contrast sensitivity function of Blakemore and Campbell (1969).

Von Békésy (1970) and Khutoryansky (2000) studied some relevant monocular properties (bar width and edge blur) of venetian blind stimuli in the search for a spatial frequency effect but found none. A spatial frequency effect in venetian

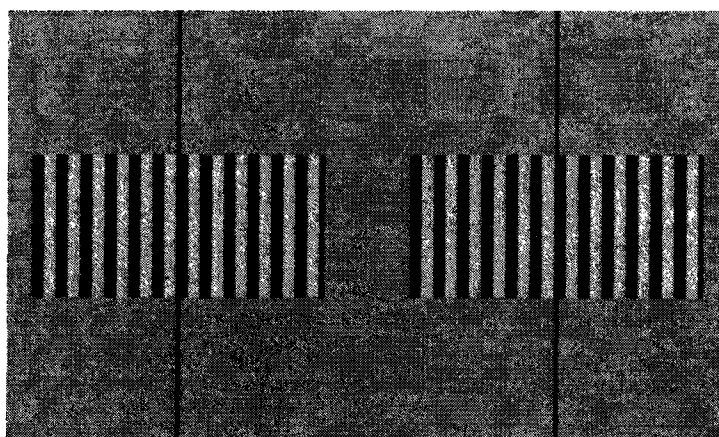


Figure 6. A stereogram containing an unmodulated carrier square-wave. The contrast in each grating (each half-image) is identical to the contrast in the other grating, and does not change when calculated according to segment. This stereogram has no contrast disparity.

blind thresholds would be useful in characterizing the venetian blind effect and potentially useful in providing additional insight into the underlying physical mechanisms involved.

Consequently, the current study examines a specifically binocular stimulus property: contrast disparity. Figure 6 shows a stereogram with no contrast disparity. The two square-wave gratings (half-images) have identical contrast, mean luminance and

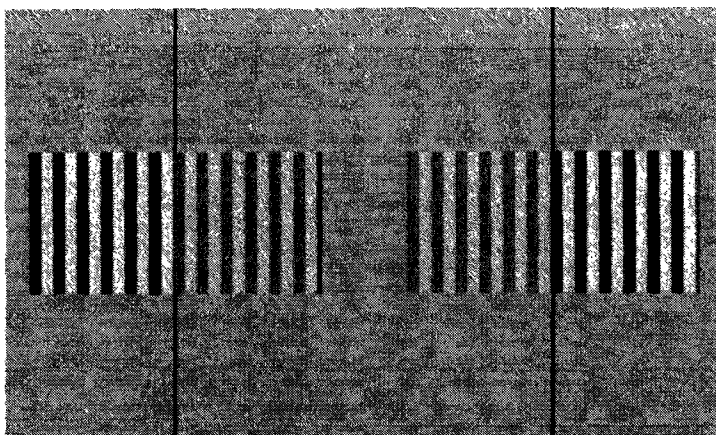


Figure 7. A stereogram with contrast disparity modulation. The contrast of the carrier square-wave is modulated so that the contrast in the left half-image has opposite phase from the contrast in the right half-image. (The mean contrast in each half-image is the same but the left half-image has a high contrast segment on the left and a low contrast segment on the right; while the right half-image has low contrast segment on the left and a high contrast segment on the right.)

spatial frequency (and should appear flat when fused). They can be considered to be unmodulated carrier square-waves. Figure 7 shows a similar stereogram but with the addition of contrast disparity. The contrast

modulation in the left half-image increases the contrast in the left segment (the left half of the left half-image in this example) and decreases the contrast in the right segment. Just over twelve cycles of carrier and just over one cycle of modulation are shown. The contrast modulation in the right half-image exactly reverses the pattern of modulation seen in the left half-image. The modulation in the two half-images is therefore in antiphase (π radians out of phase). If the unmodulated carrier contrast is 0.5 and the modulation contrast proportion is 0.25 then the resulting contrasts in corresponding segments of the half-images will be $0.5 \pm 25\%$, i.e., 0.625 and 0.375.

Because changes in contrast disparity occur abruptly in Figure 7, as in a square-wave, we call this kind of modulation "square-wave contrast disparity modulation." This kind of modulation is used in Experiments 1 and 2. In Experiment 3 we vary contrast disparity gradually, following a sine-wave function, and call the modulation "sine-wave contrast disparity modulation."

When the half-images in Figure 7 are fused (uncrossed), the left segment of the fused image will be formed from a contrast of 0.625 from the left eye and a contrast of 0.375 from the right eye. As a result, the bars in the left segment of the fused image will seem to slant so that the right side of each light bar is closer. Meanwhile, the right segment of the fused image will be formed from a contrast of 0.375 from the left eye and a contrast of 0.625 from the right eye, so the bars in the right segment of the fused image will appear to slant in the opposite direction.

Fused (uncrossed) from a distance of about 57 cm, the stereogram in Figure 7 resembles the stimulus of Experiment 1, condition 1 (carrier spatial frequency = 3.14 c/deg and modulation spatial frequency = 0.26 c/deg), notwithstanding the limitations of the printed page. (Complete samples of all stimuli are shown in Appendices 1-3.)

In all experiments, the carrier was always a square-wave. In Experiment 1 we measured thresholds for the perception of slant for contrast disparity modulation of a 3.14 c/deg carrier using square-wave modulation spatial frequencies of 0.26, 0.39, 0.79, and 1.57 c/deg. In Experiment 2 we increased spatial frequencies. We measured thresholds for the perception of slant for contrast disparity modulation of a 5.24 c/deg carrier using square-wave modulation spatial frequencies of 0.33, 0.65, 1.31, and 2.62 c/deg. In Experiment 3 we returned to the spatial frequencies of Experiment 1 but used sine-wave modulation. We measured thresholds for the perception of slant for contrast disparity modulation of a 3.14 c/deg carrier using sine-wave modulation spatial frequencies of 0.26, 0.39, 0.79, and 1.57 c/deg.

GENERAL METHOD

Subjects

Three healthy adult male subjects, ages 48, 32, and 47, identified by the initials ETF, JMS and WWS, respectively, participated in the experiments. Each subject had normal or corrected to normal vision. Although two of the subjects (ETF and WWS) had some age-related presbyopia, the viewing distance to the stimulus (130 cm) was sufficient to allow full accommodation.

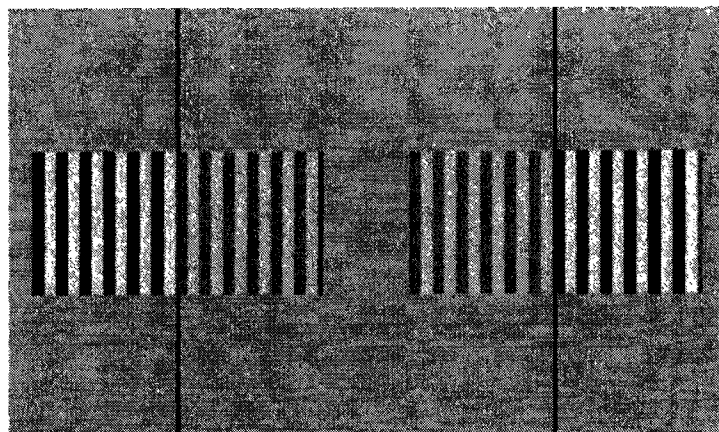
Institutional Review Board clearance and informed consent were given for all experiments (see Appendix 16).

Apparatus

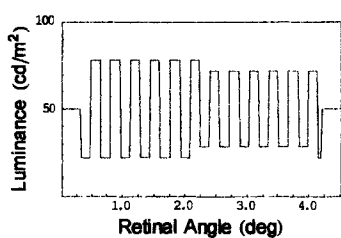
Stimuli were presented under the control of a *Mathematica*[®] 4.0 program run on a Macintosh G4 computer (OS 9.0.4) with an Apple ColorSync Display: 24 bit, 0.29 mm nominal dot pitch CRT (0.36 mm horizontal interpixel distance), 43.18 cm diagonal nominal viewable image size (40.64 cm diagonal actual viewable image size), Family Number M2935. A Minolta LS-110 photometer was used to calibrate the monitor (see Appendix 15).

Other equipment included a bite bar, 3 mm artificial pupils, masking to eliminate high luminance areas surrounding the 50 cd/m² stimulus border, baffling to prevent one eye from receiving the other eye's stimulus, and an arrangement allowing accurate positioning of the bite bar and artificial pupils.

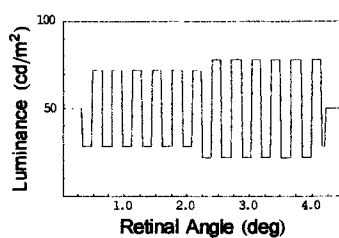
Stimuli



(a)



(b)



(c)

Figure 8. (a) Experiment 1, condition 1 stereogram layout (square-wave contrast disparity modulation spatial frequency of 0.26 c/deg and square-wave carrier spatial frequency of 3.14 c/deg), (b) Luminance plot of left image, (c) Luminance plot of right image.

Stimuli were stereo pairs of images, each pair viewed from a distance of 130 cm and containing an alternating series of dark and light vertical bars (see Figure 8a). The width of a single image from a stereo pair (e.g., a left image), excluding the gray margins on the left and right sides, was 3.88° of retinal angle (8.8 cm).

The height of an image of a stereo pair (excluding the gray margins on the top and bottom) was 1.90° of retinal angle (4.3 cm). Each image from a stereo pair was separated from the other image by 1.10° of retinal angle (2.5 cm). The stereogram pairs were placed in a 50 cd/m^2 border with an outer width of 9.55° of retinal angle (21.8 cm) and height of 5.68° of retinal angle (12.9 cm). Overlapping the outer edges of the border, a piece of cardboard with a rectangular hole cut in it covered the remaining area of the display (the high luminance region outside the stimulus). A divider prevented each eye from seeing the image displayed to the opposite eye, and allowed only uncrossed fusion.

To facilitate fusing, a dark nonius line (luminance = 0.6 cd/m^2 , width = 0.03° and length = 1.90°) was placed above and below each stereo image.

Each stereogram comprised two geometrically identical contrast disparity modulated square-wave carrier images (each image with a mean luminance of 50 cd/m^2 and a Michelson contrast of 0.5). The contrast of one carrier image (see Figure 8b) was modulated in anti-phase (i.e., π radians out of phase) relative to that of the other carrier image (see Figure 8c). For example, a contrast disparity proportion of 0.10 would increase the carrier image contrast by 10% (giving a contrast of 0.55) for a segment in one image, while decreasing the carrier image contrast by 10% (giving a contrast of 0.45) for the corresponding segment in the other image. Stimulus luminances ranged from 10 to 120 cd/m^2 (from about 70 td to about 850 td, photopic). In Experiments 1 and 2 contrast disparity was square-wave modulated (as shown in Appendix 1 and Appendix 2) but in Experiment 3, contrast disparity was sine-wave modulated (as shown in Appendix 3).

In Experiment 1, carrier spatial frequency was fixed at 3.14 c/deg, while four conditions of square-wave contrast disparity modulation spatial frequency were used: 0.26, 0.39, 0.79, and 1.57 c/deg (see Figure 9). In Experiment 2, carrier spatial frequency was fixed at 5.24 c/deg, while square-wave contrast disparity modulation spatial frequencies of 0.33, 0.65, 1.31, and 2.62 c/deg were used. In Experiment 3, carrier spatial frequency was fixed at 3.14 c/deg, while sine-wave contrast disparity modulation spatial frequencies of 0.26, 0.39, 0.79, and 1.57 c/deg were used.

Task and procedure

In each experiment, the subject bit onto a bite bar and pressed a key to start the program that controlled the experiment. The program then displayed a stimulus to allow final alignment. With one eye the subject fixated the center of the corresponding stimulus and, without changing fixation point, aligned a pair of pins so as to site across their tops to the center of the image. Keeping the artificial pupil as close as possible to the cornea without touching it, the subject partially closed the artificial pupil and aligned it horizontally and vertically to form a clear, unoccluded, consistently bright image. The subject then repeated this procedure for the other eye. After the subject was roughly aligned in this way, the researcher completed the final centering of the artificial pupils by siting down the alignment pins at the subject's natural pupils. The alignment pins were removed, the artificial pupils were adjusted to a diameter of 3 mm, and a final check was performed by both subject and researcher.

Upon completing all adjustments, the subject entered his initials and the room lights were turned out, so that the only light remaining in the room came from the monitor (except for a very small amount of light from under the closed laboratory door). The subject then pressed a key to begin adapting to a uniform luminance of 50 cd/m² for 5 minutes.

After adapting the subject, the program cycled through 250 stimuli (8 sec. of stimulus presentation and 8 sec. of ISI used for re-adapting to 50 cd/m²). On each trial an in-phase modulated image was randomly placed on the left or right side, while an anti-phase modulated image was placed on the opposite side. The subject's

task in Experiments 1-3 was to respond "Yes" if some of the bars appeared to slant differently from others; and otherwise to respond "No."

A stochastic approximation procedure (Robbins and Monro, 1951; Treutwein, 1995) was used to measure contrast disparity thresholds. Stochastic approximation is a non-parametric adaptive procedure (non-parametric because it does not assume a particular distribution of thresholds for a given stimulus strength; adaptive because the stimulus strength on any given trial is a function of the subject's response on previous trials).

$$\text{Equation 1} \quad S_{i+1} = S_i - (z_i - \phi) \delta_i$$

$$\text{Equation 2} \quad \delta_i = \delta_1 / i$$

Equation 1 describes how stimulus strength (contrast disparity, in our experiments) was varied over a sequence of trials 1 through n during measurement of contrast disparity threshold. S_{i+1} represents stimulus strength on trial $i+1$. S_i is stimulus strength on trial i . z_i is the subject's response on trial i (0 for a "No" or 1 for a "Yes") and ϕ is the probability of a "Yes" (always 0.5 in our experiments) toward which the sequence is set to converge as threshold is measured. δ_i is the step-size on trial i . Equation 2 describes how step-size, δ_i , decreased over a sequence of trials: $\delta_1 = \delta_1 / 1$, $\delta_2 = \delta_1 / 2$, $\delta_3 = \delta_1 / 3$, etc.

An initial step-size, δ_1 , was selected prior to any trials and ϕ was set to 0.5. On trial 1 stimulus strength, S_1 , was randomly selected from a range of possible strengths. If on trial 1 the subject responded "Yes" then $z_1 = 1$, $(z_1 - \phi) = 0.5$, and $S_2 = S_1 - 0.5 \delta_1$; i.e., stimulus strength on trial 2 was decreased by half the step-size from trial 1. On the other hand, if on trial 1 the subject responded "No" then $z_1 = 0$, $(z_1 - \phi) = -0.5$, and

$S_2 = S_1 + 0.5 \delta_1$: stimulus strength on trial 2 was increased by half the step-size from trial 1. Generally, if the subject responded "Yes" on trial i then stimulus strength on trial $i + 1$ was decreased by half the step-size from trial i ; if the subject responded "No" on trial i then stimulus strength on trial $i + 1$ was increased by half the step-size from trial i . This process continued through all n trials of a sequence, changing S_i by $\pm \delta_i / i$ on each trial, and converging toward a probability of 0.5 that the subject will say "Yes."

Each subject ($n = 3$) ran 8 sessions per experiment. Each session included 10 sequences of 25 trials (randomly interleaved to assure independence of trials), for a total of 250 trials per session. Two sequences per session were dedicated to each of the 4 experimental conditions (giving 2 threshold measurements per condition) and the remaining two sequences were dedicated to catch trials.

EXPERIMENT 1

Introduction

Threshold functions for detection of disparity modulation as a function of spatial frequency in random dot stereograms have a bandpass shape, with the lowest thresholds in the range of 0.3 to 0.5 c/deg (Rogers & Graham, 1982; Bradshaw & Rogers, 1993; Ioannou et al., 1993).¹³ We therefore expected that if we did find a spatial frequency effect in Experiment 1, we would find a similar bandpass threshold function. Specifically, we expected to find the lowest contrast disparity thresholds for slant perception at a modulation spatial frequency of 0.26 c/deg or 0.39 c/deg, with increasing thresholds to 1.57 c/deg.

Methods

Subjects

ETF, JMS and WWS participated in Experiment 1.

Apparatus

Apparatus was as described under GENERAL METHOD.

Stimuli

Stimuli were stereograms as described under GENERAL METHOD. The square-wave carrier spatial frequency was fixed at 3.14 c/deg. Square-wave contrast

¹³ Shumer & Julesz (1984) found this same bandpass shape for disparity modulated random dot stereograms with no disparity pedestal, although they also found a systematic shift in bandpass toward lower spatial frequencies (around 0.2 c/deg) when stereograms were placed on crossed or uncrossed disparity pedestals.

disparity modulation spatial frequencies in the four conditions were 0.26 c/deg, 0.39 c/deg, 0.79 c/deg, and 1.57 c/deg (Figure 9a-d, respectively).

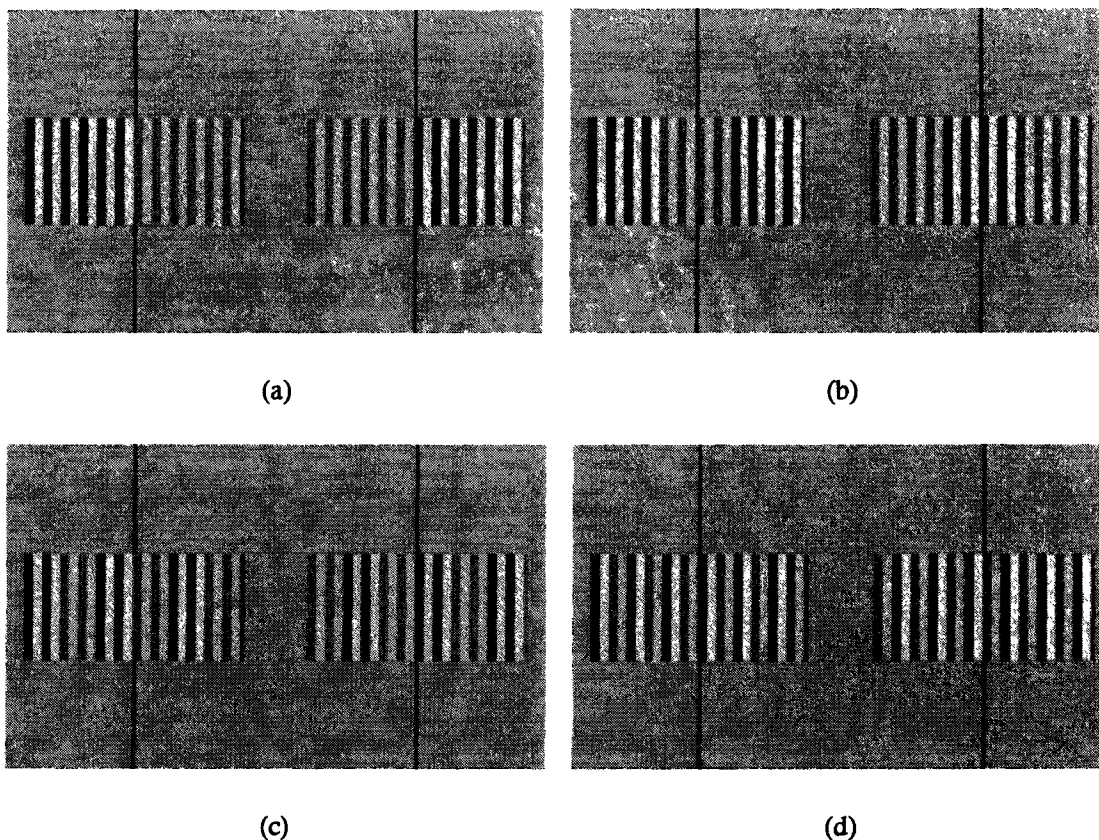


Figure 9. Experiment 1 stimuli (not shown at actual size or luminance). The carrier is a 3.14 c/deg square-wave for all 4 conditions. (a) condition 1: 0.26 c/deg square-wave contrast disparity modulation, (b) condition 2: 0.39 c/deg square-wave contrast disparity modulation, (c) condition 3: 0.79 c/deg square-wave contrast disparity modulation, (d) condition 4: 1.57 c/deg square-wave contrast disparity modulation.

Procedure

The procedure in Experiment 1 was as described under GENERAL METHOD. Square-wave carrier spatial frequency was fixed at 3.14 c/deg and contrast disparity thresholds for perception of apparent slant were measured for square-wave contrast disparity modulation spatial frequencies of 0.26 c/deg, 0.39 c/deg, 0.79 c/deg, and 1.57 c/deg. Ten sequences per session were presented, interleaved in random order,

including two sequences at each of four modulation spatial frequencies and two sequences of catch trials (noise).

Results

Contrast disparity thresholds for seeing slant from Experiment 1 are plotted as a function of spatial frequency of square-wave modulation for ETF, JMS, and WWS in Figure 10, Figure 11, and Figure 12, respectively. For each subject, four plots are shown. The first plot in each case is a log-log plot of mean thresholds for seeing slant for all sessions, with error bars representing standard error of the mean. The second plot is a log-log plot of session matched mean thresholds for seeing slant, with error bars representing standard error of the mean. Sessions are matched by shifting individual session curves to the same overall level (subtracting session means and adding the grand mean). Then error bars are calculated for the shifted means, which removes session differences in overall level, resulting in smaller error bars, and highlighting the plot shape. The third plot is a log-log plot of median thresholds for seeing slant, with error bars equal to 1.483 times the median absolute deviation $/\sqrt{n}$, which is a robust estimator of the standard error of the mean for a normally distributed random variable. The fourth plot is a log-log plot of session matched median thresholds for seeing slant, with error bars equal to 1.483 times median absolute deviation $/\sqrt{n}$. Again, sessions are matched by shifting individual session curves to the same overall level (subtracting session medians and adding the grand median). Because the plots were quite similar in each case, session matched median threshold plots are enlarged.

ETF

Figure 10a-d show results of Experiment 1 for ETF. Contrast disparity thresholds for seeing slant generally decreased with increasing spatial frequency of square-wave contrast disparity modulation. The shapes of the response curves for the four plots were similar. Thresholds were highest for a square-wave contrast disparity modulation spatial frequency of 0.39 c/deg, and decreased with increasing spatial frequency. A flattening or a dip in contrast disparity threshold for seeing slant can be seen at the lowest modulation spatial frequency (0.26 c/deg). In Figure 10a and c, which do not match overall levels of sessions, the error bars are large enough to overwhelm the apparent dip in threshold for the 0.26 c/deg threshold relative to the 0.39 c/deg threshold, leaving a flattening. However, in Figure 10b and d, which do match sessions, the difference between the two points seems clearer.

JMS

Figure 11a-d show results of Experiment 1 for JMS. Once again, the four plots are similar to one another. Again, contrast disparity thresholds for seeing slant generally decreased with increasing spatial frequency of square-wave contrast disparity modulation and the overall threshold level is similar to that for ETF, although the slope is slightly less than it is for ETF. Some flattening can be seen at the lowest modulation spatial frequency (0.26 c/deg) but for JMS the drop is less pronounced than it is for ETF and the shape of the decreasing thresholds plot for JMS is nearly a straight line. Even after session matching, the error bars are large enough to overwhelm the apparent dip in threshold for the 0.26 c/deg, leaving a flattening.

WWS

Figure 12a-d show results of Experiment 1 for WWS. The four plots are again similar to one another. As for ETF and JMS, contrast disparity thresholds for seeing slant generally decreased with increasing spatial frequency of square-wave contrast disparity modulation. The slope of the threshold plot is close to the slope for JMS but the overall threshold level is higher than that for ETF or JMS. A flattening can be seen for WWS at the lowest modulation spatial frequency (0.26 c/deg) and again at the highest modulation spatial frequency (1.57 c/deg). In the session matched median thresholds plot the drop in threshold from 0.39 c/deg to 0.79 c/deg is slightly larger than those for ETF or JMS.

Discussion

Figure 13 shows session matched median thresholds for seeing slant for all three subjects in Experiment 1. Contrary to expectations based on Ioannou et al.(1993), thresholds generally decreased with increasing modulation spatial frequency. Our results more closely resemble monocular contrast thresholds and some may infer that contrast disparity modulation is tapping into monocular limits to contrast sensitivity, rather than into binocular limits to the detection of retinal disparities, as measured by random dot corrugations.

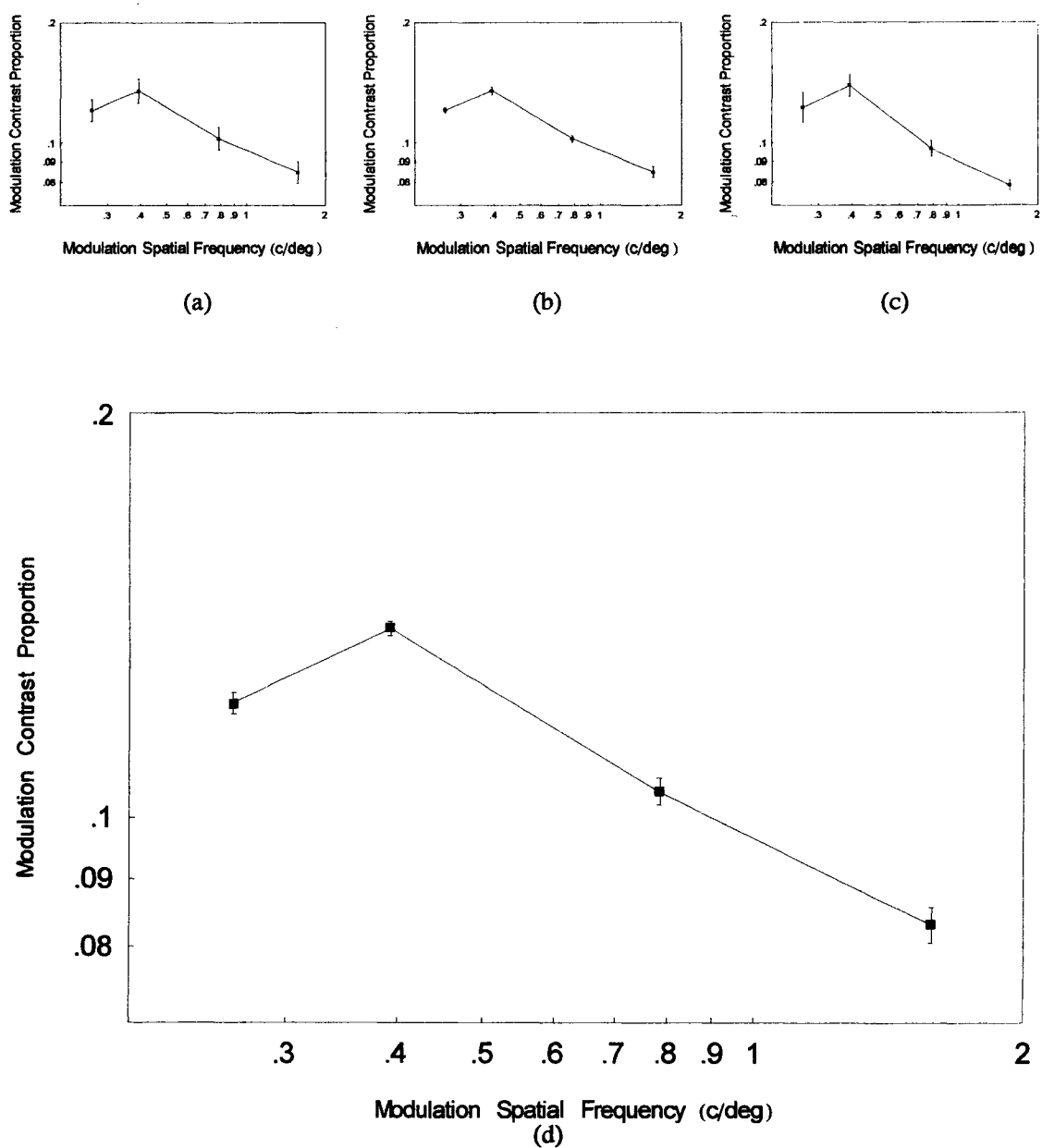


Figure 10. ETF, Experiment 1 contrast disparity thresholds. Square-wave contrast disparity modulation spatial frequencies are 0.26 c/deg, 0.39 c/deg, 0.79 c/deg and 1.57 c/deg. Square-wave carrier spatial frequency is 3.14 c/deg. (a) mean thresholds; error bars are \pm standard error of the mean, (b) session matched mean thresholds; error bars are \pm standard error of the mean, (c) median thresholds; error bars are ± 1.483 median absolute deviation/ \sqrt{n} , (d) session matched median thresholds; error bars are ± 1.483 median absolute deviation/ \sqrt{n} . ($n=8$ for all plots).

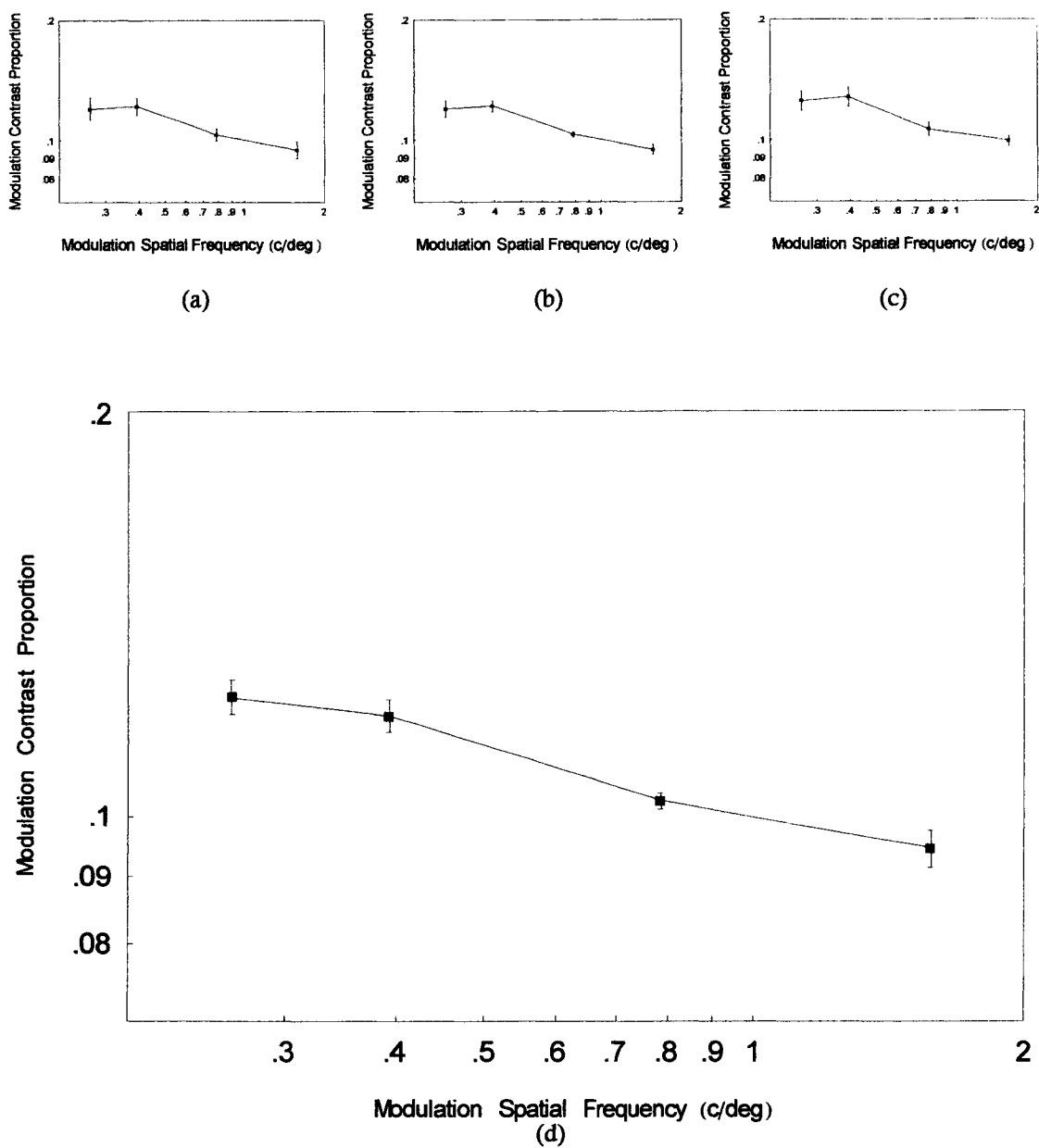


Figure 11. JMS, Experiment 1 contrast disparity thresholds. Square-wave contrast disparity modulation spatial frequencies are 0.26 c/deg, 0.39 c/deg, 0.79 c/deg and 1.57 c/deg. Square-wave carrier spatial frequency is 3.14 c/deg. (a) mean thresholds; error bars are \pm standard error of the mean, (b) session matched mean thresholds; error bars are \pm standard error of the mean, (c) median thresholds; error bars are ± 1.483 median absolute deviation/ \sqrt{n} , (d) session matched median thresholds; error bars are ± 1.483 median absolute deviation/ \sqrt{n} . ($n=8$ for all plots).

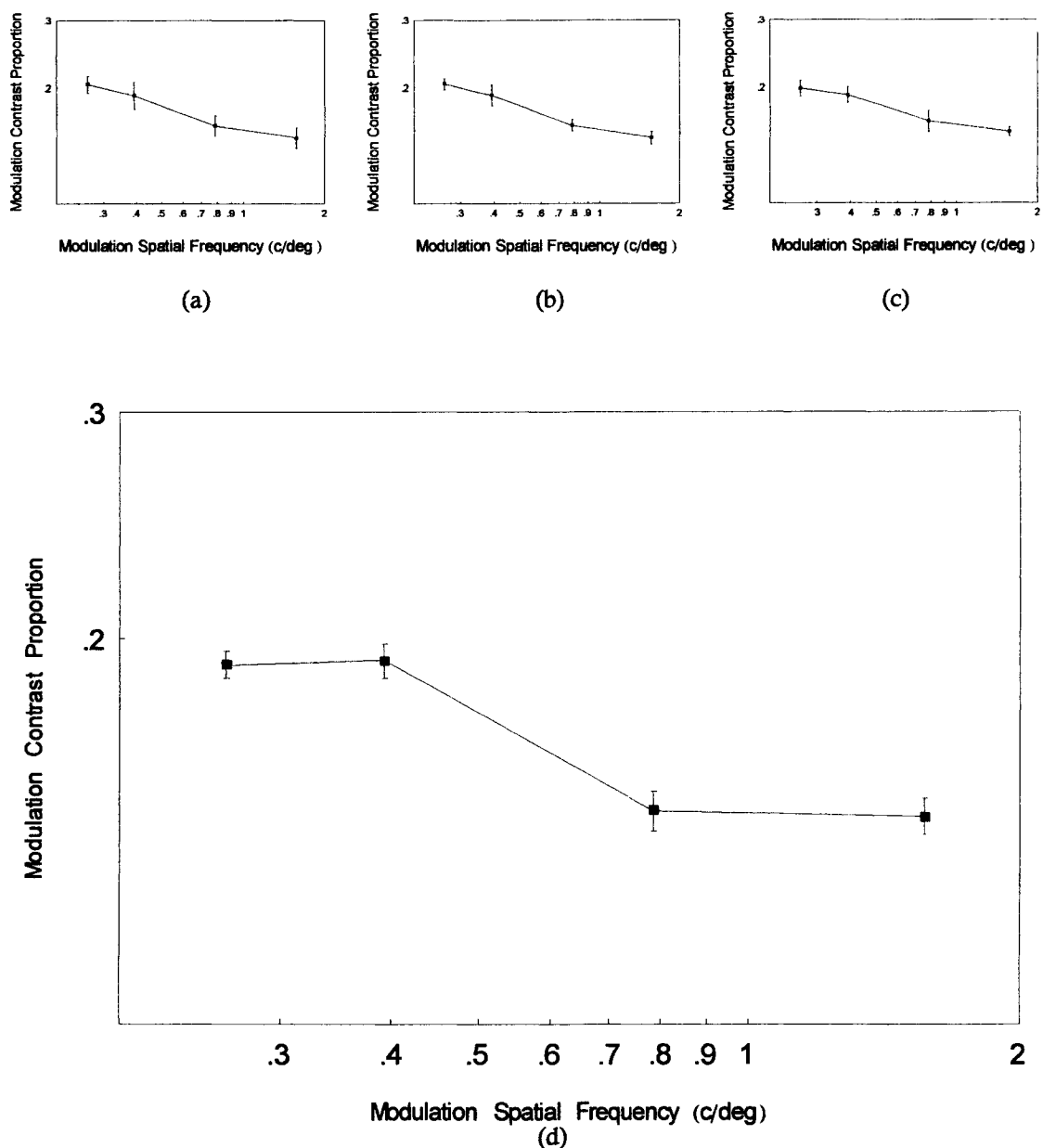


Figure 12. WWS, Experiment 1 contrast disparity thresholds. Square-wave contrast disparity modulation spatial frequencies are 0.26 c/deg, 0.39 c/deg, 0.79 c/deg and 1.57 c/deg. Square-wave carrier spatial frequency is 3.14 c/deg. (a) mean thresholds; error bars are \pm standard error of the mean, (b) session matched mean thresholds; error bars are \pm standard error of the mean, (c) median thresholds; error bars are ± 1.483 median absolute deviation/ \sqrt{n} , (d) session matched median thresholds; error bars are ± 1.483 median absolute deviation/ \sqrt{n} . ($n=8$ for all plots).

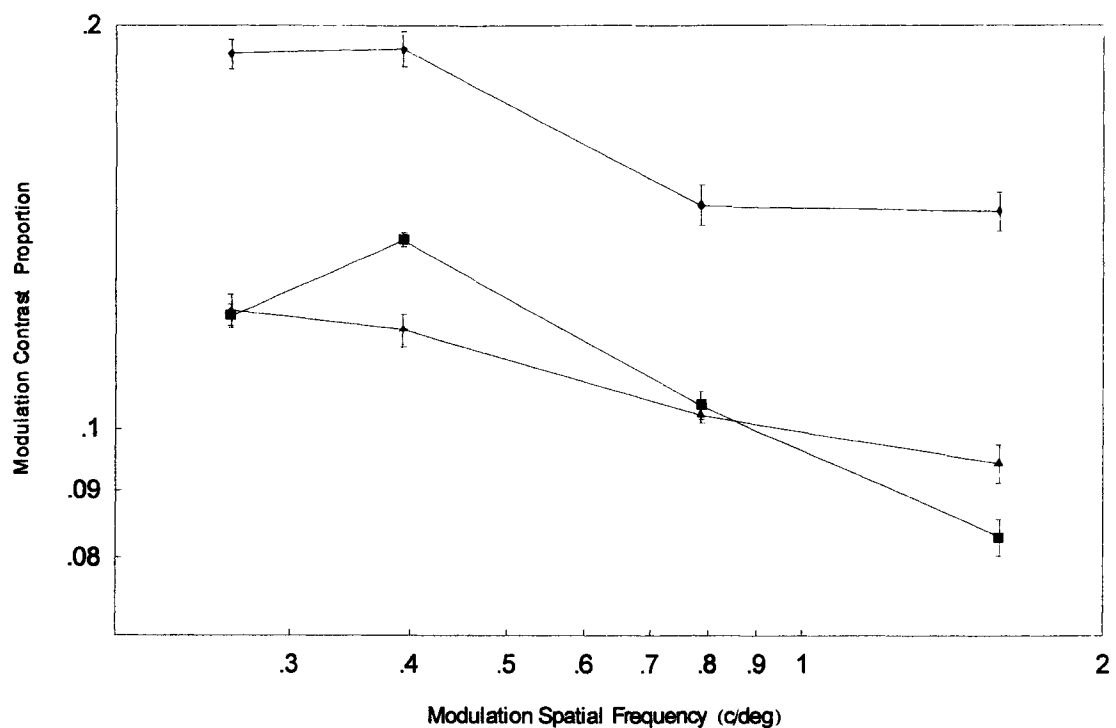


Figure 13. Experiment 1 session matched median contrast disparity thresholds plotted as a function of spatial frequency in c/deg for ETF (boxes), JMS (triangles), and WWS (diamonds). Error bars are ± 1.483 median absolute deviation / \sqrt{n} . Square-wave contrast disparity modulation spatial frequencies are 0.26 c/deg, 0.39 c/deg, 0.79 c/deg and 1.57 c/deg. Square-wave carrier spatial frequency is 3.14 c/deg.

EXPERIMENT 2

Introduction

Von Békésy (1970) found no spatial frequency effects of luminance disparity on the angular disparity required to null the perception of slant in the venetian blind effect. Khutoryansky (2000) looked for spatial frequency effects of luminance disparity and contrast disparity on thresholds for seeing slant in venetian blind stimuli but found none.¹⁴ We therefore did not expect changes in the shape of the threshold function as we increased the spatial frequency of the square-wave carrier in Experiment 2. In Experiment 2 we expected that the shape of the threshold function would replicate that of Experiment 1 for overlapping modulation spatial frequencies, that thresholds would continue to drop with higher modulation spatial frequencies, and that no interaction between carrier spatial frequency and modulation spatial frequency would be found.

Methods

Subjects

ETF, JMS and WWS participated in Experiment 2.

Apparatus

Apparatus was as described under GENERAL METHOD.

¹⁴ By definition, for a non-zero contrast disparity, setting the square-wave contrast disparity modulation spatial frequency to zero would produce two gratings of different contrasts but having no changes in contrast within a single grating. At appropriate carrier spatial frequencies, such stimuli would resemble those of Khutoryansky (2000), Experiment 3. In effect, Khutoryansky (2000) Experiment 3 varied the carrier spatial frequency, not the modulation spatial frequency.

Stimuli

Stimuli were stereograms as described under GENERAL METHOD. The square-wave carrier spatial frequency was fixed at 5.24 c/deg. Square-wave contrast disparity modulation spatial frequencies in the four conditions were 0.33 c/deg, 0.65 c/deg, 1.31 c/deg, and 2.62 c/deg (Figure 14a-d, respectively).

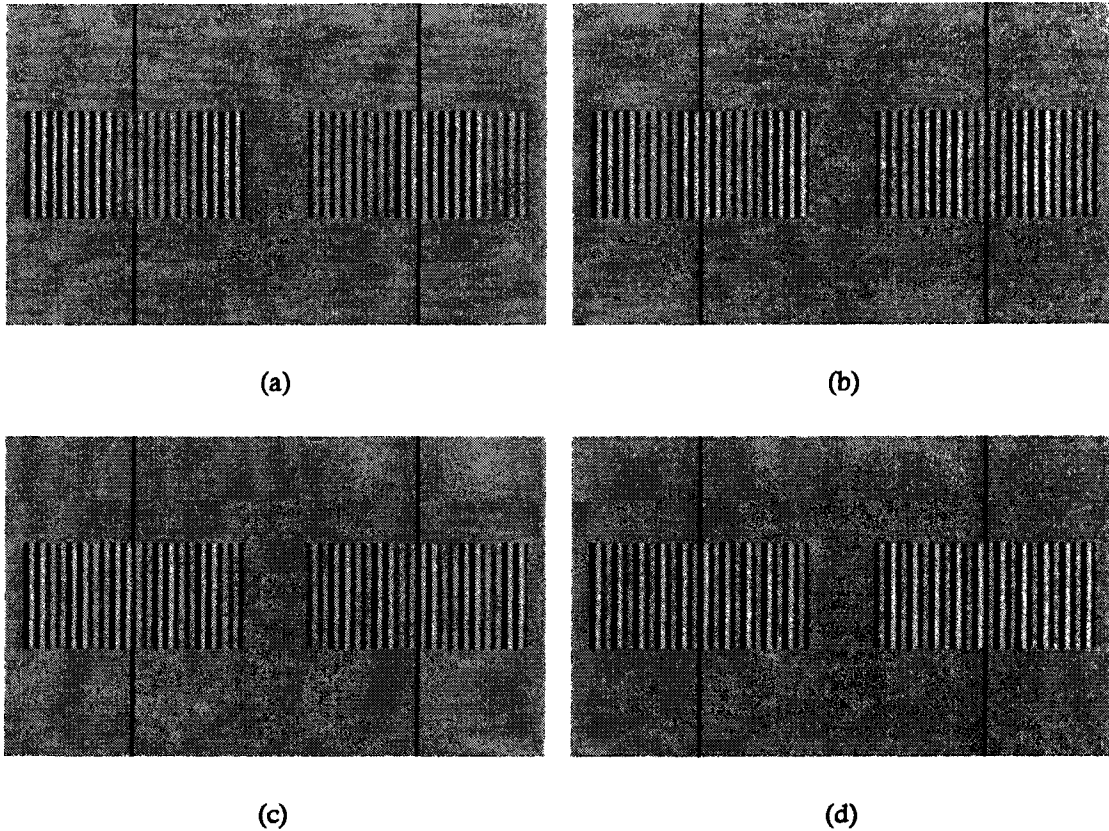


Figure 14. Experiment 2 stimuli (not shown at actual size or luminance levels). For all conditions, the carrier is a 5.24 c/deg square-wave. (a) condition 1: 0.33 c/deg square-wave contrast disparity modulation, (b) condition 2: 0.65 c/deg square-wave contrast disparity modulation, (c) condition 3: 1.31 c/deg square-wave contrast disparity modulation, (d) condition 4: 2.62 c/deg square-wave contrast disparity modulation.

Procedure

The procedure in Experiment 2 was as described under GENERAL METHOD. Experiment 2 was basically like Experiment 1 but used a higher square-wave carrier spatial frequency and a higher range of square-wave contrast disparity modulation spatial frequencies (that partially overlapped the modulation spatial frequency range from Experiment 1). The square-wave carrier spatial frequency was fixed at 5.24 c/deg and contrast disparity thresholds for perception of apparent slant were measured for square-wave contrast disparity modulation spatial frequencies of 0.33 c/deg, 0.65 c/deg, 1.31 c/deg, and 2.62 c/deg. Again, ten sequences per session were presented, including two sequences at each of four modulation spatial frequencies and two sequences of catch trials.

Results

Experiment 2 contrast disparity thresholds for seeing slant for ETF, JMS and WWS are shown in Figure 15, Figure 16, Figure 17, respectively. As in Experiment 1, four log-log plots are shown for each subject: mean thresholds for seeing slant, session matched mean thresholds, median thresholds, and session matched median thresholds. Error bars are as in Experiment 1 and sessions are again matched by shifting individual session curves to the same overall level. Session matched median threshold plots are enlarged.

ETF

Figure 15a-d show results for ETF in Experiment 2. Contrast disparity thresholds for seeing slant again decreased with increasing spatial frequency of square-wave

contrast disparity modulation. The shapes of the response curves for the four plots were similar. Thresholds were highest for a square-wave contrast disparity modulation spatial frequency of 0.33 c/deg, and decreased monotonically with increasing spatial frequency, although again, some flattening in the plot can be seen at the lowest modulation spatial frequency. Unlike Experiment 1, the flattening is not enough to be seen as an actual dip in threshold level, and is not overwhelmed by error bars in any of the plots. The overall level is close to that of ETF Experiment 1 but slightly higher.

JMS

Figure 16a-d plot the results for JMS in Experiment 2. Again, the four plots are similar to one another and they continue the trend of decreasing contrast disparity thresholds for seeing slant with increasing spatial frequency of square-wave modulation. Unlike the result for JMS in Experiment 1, no flattening is seen at the lowest modulation spatial frequency (0.33 c/deg). The threshold even rises slightly but the shape of the decreasing thresholds function for JMS in Experiment 2 is again fairly flat and the error bars are small. The overall level of thresholds for JMS in Experiment 2 is slightly lower than it was in Experiment 1.

WWS

Figure 17a-d show results for WWS in Experiment 2. The shapes of the four plots appear somewhat different from each other, although the error bars are large enough to overwhelm most of the apparent differences. The most striking difference in shape is seen in Figure 17a (mean thresholds). However, that difference results

largely from the threshold for the 1.31 c/deg modulation point, which has large error bars. Contrast disparity thresholds for seeing slant still generally decreased with increasing spatial frequency of square-wave contrast disparity modulation. The decreasing slope of the threshold plot is close to the slope for ETF, though the overall threshold levels for WWS are closer to those for JMS. Instead of a flattening at the lowest modulation spatial frequency (as in WWS, Experiment 1), the threshold rises somewhat. Still, overall shape of the plot could almost be a straight decreasing line.

Discussion

Figure 18 shows session matched median thresholds for perception of slant for all three subjects in Experiment 2. For ETF and JMS the shape of the threshold function in Experiment 2 replicated the shape of the function in Experiment 1 for overlapping spatial frequencies. For WWS the threshold function in Experiment 2 was steeper and straighter than it was in Experiment 1. As in Experiment 1, thresholds for all subjects decreased with increasing modulation spatial frequency, resembling monocular contrast thresholds.

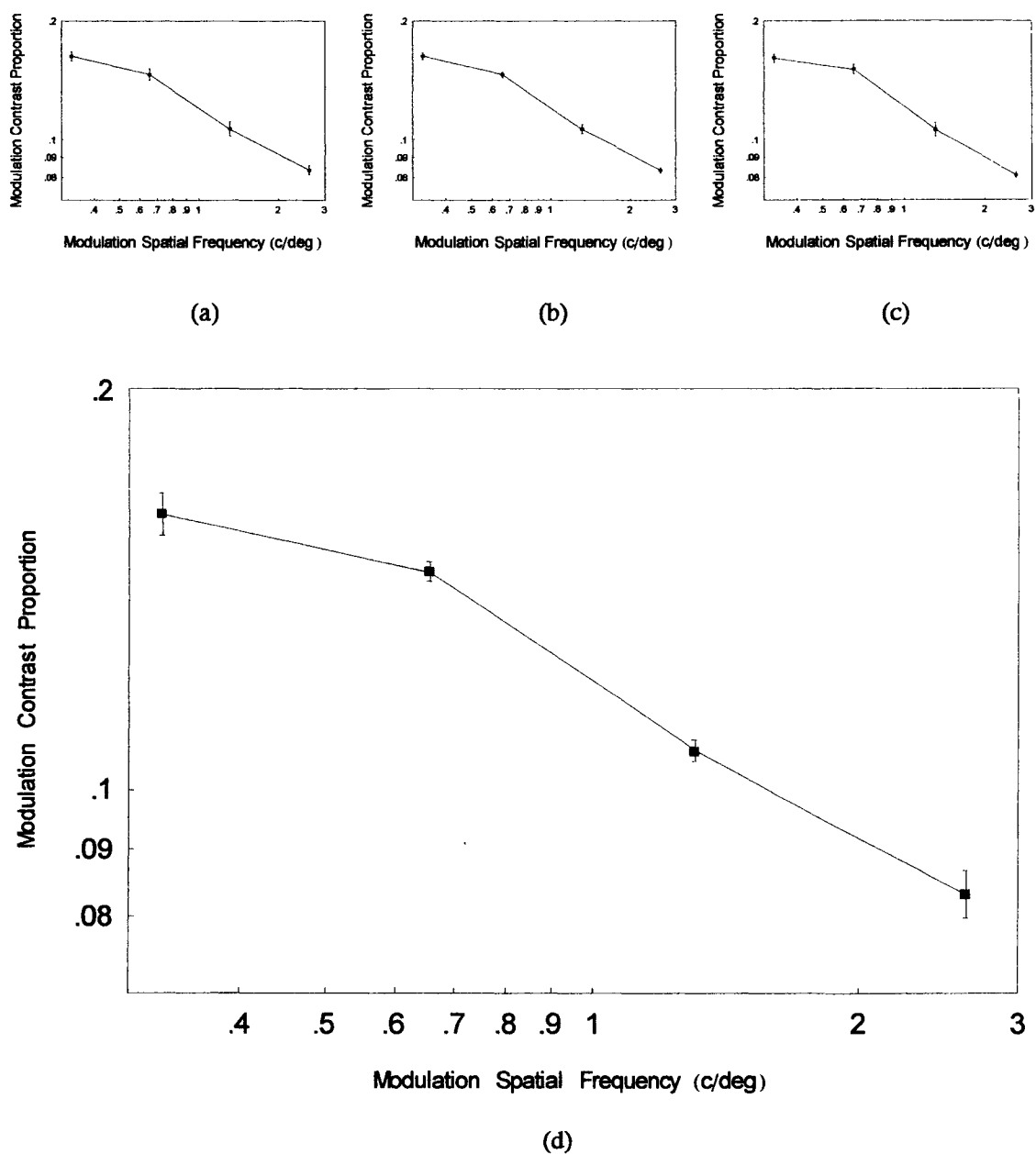


Figure 15. ETF, Experiment 2 contrast disparity thresholds. Square-wave contrast disparity modulation spatial frequencies are 0.33 c/deg, 0.65 c/deg, 1.31 c/deg and 2.62 c/deg. Square-wave carrier spatial frequency is 5.24 c/deg. (a) mean thresholds; error bars are \pm standard error of the mean, (b) session matched mean thresholds; error bars are \pm standard error of the mean, (c) median thresholds; error bars are ± 1.483 median absolute deviation/ \sqrt{n} , (d) session matched median thresholds; error bars are ± 1.483 median absolute deviation/ \sqrt{n} . ($n=8$ for all plots).

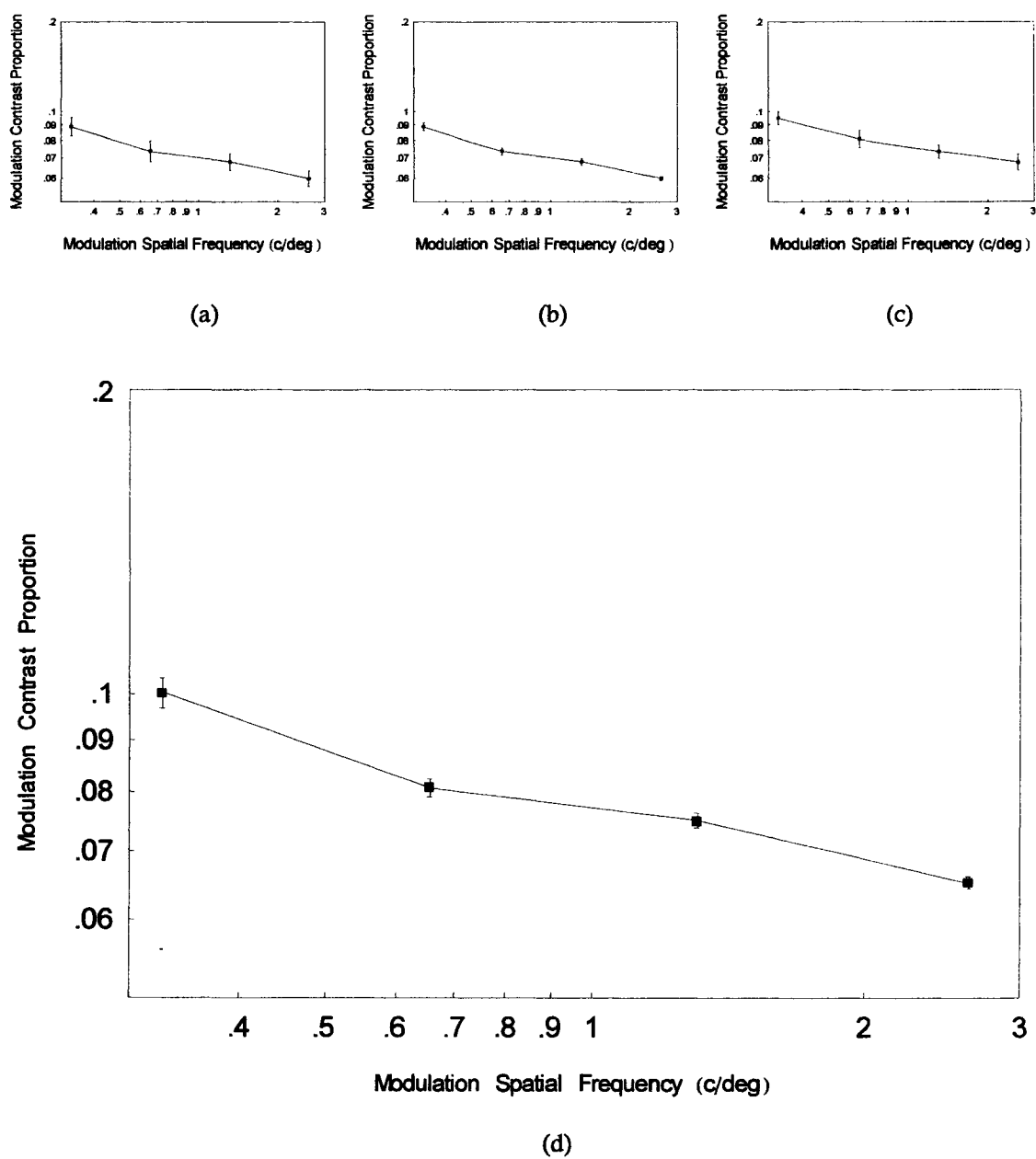


Figure 16. JMS, Experiment 2 contrast disparity thresholds. Square-wave contrast disparity modulation spatial frequencies are 0.33 c/deg, 0.65 c/deg, 1.31 c/deg and 2.62 c/deg. Square-wave carrier spatial frequency is 5.24 c/deg. (a) mean thresholds; error bars are \pm standard error of the mean, (b) session matched mean thresholds; error bars are \pm standard error of the mean, (c) median thresholds; error bars are ± 1.483 median absolute deviation/ \sqrt{n} , (d) session matched median thresholds; error bars are ± 1.483 median absolute deviation/ \sqrt{n} . ($n=8$ for all plots).

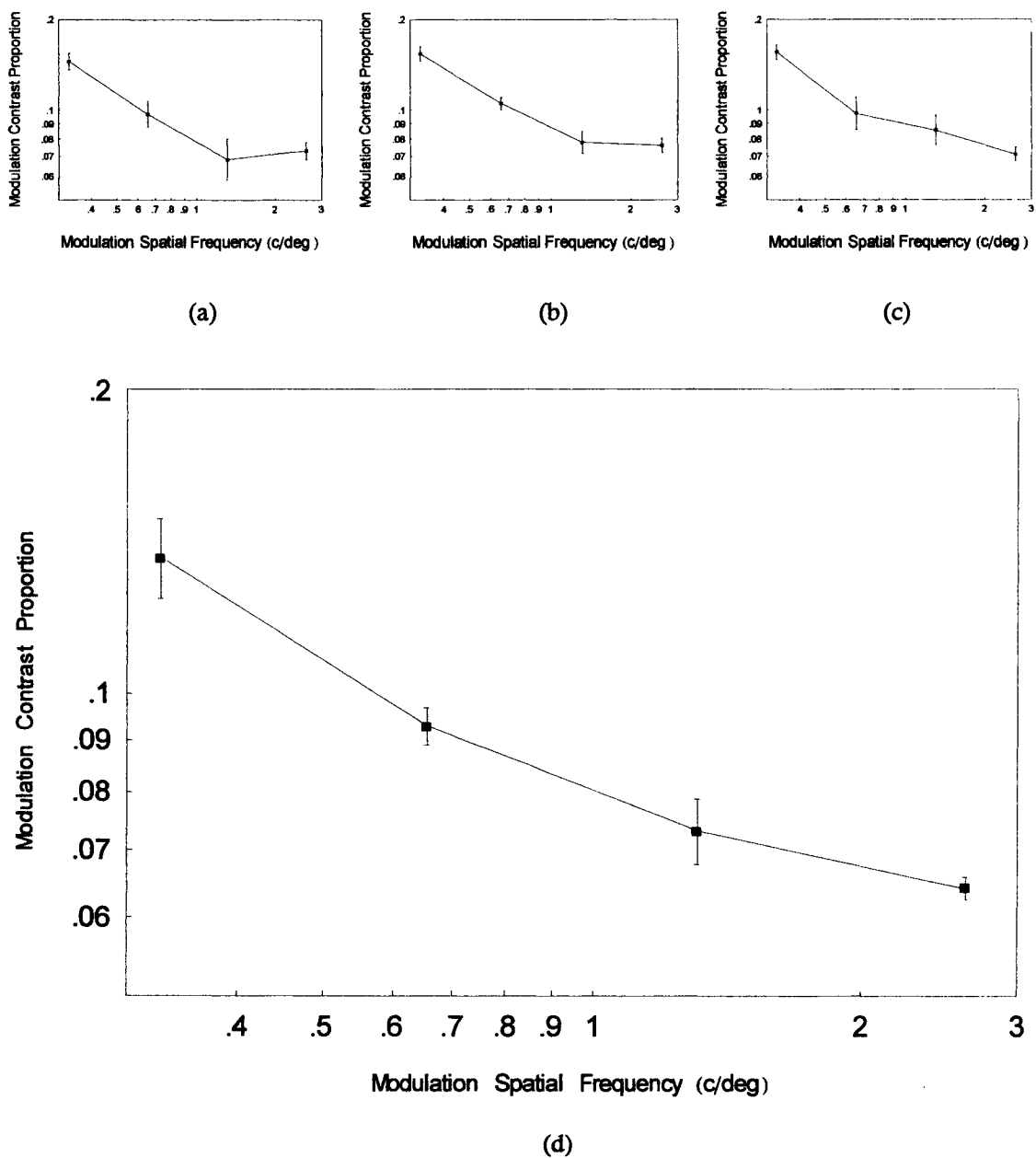


Figure 17. WWS, Experiment 2 contrast disparity thresholds. Square-wave contrast disparity modulation spatial frequencies are 0.33 c/deg, 0.65 c/deg, 1.31 c/deg and 2.62 c/deg. Square-wave carrier spatial frequency is 5.24 c/deg. (a) mean thresholds; error bars are \pm standard error of the mean, (b) session matched mean thresholds; error bars are \pm standard error of the mean, (c) median thresholds; error bars are ± 1.483 median absolute deviation/ \sqrt{n} , (d) session matched median thresholds; error bars are ± 1.483 median absolute deviation/ \sqrt{n} . ($n=7$ for all plots).

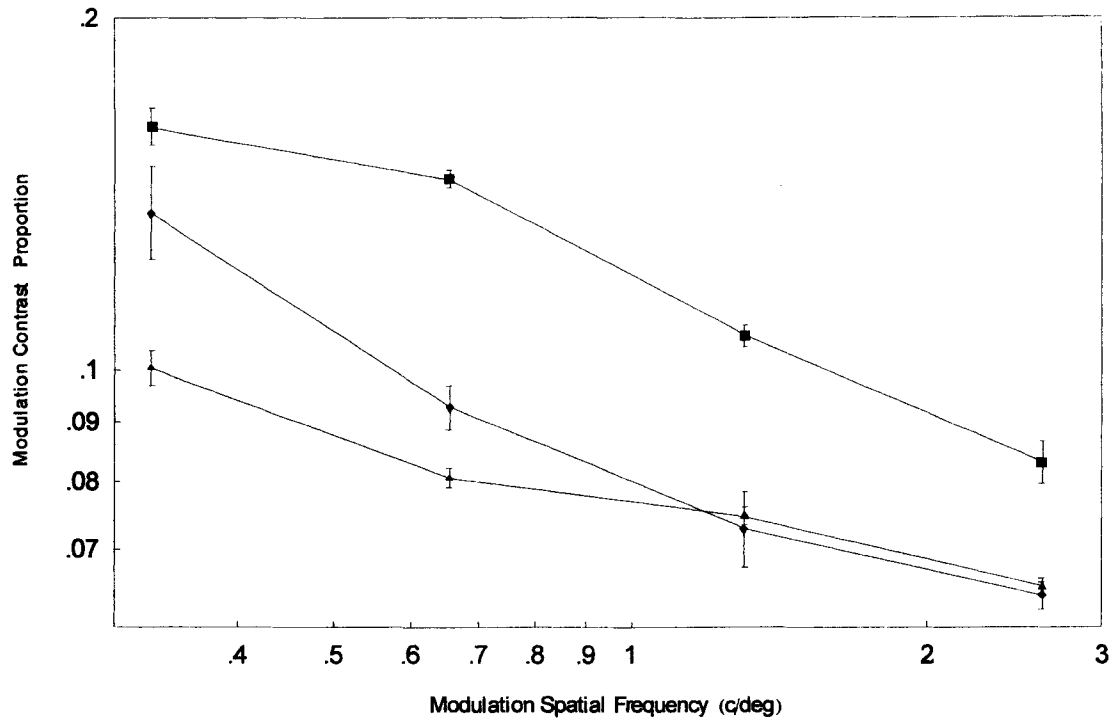


Figure 18. Experiment 2 session matched median contrast disparity thresholds plotted as a function of spatial frequency in c/deg for ETF (boxes), JMS (triangles), and WWS (diamonds). Error bars are ± 1.483 median absolute deviation / \sqrt{n} . Square-wave contrast disparity modulation spatial frequencies are 0.33 c/deg, 0.65 c/deg, 1.31 c/deg and 2.62 c/deg. Square-wave carrier spatial frequency is 5.24 c/deg.

EXPERIMENT 3

Introduction

Recall that in Experiment 1 the third harmonic (0.78 c/deg) for the modulation square-wave of our lowest spatial frequency (0.26 c/deg) falls in the low threshold region of our response curve. The third harmonic therefore may be expected to contribute to sensitivity at the lowest spatial frequency of square-wave modulation in Experiment 1. In Experiment 3, we sought to test this hypothesis by using sine-wave modulation, instead of square-wave modulation.

Methods

Subjects

ETF, JMS and WWS participated in Experiment 3.

Apparatus

Apparatus was as described under GENERAL METHOD.

Stimuli

Stimuli were stereograms as described under GENERAL METHOD. The square-wave carrier spatial frequency was fixed at 3.14 c/deg. Sine-wave contrast disparity modulation spatial frequencies in the four conditions were 0.26 c/deg, 0.39 c/deg, 0.79 c/deg, and 1.57 c/deg (Figure 19a-d, respectively).

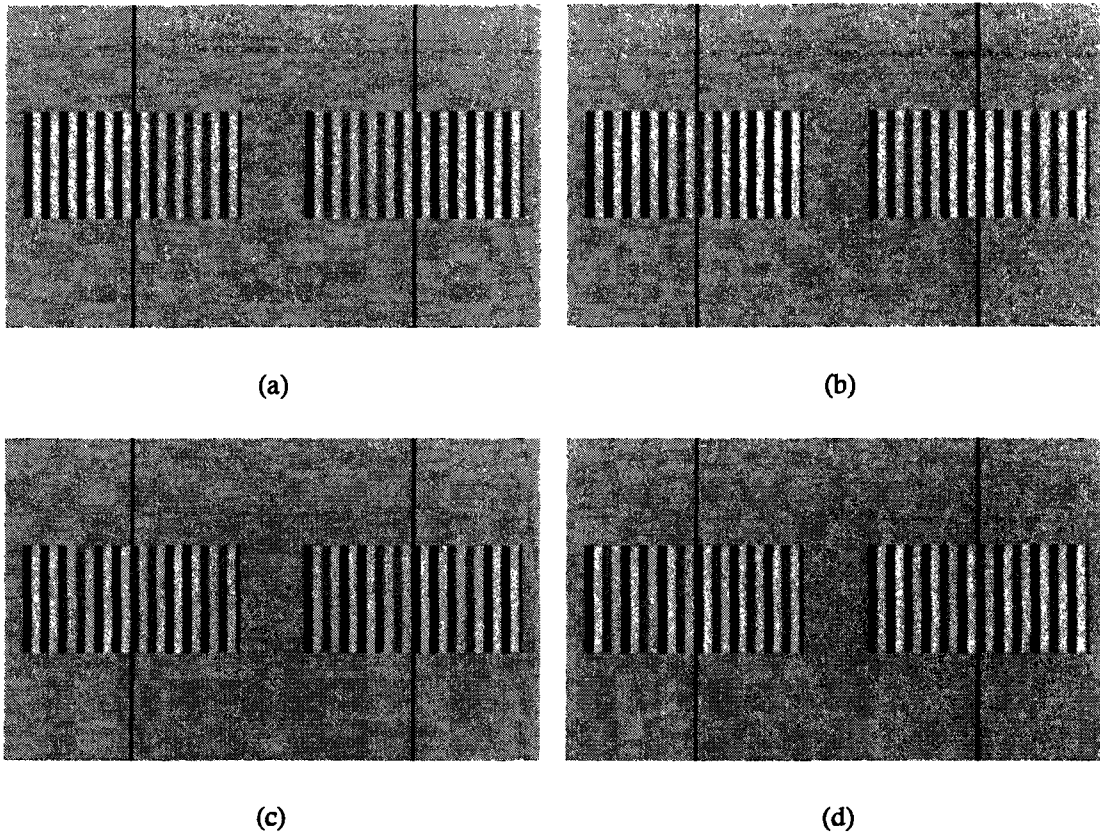


Figure 19. Experiment 3 stimuli (not shown at actual size or luminance levels). For all conditions, the carrier is a 3.14 c/deg square-wave. (a) condition 1: 0.26 c/deg sine-wave contrast disparity modulation, (b) condition 2: 0.39 c/deg sine-wave contrast disparity modulation, (c) condition 3: 0.79 c/deg sine-wave contrast disparity modulation, (d) condition 4: 1.57 c/deg sine-wave contrast disparity modulation.

Procedure

The procedure in Experiment 3 was as described under GENERAL METHOD.

Experiment 3 was identical to Experiment 1, except that it used sine-wave modulation, instead of square-wave modulation. The square-wave carrier spatial frequency was again fixed at 3.14 c/deg and contrast disparity thresholds for perception of apparent slant were measured for sine-wave contrast disparity modulation spatial frequencies of 0.26 c/deg, 0.39 c/deg, 0.79 c/deg, and 1.57

c/deg. Again, ten sequences per session were presented, including two sequences at each of four modulation spatial frequencies and two sequences of catch trials.

Results

Experiment 3 contrast disparity thresholds for seeing slant for ETF, JMS and WWS are shown in Figure 20, Figure 21, Figure 22, respectively. As in Experiments 1 and 2, the plots show thresholds for seeing slant plotted as a function of modulation spatial frequency. Plots again include session matched mean thresholds, median thresholds, and session matched median thresholds. Session matching and error bars are as in previous experiments. Session matched median threshold plots are enlarged.

ETF

Figure 20a-d show the results for ETF in Experiment 3. Contrast disparity thresholds for seeing slant decreased with increasing spatial frequency of sine-wave contrast disparity modulation. The shapes of the response curves for the four plots were similar, and nearly a straight line. Thresholds were highest for a sine-wave contrast disparity modulation spatial frequency of 0.26 c/deg, and decreased monotonically with increasing modulation spatial frequency. The overall level is close to that of ETF Experiment 1 and Experiment 2 but slightly higher than both.

JMS

Figure 21a-d plot the results for JMS in Experiment 3. Again, contrast disparity thresholds for seeing slant were highest for a sine-wave contrast disparity modulation of 0.26 c/deg, and decreased monotonically with increasing modulation spatial frequency. The shapes of the response curves for the four plots were similar, and

nearly a straight line. The plot closely resembles the plot of JMS in Experiment 2. The plot also resembles that for JMS in Experiment 1, although in Experiment 3 the overall level is a bit lower and the slope is slightly steeper. The plot also resembles that for ETF in Experiment 3, although the slope is smaller for JMS.

WWS

Figure 22a-d show results of Experiment 3 for WWS. The overall threshold level for WWS is higher than it is for ETF or JMS and, unlike those two subjects, WWS shows a decrease in threshold at a modulation spatial frequency of 0.26 c/deg. Aside from the 0.26 c/deg condition, contrast disparity thresholds in the session matched median plot (Figure 22d) appear to decrease with increasing modulation spatial frequency. However, the other three plots do not seem to fit this pattern.

Discussion

Figure 23 plots session matched median thresholds for seeing slant for all three subjects in Experiment 3. Thresholds tend to decrease with increasing modulation spatial frequency for two out of three subjects (ETF and JMS) but the drop is not as clear for the remaining subject (WWS).

In each experiment, stimulus presentations were randomly interleaved but the three experiments were performed sequentially, so interpreting levels between experiments is problematic and criterion changes could play a role.¹⁵

¹⁵ Appendix 10 plots the time series of false alarms by session for each subject. No obvious pattern across subjects emerges. An argument can be made that criterion changes account for overall levels for WWS.

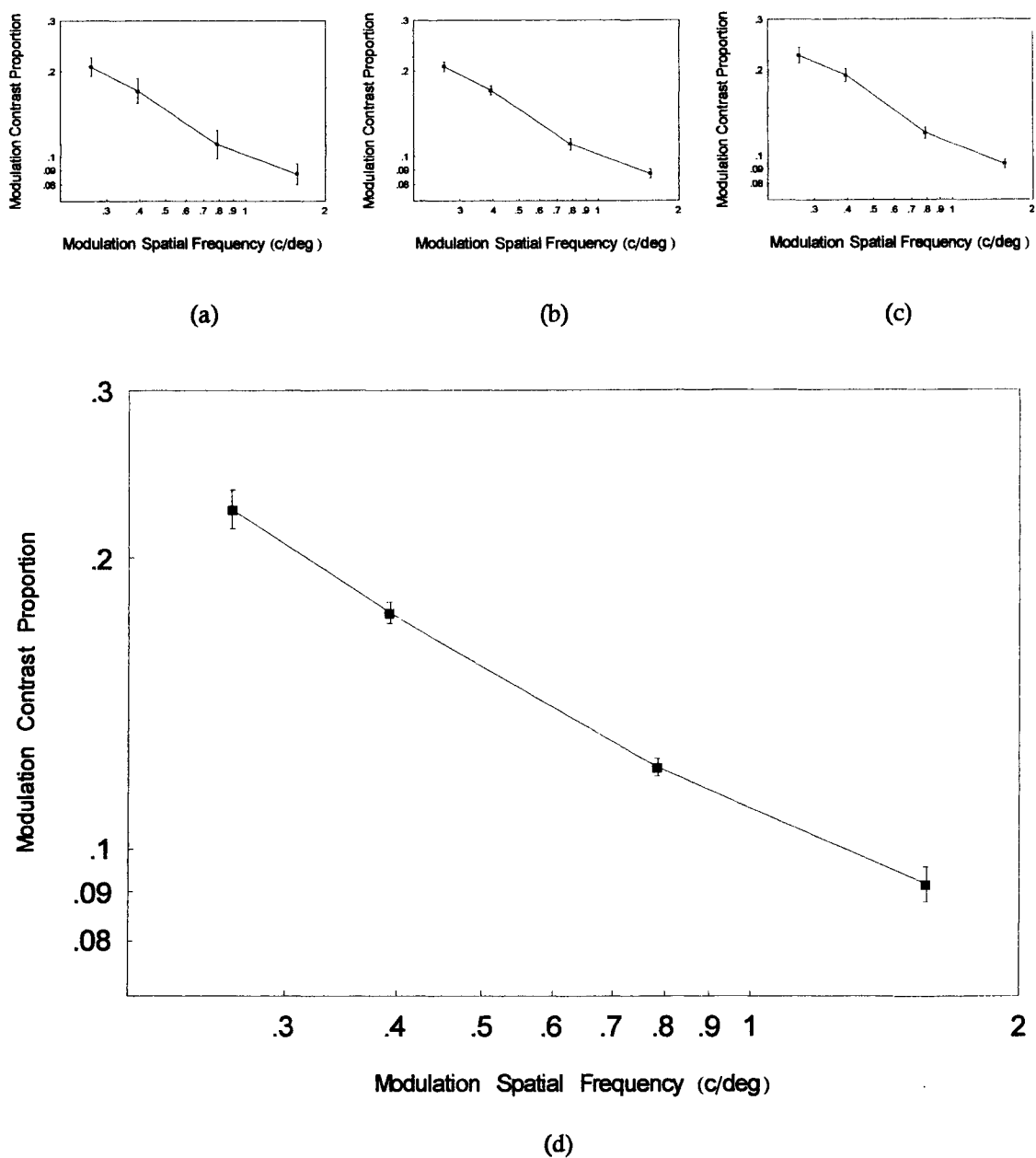


Figure 20. ETF, Experiment 3 contrast disparity thresholds. Sine-wave contrast disparity modulation spatial frequencies are 0.26 c/deg, 0.39 c/deg, 0.79 c/deg and 1.57 c/deg. Square-wave carrier spatial frequency is 3.14 c/deg. (a) mean thresholds; error bars are \pm standard error of the mean, (b) session matched mean thresholds; error bars are \pm standard error of the mean, (c) median thresholds; error bars are ± 1.483 median absolute deviation/ \sqrt{n} , (d) session matched median thresholds; error bars are ± 1.483 median absolute deviation/ \sqrt{n} . ($n=8$ for all plots).

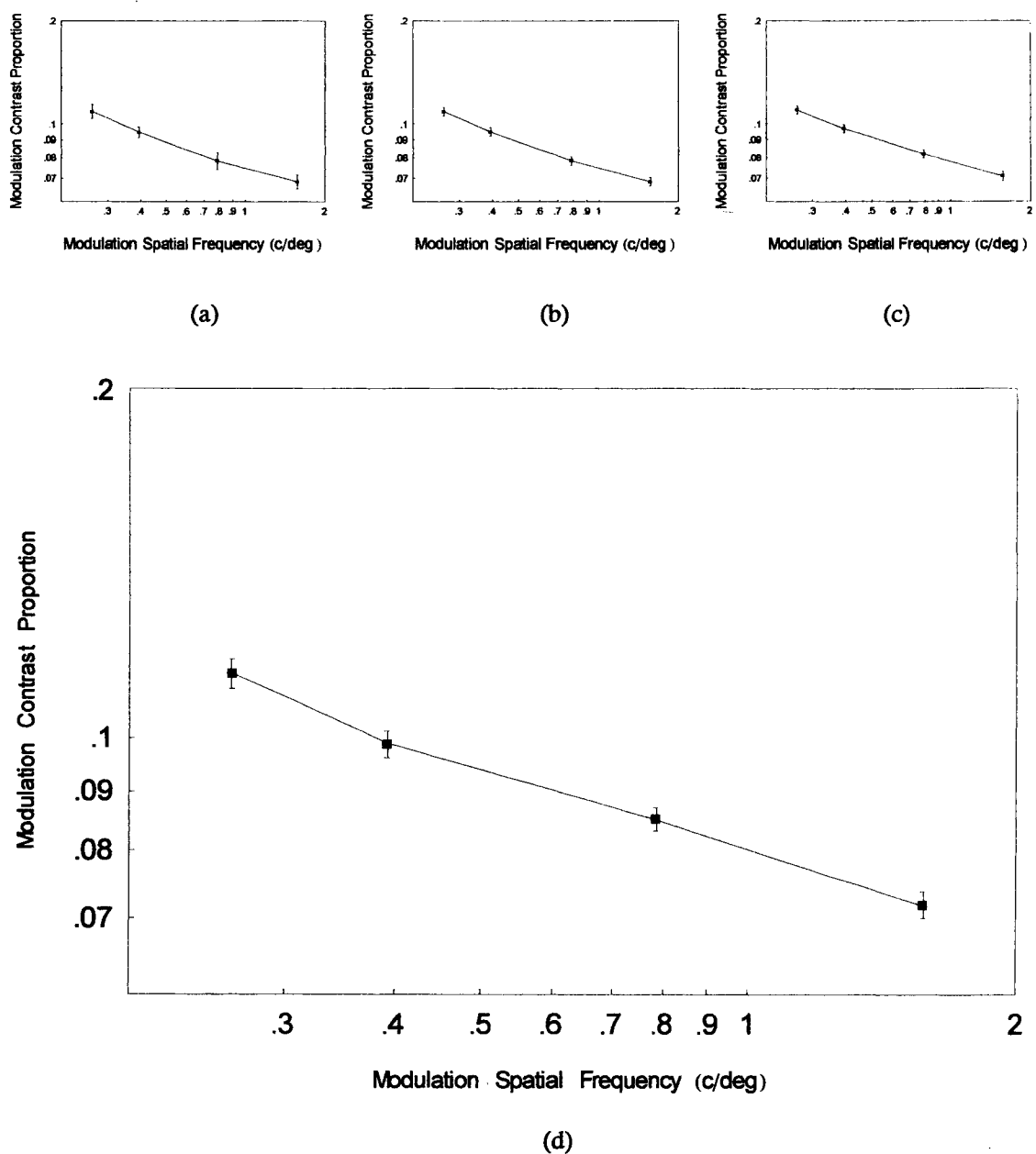


Figure 21. JMS, Experiment 3 contrast disparity thresholds. Sine-wave contrast disparity modulation spatial frequencies are 0.26 c/deg, 0.39 c/deg, 0.79 c/deg and 1.57 c/deg. Square-wave carrier spatial frequency is 3.14 c/deg. (a) mean thresholds; error bars are \pm standard error of the mean, (b) session matched mean thresholds; error bars are \pm standard error of the mean, (c) median thresholds; error bars are ± 1.483 median absolute deviation/ \sqrt{n} , (d) session matched median thresholds; error bars are ± 1.483 median absolute deviation/ \sqrt{n} . ($n=8$ for all plots).

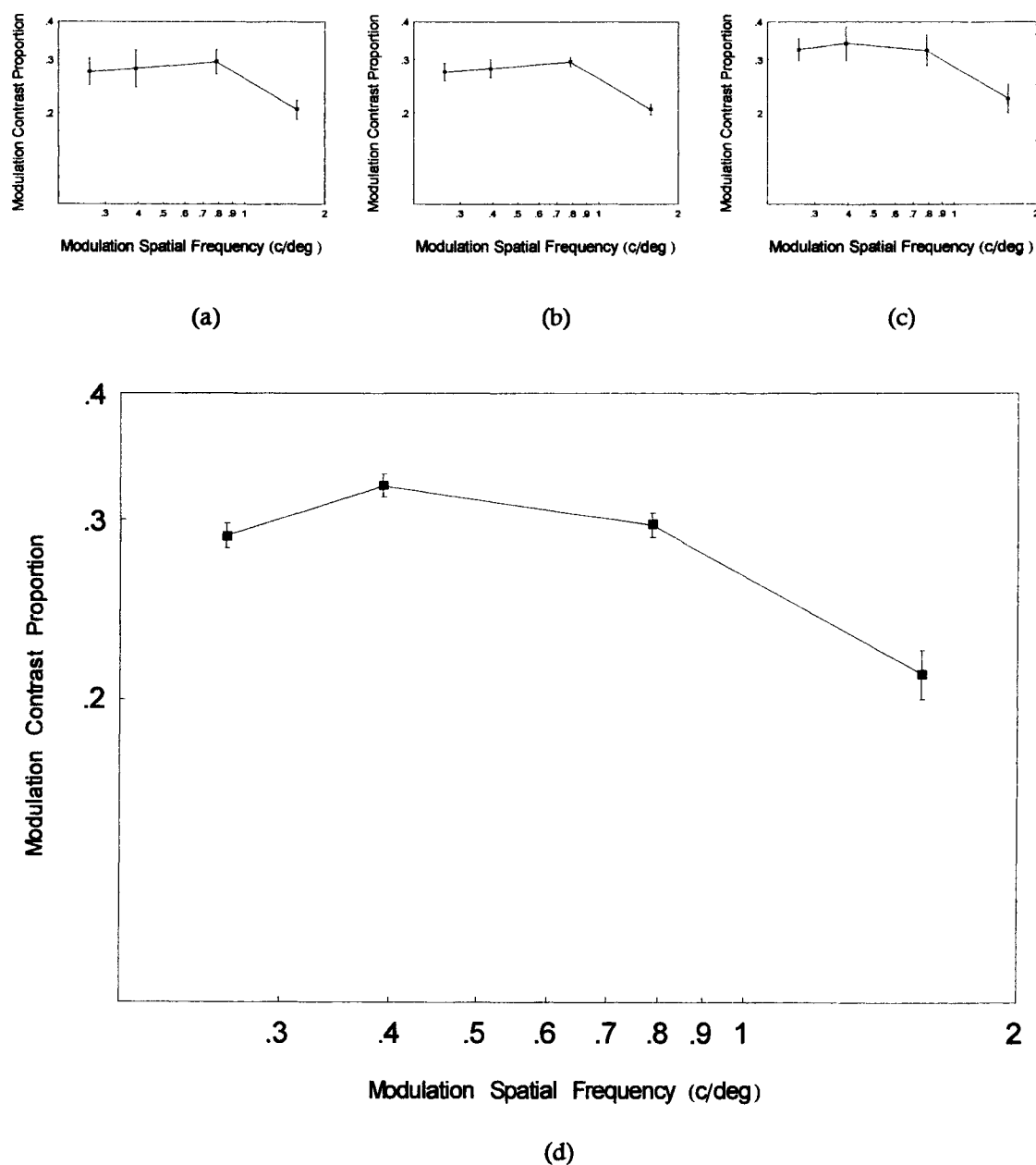


Figure 22. WWS, Experiment 3 contrast disparity thresholds. Sine-wave contrast disparity modulation spatial frequencies are 0.26 c/deg, 0.39 c/deg, 0.79 c/deg and 1.57 c/deg. Square-wave carrier spatial frequency is 3.14 c/deg. (a) mean thresholds; error bars are \pm standard error of the mean, (b) session matched mean thresholds; error bars are \pm standard error of the mean, (c) median thresholds; error bars are ± 1.483 median absolute deviation/ \sqrt{n} , (d) session matched median thresholds; error bars are ± 1.483 median absolute deviation/ \sqrt{n} . ($n=8$ for all plots).

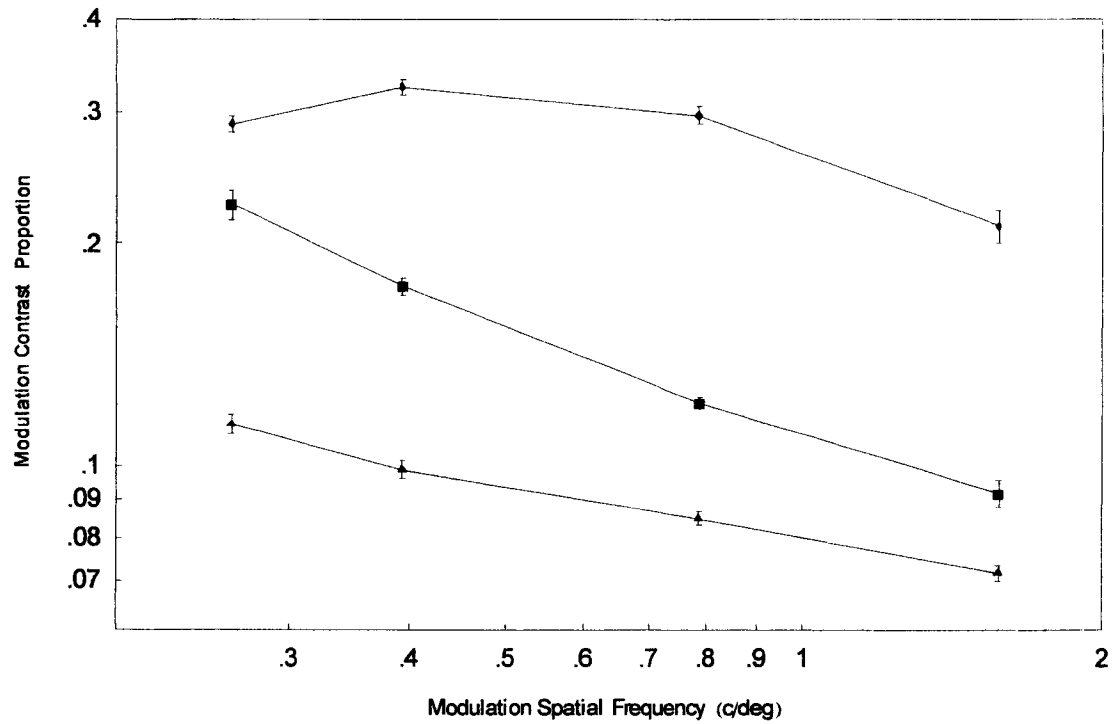


Figure 23. Experiment 3 session matched median contrast disparity thresholds plotted as a function of spatial frequency in c/deg for ETF (boxes), JMS (triangles), and WWS (diamonds). Error bars are ± 1.483 median absolute deviation / \sqrt{n} . Sine-wave contrast disparity modulation spatial frequencies are 0.26 c/deg, 0.39 c/deg, 0.79 c/deg and 1.57 c/deg. Square-wave carrier spatial frequency is 3.14 c/deg.

GENERAL DISCUSSION

The following discussion will (i) give a brief overview of the application of Fourier analysis to the results of the three experiments, (ii) describe three models of the results based on Fourier analysis and (iii) discuss some possible future directions for research.

In Experiments 1-3 we measured thresholds for the perception of slant in venetian blind stimuli as a function of the spatial frequency of square-wave contrast disparity modulations and sine-wave contrast disparity modulations. The results of Experiments 1-3 more closely resemble monocular contrast thresholds than stereo disparity thresholds for the detection of depth in random dot corrugations, so initially it is tempting to infer that contrast disparity modulation is tapping into monocular limits to contrast sensitivity, not binocular limits for the detection of retinal disparities. The drop in threshold for ETF at a modulation spatial frequency of 0.26 c/deg in Experiment 1 (which used square-wave modulation) relative to the corresponding threshold in Experiment 3 (which used sine-wave modulation) might then be accounted for on the basis of the presence of square-wave harmonics available for detection in Experiment 1 but not in Experiment 3. However, that approach would not be a fully adequate way to look at the results.

The stereo system should respond specifically to the binocular aspect of stimuli, i.e., to disparities of some kind between the images in the two eyes. Exactly how those disparities should be defined is an open question. If a subject's contrast sensitivity function explained that subject's threshold functions in Experiments 1-3

then a plausible way to incorporate it into a model would be to Fourier transform each half-image of a stereogram, adjust each resulting spectrum for the contrast sensitivity function, perform an inverse Fourier transform on each spectrum to return to the spatial domain, subtract luminances of one half-image from the other, and then Fourier transform the difference of luminances. (This is, in fact, equivalent to what we actually did.) If the contrast sensitivity function explained the contrast disparity thresholds in our experiments, then one might expect a subject to have equal power in the resulting spectra for the four conditions of an experiment. In a somewhat more complicated situation, if the four spectra did not have equal power, then one might still expect a systematic relationship across experiments. In that case, it should be possible to predict a subject's results in one experiment based on that subject's results in another. Because Experiment 3 used sine-wave contrast disparity

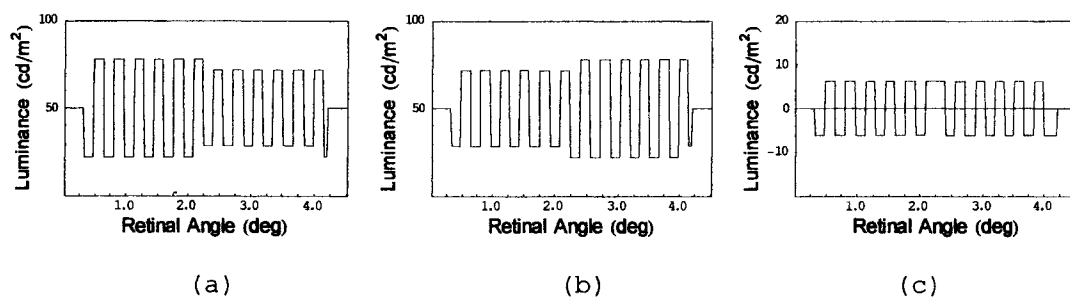


Figure 24. (a) Luminance plot of left image, (b) Luminance plot of right image, (c) Luminance plot of difference of luminances between left and right image

modulation instead of square-wave contrast disparity modulation, an initial guess might be that it would have somewhat cleaner spectra and be a good choice for predicting the other experiments. It turns out that the spectra of the binocular aspect of the stimuli in our experiments are not as simple as might be supposed. (Contrast disparity modulation leads to sum and difference spikes in the frequency domain.)

The stimuli in all experiments are fairly similar, so any experiment could be used to predict any other without altering the quality of the resulting model. Details of our Fourier analyses and subsequent models will now be presented.

To isolate the binocular aspect of the stimulus in each case, the luminance values in the right image were subtracted from the luminance values in the left image. (The Nyquist sampling criterion was met in all cases to avoid aliasing.¹⁶) A discrete Fourier transformation was performed on the resulting list of luminance differences (Figure 24) by application of Equation 3:

Equation 3

$$b_s = \frac{1}{\sqrt{n}} \sum_{r=1}^n u_r e^{2\pi i(r-1)(s-1)/n}$$

where u_r is the r^{th} element (each element is a sample point and corresponds to one pixel or 0.0159° of retinal angle) in a list of luminance differences (cd/m^2) to be Fourier transformed, n is the total number of elements in the untransformed list (284 pixels, corresponding to 4.519° of retinal angle), b_s is the s^{th} element in the transformed list, and of course $i = \sqrt{-1}$. This produces a frequency domain representation of the stimulus.

The first element in the transformed list ($s = 1$) is a real number representing the amplitude of the zero spatial frequency component of the stimulus (i.e., the mean

¹⁶ Aliasing is the appearance of frequencies in the Fourier transformed list that are not actually present in the sampled signal. The Nyquist sampling theorem states that in order to avoid aliasing, "the sampling rate must be at least twice the frequency of the highest component in the waveform being sampled" (Ramirez, 1985, p. 115). In our stimuli, a pixel constitutes a sample point. Our highest carrier spatial frequency was 5.24 c/deg, corresponding to 12 pixels/cycle (Experiment 2). Its fifth harmonic (26.2 c/deg or 2.4 pixels/cycle) includes slightly more than two sample points (pixels) per cycle. We therefore meet the Nyquist criterion for up to the fifth harmonic of our highest spatial frequency.

luminance, 50 cd/m²). The second element in the list ($s = 2$) is a complex number representing the phase and amplitude of the lowest spatial frequency present in the sample (0.2 c/deg). The last element in the list is the complex conjugate of the second element in the list. The third element ($s = 3$) is a complex number representing the phase and amplitude of the next higher sampled frequency (0.4 c/deg); and the penultimate element is the complex conjugate of the third element. Elements are paired off in this way, working toward the center of the list, until the highest sampled frequency (32 c/deg) is reached at the center ($s = 143$).

The spectrum list produced above was then "folded" to produce the "power spectrum," a plottable list of real numbers corresponding to amplitudes of sampled spatial frequencies, ordered from lowest spatial frequency to highest. The term "power spectrum" is conventional but is not quite correct because the values in it take the same units (cd/m² in our case) as the untransformed list (James, 1995, p.12). Nevertheless, the values are proportional to the power. Folding was accomplished by discarding the zero frequency element of the transformed list and then finding one real number (representing amplitude) per conjugate pair by application of Equation 4:

Equation 4
$$f = \sqrt{|b_1|^2 + |b_2|^2}$$

where $|b_1|$ is the modulus (i.e., absolute value) of the first element of the conjugate pair, $|b_2|$ is the modulus of the second element of the conjugate pair, and f is the resulting amplitude for that spatial frequency. The highest spatial frequency, occurring at the center of the unfolded list, had only a single element and so played the roles of both b_1 and b_2 in Equation 4, producing an amplitude equal to $\sqrt{2}$ times the actual amplitude, which was then divided by $\sqrt{2}$.

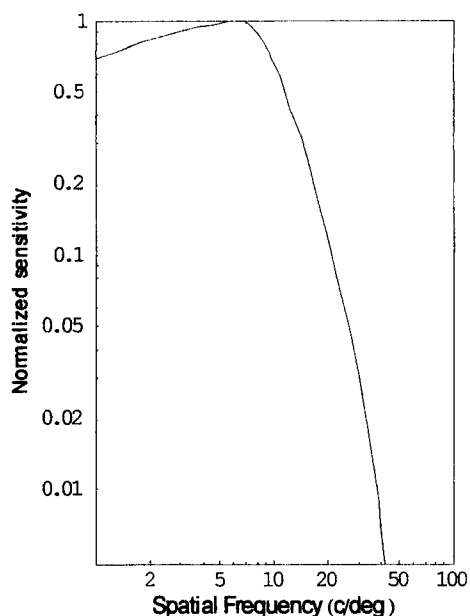


Figure 25. Normalized contrast sensitivity function based on data from C. Blakemore and F. W. Campbell (1969).

An adjustment for contrast sensitivity function was then applied to the folded spectrum list by multiplying it by the normalized contrast sensitivity function (Figure 25) derived from data from Blakemore and Campbell (1969).¹⁷ An example of a Fourier plot for condition 1 of Experiment 1, after adjustment for contrast sensitivity function is shown in Figure 26. (Complete examples of stimuli, luminance plots and Fourier plots appear in Appendices 1-3.) The spatial frequency of the square-wave carrier is 3.14

c/deg and the spatial frequency of the square-wave modulation is 0.26 c/deg. The

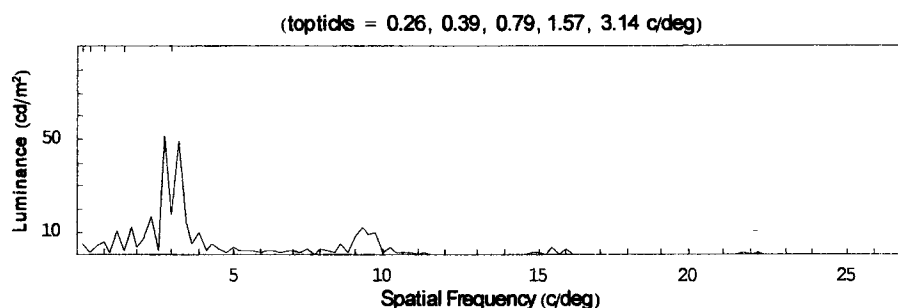
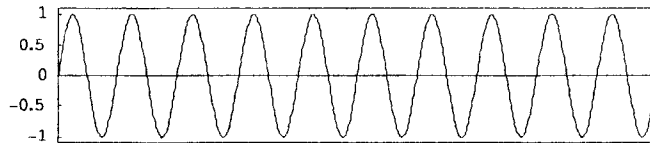


Figure 26. Fourier plot (adjusted for human contrast sensitivity function) of the difference in luminances between left and right images of a stereogram.

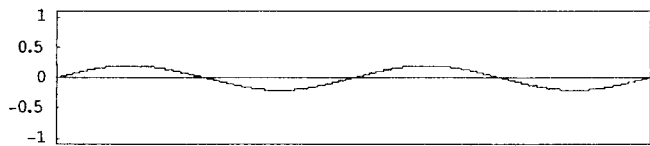
¹⁷ Cornsweet (1970) reports a peak for the contrast sensitivity function in the range of 4 c/deg. As a check, we also did our calculations using Cornsweet's contrast sensitivity function but our results were essentially unchanged.

ticks on the upper x-axis indicate the four spatial frequency conditions of square-wave modulation in Experiment 1, as well as the square-wave carrier spatial frequency.

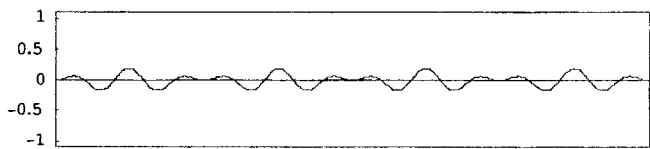
Note that no spike occurs at the spatial frequency of the carrier but a spike appears immediately to either side. These spikes (3.4 c/deg and 2.88 c/deg) are sum



(a)



(b)



(c)

Figure 27. (a) 10 c/deg carrier sine-wave, (b) 2 c/deg modulation sine-wave, (c) modulated carrier wave. Note that the modulation goes negative every half cycle, introducing into the result a 180° phase shift with every half cycle of the carrier.

and difference spatial frequencies of the carrier and modulation, not harmonics.

Recall from Figure 24 that, to isolate the binocular aspect of the stimulus, the luminance values of the right image were subtracted from the luminance values of the left image and the resulting difference of

luminances list was Fourier

analyzed. An examination of

Figure 24 shows that the image

having a higher contrast

switches from one image to the other (left to right or right to left) with every half cycle of modulation. (This applies to all conditions in all experiments.) The sum and difference spikes in the Fourier plot (Figure 26) are caused by the resulting 180° phase

shift in the difference luminances, as demonstrated for a simple case in Figure 27 and Figure 28.

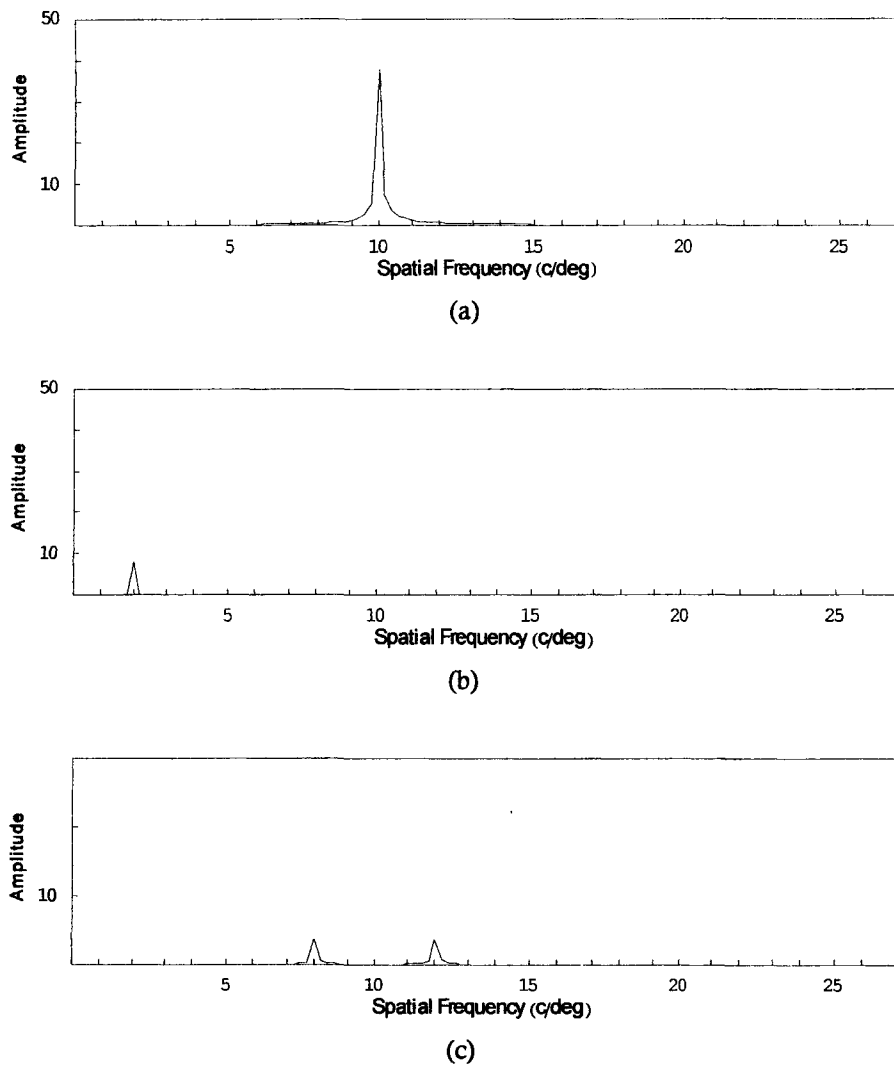


Figure 28. (a) Fourier plot 10 c/deg carrier sine-wave, (b) Fourier plot of 2 c/deg modulation sine-wave, (c) Fourier plot of result of modulation. In (c), sum and difference spikes appear at 8 c/deg and 12 c/deg.

Figure 27a-c show a 10 c/deg carrier sine-wave, a 2 c/deg modulation sine-wave, and the result of modulating the carrier by multiplying its amplitude by the amplitude of the modulation sine-wave. Figure 28a-c show the corresponding Fourier

plots. The sum and difference frequencies seen in Figure 28c are produced by the 180° phase shift occurring with every half-cycle of modulation in Figure 27c. Adding a constant offset to the modulation sine-wave to prevent it from ever going negative removes the 180° phase shift in the modulated waveform and eliminates sum and difference frequencies in the Fourier plot.¹⁸

In Figure 26, harmonics of the sum and difference spikes can be seen at three times their spatial frequencies, and again at five times their spatial frequencies. (Recall that a square-wave consists of an infinite number of sinusoids: the fundamental at the frequency of the square-wave, a sinusoid with one third the amplitude of the fundamental at three times the frequency, a sinusoid with one fifth the amplitude of the fundamental at five times the frequency, etc.)

Fourier analyses, including adjustment for contrast sensitivity function, were performed on all threshold stimuli for all subjects in all experiments. (Complete Fourier plots for all results are shown in Appendices 4-6.) We then used the results of the Fourier analyses in calculating three different models: a one parameter model, a two parameter model, and a three parameter model.

In our one parameter model, for each subject separately, we used a subject's session matched median thresholds from Experiment 3 to predict that subject's session matched median thresholds in Experiments 1 and 2 jointly. We fixed our free parameter, AL_3 , to an arbitrary initial value for the first iteration of the model. AL_3

¹⁸ Sum and difference frequencies also appear in a Fourier plot of a wave constructed from, say, 6 cycles of sine-wave centered around a mean level of 0, followed by 6 cycles of the sine-wave shifted

can be thought of as a horizontal line placed across a Fourier plot. We took the four difference of luminance Fourier plots corresponding to session matched median thresholds for the subject in conditions 1-4 of Experiment 3. For each of the four Fourier plots separately (but using the same AL_3 value), we summed the amplitudes of all spikes that reached or exceeded AL_3 to estimate the power required to see slant in that condition. With the stipulation that the initial value of AL_3 was arbitrary, we now had a list of four theoretical powers required to see slant in conditions 1-4 of Experiment 3.

AL_1 and AL_2 can also be thought of as horizontal lines placed across Fourier plots but, unlike AL_3 , they were not free parameters. Rather, values of AL_1 and AL_2 were fixed to the value of AL_3 times a factor correcting for the change in overall level between experiments by application of Equation 5 and Equation 6:

$$\text{Equation 5} \quad AL_1 = AL_3 \frac{E_1}{E_3}$$

$$\text{Equation 6} \quad AL_2 = AL_3 \frac{E_2}{E_3}$$

where E_1 , E_2 and E_3 were the means of the four session matched median thresholds for the subject in Experiments 1, 2, and 3, respectively.

Next we took the four difference of luminance Fourier plots corresponding to session matched median thresholds for the subject in Experiment 1. For each of the four Fourier plots separately, we summed the amplitudes of all spikes that reached or exceeded AL_1 to find the power required to see slant in that condition. (If the four

180°. Sum and difference frequencies remain if the level of the wave is shifted so that the resultant wave does not go negative.

powers found in Experiment 1 were perfectly predicted by those found in Experiment 3, then they would have exactly the same four values as the powers in Experiment 3.) We repeated this process for Experiment 2 to predict the four powers required in that experiment from those in Experiment 3.

As a measure of the quality of our initial predictions, we calculated prediction error as a coefficient of variation of the actual thresholds divided by the predicted thresholds, point by point. In the one parameter model, each subject had eight ratios (four for Experiment 1 and four for Experiment 2) that went into a single coefficient of variation.¹⁹ For each subject separately, we repeated all of the above calculations for a range of AL_3 values to determine the AL_3 value giving the smallest error.

In addition to the one parameter model, we produced two more very similar models: a two parameter model and a three parameter model. As was the case for the one parameter model, the two and three parameter models were calculated for each subject separately. The only difference of the two parameter model from the one parameter model was that, instead of predicting the results of Experiments 1 and 2 together using a single AL_3 (as was done in the one parameter model), Experiment 1 was predicted alone from Experiment 3, and Experiment 2 was predicted alone from Experiment 3. This gave two independent AL_3 values (one per experiment) for each subject in the two parameter model. Two independent prediction errors were found: a coefficient of variation of the actual Experiment 1 thresholds divided by the predicted Experiment 1 thresholds, point by point; and a coefficient of variation of

the actual Experiment 2 thresholds divided by the predicted Experiment 2 thresholds, point by point.

In the three parameter model, all three *ALs* were varied independently to find the combination producing the lowest error for the three experiments. Thus we had six coefficients of variation (two for each subject, i.e., one for Experiment 1 and one for Experiment 2). Each coefficient of variation was based on four ratios. (Complete model predictions superimposed on plots of experimental results are given in Appendices 7-9.)

Although the models predict fairly well for two out of three subjects (ETF and JMS), they are not as successful at predicting the third subject (WWS). For example, consider the actual and predicted thresholds for WWS in Experiment 1 (Figure 50c, Figure 52c, and Figure 54c) and Experiment 2 (Figure 51c, Figure 53c, and Figure 55c). In every case, the shapes of those plots for predicted and actual thresholds differ substantially. The condition 1 prediction is always too low, while the condition 3 prediction is always too high. On the other hand, the predictions for ETF (Figure 50a through Figure 55a), and the predictions for JMS (Figure 50b through Figure 55b) are moderately good and tend to improve steadily from the one parameter model to the three parameter model. The three parameter fit for ETF Experiment 2 and the three parameter fit for JMS Experiment 1 are excellent. Although the fits for ETF and WWS are better overall, the same pattern of predictions that are too low for condition 1 and too high for condition 3 can be seen in Experiment 2 (with the

¹⁹ Coefficient of variation is a relative measure of dispersion given by $CV = \sigma_x / \bar{x}$.

exceptions of condition 3 for ETF Experiment 2 using the one parameter model, and conditions 1-4 for ETF Experiment 2 using the three parameter model, all of which are too close to call).

The systematic deviation from predictions in Experiment 2 suggests that the models could be adjusted to improve prediction. However, that approach should be considered with some skepticism because it is possible to model phenomena without sufficient physical insight, to reduce error without increasing the ability to predict. Theoretically, it may be possible to get more accurate model predictions by measuring a single subject's contrast sensitivity function and repeating the three experiments and calculations for that subject but that seems unlikely. In a deep sense, our models probably have not captured the right predictors and it is unclear how much progress could be made by tweaking the models. On the other hand, the systematic deviations from prediction in Experiment 2 are intriguing and such deviations could probably be fit with narrowly tuned spatial frequency channels at the appropriate spatial frequencies. (Again, caution is in order because, in some sense, one can fit anything.) It may be possible to perform adaptation procedures, analogous to those used by Blakemore & Campbell (1969), to measure the sensitivity and bandwidth of such putative channels.

We have tentatively ruled out some simple explanations for the results of Experiments 1-3. Monocular contrast sensitivity functions do not explain the results in a simple way. (If they did then the power levels in the difference of luminance Fourier plots should have had, after adjustment for contrast sensitivity function, the same power in conditions 1-4.)

A number of directions could be taken. Banks (1985, p. 32) states while discussing how to characterize visual stimuli, "At the beginning of a search, one is far better off with a rough map containing most of the major landmarks, but not details, than with a detailed map of just one neighborhood." That advice may be apt for venetian blind research, so we will now consider several possible directions for research.

It would be natural to follow up the current study with a study measuring luminance disparity modulation thresholds as a function of spatial frequency to learn whether or not the pattern of decreasing thresholds seen with increasing spatial frequency generalizes to luminance disparity modulation.

One interesting feature of the current study is the appearance of sum and difference spatial frequency spikes in the difference of luminance Fourier plots. To our knowledge, sum and difference spikes, and their production by interocular phase differences, have not been investigated in the context of spatial vision. If such phase differences are environmentally common, one might expect the stereo system to be adept at their detection. This suggests the possibility of cortical stereo receptive fields specialized for the detection of sum and difference spikes.

Another interesting point was noted by two subjects (ETF and WWS) in Experiment 2. Sometimes a bar seemed to slant when they looked away from it. Because peripheral contrast sensitivity (a bandpass function) peaks at lower spatial frequencies than does foveal contrast sensitivity (Thibos et al., 1996), one might hope to explain this non-foveal perception of slant by reference to a low spatial frequency range in which peripheral contrast sensitivity exceeds foveal contrast sensitivity.

However, that explanation can be ruled out because contrast sensitivity for any given spatial frequency decreases monotonically with increasing retinal eccentricity (Rovamo et al., 1978).

At least two further explanations for seeing slant when looking away from the venetian blind stimulus could be examined. First, for retinal eccentricities from 0° to 8° , stereoacuity from horizontal retinal disparity decreases with increasing stimulus eccentricity (Rawlings and Shipley, 1969). This suggests that subjects performing a depth discrimination task may search for and successively foveate relatively informative stimulus regions. However, Blakemore (1970) reported that if two stimuli whose relative depth is to be discriminated are placed on a depth pedestal (i.e., the stimuli are placed some distance beyond the subject's fixation depth) then the rate of decrease in stereoacuity drops. Blakemore's data imply (Krekling, 1974) that stimuli on a depth pedestal of 80 arc min actually have lower thresholds for horizontal retinal disparity at a retinal eccentricity of 5° than they do at 0° . If the visual systems of subjects in our experiments sometimes interpreted contrast disparity as a depth pedestal (where none actually exists) then this might enhance slant detection for images that are slightly non-foveal. One problem for this hypothesis is that depth in venetian blind stimuli is not produced in an obvious way by geometric retinal disparities.

A second possibility is that eye movements themselves sometimes produce a temporarily greater contrast sensitivity. Our Experiments 1-3 did not control or measure eye movements or fixation, so it is not known how much variability these might have contributed. Kelly (1979) measured contrast sensitivity for vertically

oriented sine-wave gratings (about 0.2 c/deg to about 12 c/deg) drifting across the retina at various speeds ($0^\circ/\text{s}$, $0.012^\circ/\text{s}$, $0.15^\circ/\text{s}$, $3^\circ/\text{s}$, $11^\circ/\text{s}$, and $32^\circ/\text{s}$). Drift rates above about $0.1^\circ/\text{s}$ produced a contrast sensitivity curve of similar shape (bandpass) but with a peak sensitivity that shifted toward lower spatial frequencies as drift rate increased, so a spatial frequency that was invisible to the visual system at a slow drift rate became visible at a higher drift rate. If visually scanning the stimulus can sometimes simulate drift then eye movements might sometimes lead to slant perception.

However, visual scanning of static stimuli is generally performed by saccades, extremely rapid eye movements, during which saccadic suppression typically occurs. In saccadic suppression, visual sensitivity is reduced to one third of its usual level around the time of the saccade (Chase and Kalil, 1972). Although the mechanisms of saccadic suppression are not entirely understood, some of them appear to operate early in the visual system. Adey and Noda (1973) found suppressed cell response in the lateral geniculate nuclei during saccades. Matin, Clymer, and Matin (1972) suggested backward masking of the blurred saccadic image by the unblurred pre-saccadic image. Campbell and Wurtz (1978) reported forward masking of the saccadic image by the post-saccadic image. Typically, saccadic suppression would overwhelm any low spatial frequency contrast sensitivity enhancement, so incomplete saccadic suppression would need to occur. Although a possible non-foveal depth effect for the venetian blind effect is interesting, the effect is not stable and may prove difficult to replicate unless eye tracking is used.

REFERENCES

- Adey, W. R. & Noda, H. (1973). Influence of eye movements on geniculo-striate excitability in the cat. Journal of Physiology, 235, 805-821.
- von Békésy, G. (1970). Apparent image rotation in stereoscopic vision: The unbalance of the pupils. Perception & Psychophysics, 8 (5B), 343-347.
- Bex, P. J. & Edgar, G. K. (1996). Shifts in perceived location of a blurred edge increase with contrast. Perception & Psychophysics, 58 (1), 31-33.
- Blake, R. & Cormack, R. H. (1979). Does contrast disparity alone generate stereopsis? Vision Research, 19, 913-915.
- Blakemore, C. & Campbell, F. W. (1969). On the existence of neurones in the human visual system selectively sensitive to the orientation and size of retinal images. Journal of Physiology, 203, 237-260.
- Blakemore, C. (1970). The range and scope of binocular depth discrimination in man. Journal of Physiology, 211, 599-622.
- Bradshaw, M. F. & Rogers, B. J. (1993). Sensitivity to horizontally and vertically oriented stereoscopic corrugations as a function of corrugation frequency. Perception, 22, (Abstract Supplement), 117.
- Campbell, F. W. & Robson, J. G. (1968). Application of Fourier analysis to the visibility of gratings. Journal of Physiology, 197, 551-566.
- Campbell, F. W. & Wurtz, R. H. (1978). Saccadic omission: Why we do not see a grey-out during a saccadic eye movement. Vision Research, 18, 1297-1303.
- Chase, R. & Kalil, R. E. (1972). Suppression of visual evoked responses to flashes and pattern shifting during voluntary saccades. Vision Research, 12, 215-220.
- Cibis, P. A. & Haber, H. (1951). Anisopia and perception of space. Journal of the Optical Society of America, 41, 676-683.
- Cornsweet, T. N. (1970). Visual perception. Academic Press. New York.
- De Veaux, R. D., Velleman, P. F., & Bock, D. E. (2005). Stats: Data and Models. Boston: Addison-Wesley.
- Filley, E. T. (1998). An investigation of the Venetian blind effect. Unpublished masters thesis, University of New Hampshire.
- Filley, E. T., & Stine, W. W. (1998). Characterizing the 'Venetian blind' effect. Perception, 27 Supplement, 98.
- Fiorentini, A. & Maffei, L. (1971). Binocular depth perception without geometrical cues. Vision Research, 11, 1299-1305.

- Frisby, J. P. & Mayhew, J. E. W. (1978). Contrast sensitivity function for stereopsis. Perception, 7, 1299-1305.
- Howard, I. P. & Rogers, B. J. (1995a). Binocular vision and stereopsis. (pp. 310-311) Oxford University Press, Inc. New York.
- Howard, I. P. & Rogers, B. J. (1995b). Binocular vision and stereopsis. (pp. 159-166) Oxford University Press, Inc. New York.
- Ioannou, G. L., Rogers, B. J., Bradshaw M. F., and Glennerster A. (1993). Threshold and supra-threshold sensitivity functions for stereoscopic surfaces. Investigative Ophthalmology and Visual Science, 34, (ARVO Abstracts), 1186.
- James, J. F. (1995). A Student's Guide to Fourier Transforms. Cambridge University Press, Cambridge.
- Kelly, D. H. (1979). Motion and vision. II. Stabilized spatio-temporal threshold surface. Journal of the optical society of America, 69, (10), 1340-1349.
- Khutoryansky, N. (2000). An investigation of the influence of blurry edges on the Venetian Blind effect. Unpublished masters thesis, University of New Hampshire.
- Krekling, S. (1974). Stereoscopic threshold within the stereoscopic range in central vision. American Journal of Physiological Optics, 51, 626-634.
- Losada, M. A., Navarro, R. & Santa Maria, J. (1993). Relative contributions of optical and neural limitations to human contrast sensitivity at different luminance levels. Vision Research, 33, (16), 2321-2336.
- Matin, E., Clymer, A. B., & Matin, L. (1972). Metacontrast and saccadic suppression. Science, 178, 179-181.
- Michelson, A. A. (1927). Studies in Optics, p. 40, University of Chicago Press, Ltd. (1962 reprint)
- Münster, C. (1941). Über den Einfluss von Helligkeits Unterscheiden in Beiden Augen auf die stereoskopische Wahrnehmung. [The influence of interocular brightness differences on stereoscopic perception] Zeitschrift für Sinnesphysiologie, 69, 245-260.
- Ogle, K. N. (1952). Letter to the editor. Journal of the Optical Society of America, 42, 142.
- Ogle, K. N. (1962). Spatial localization through binocular vision. In H. Davson (Ed.), The Eye: Vol. 4. Visual optics and the optical space sense, 302-303. New York: Academic Press.
- Ramirez, R. W. (1985). The FFT: Fundamentals and Concepts. Prentice Hall, Inc. Englewood Cliffs, NJ.
- Rawlings, S. C., & Shipley, T. (1969). Stereoscopic acuity and horizontal angular distance from fixation. Journal of the Optical Society of America, 59, 991-993.
- Robbins, H. & Monro, S. (1951). A stochastic approximation method. Annals of Mathematical Statistics, 22, 400-407.

Robson, T. (1999). Topics in computerized visual-stimulus generation. In R. Carpenter & J. Robson (Eds.), Vision Research: A practical guide to laboratory methods, 81-105. New York: Oxford University Press.

Rogers, B. J., & Bradshaw, M. F. (1994). Is dif-frequency a stimulus for stereoscopic slant? Investigative Ophthalmology and Visual Science, 35, (ARVO Abstracts), 1316.

Rogers, B. J., & Graham, M. E. (1982). Similarities between motion parallax and stereopsis in human depth perception. Vision Research, 22, 216-270.

Rovamo, J., Virsu, V., & Nasaren, R. (1978). Cortical magnification factor predicts the photopic contrast sensitivity of peripheral vision. Nature, 271, 54-56.

Shumer, R. A., & Julesz, B. (1984). Binocular disparity modulation sensitivity to disparities offset from the plane of fixation. Vision Research, 24, 533-542.

Stine, W. W., & Filley, E. T. (1998). Modeling the 'Venetian blind' effect. Perception, 27 Supplement, 98.

Thibos, L. N., Still, D. L., & Bradley, A. (1996). Characterization of spatial aliasing and contrast sensitivity in peripheral vision. Vision Research, 36 (2), 249-258.

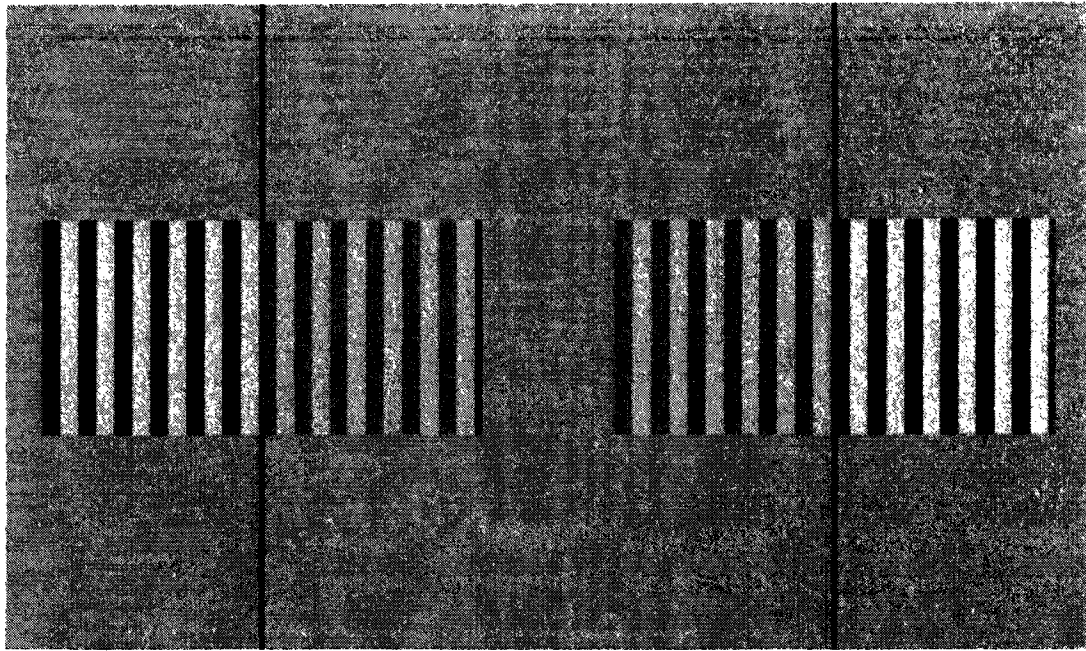
Treutwein, B. (1995). Minireview: Adaptive psychophysical procedures. Vision Research, 35, 2503-2522.

Tyler, C. W., Schor, C. M., and Coletta, N. J. (1992). Spatiotemporal limitations of vernier and stereoscopic alignment acuity. Proceedings of the International Society for Optical Engineering, 1669, 112-121.

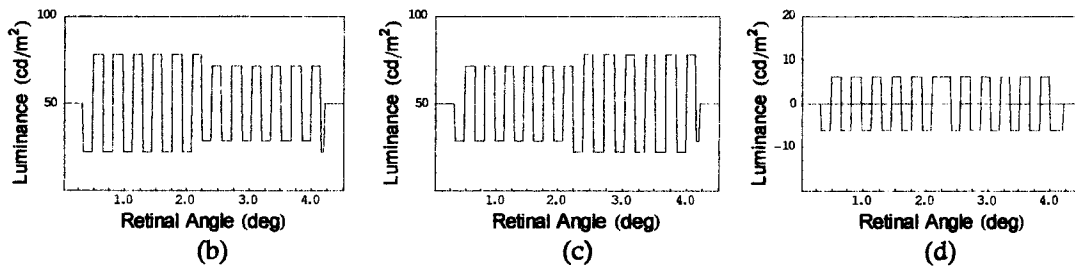
Tyler, C. W., & Sutter, E. E., (1979). Depth from spatial frequency difference: An old kind of stereopsis? Vision Research, 19, 859-865.

APPENDICES

Appendix 1. Exp. 1 Sample Stimuli, Luminance Plots, Fourier's



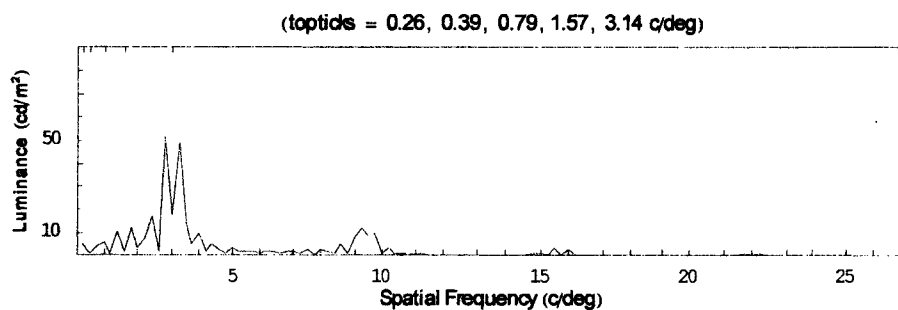
(a)



(b)

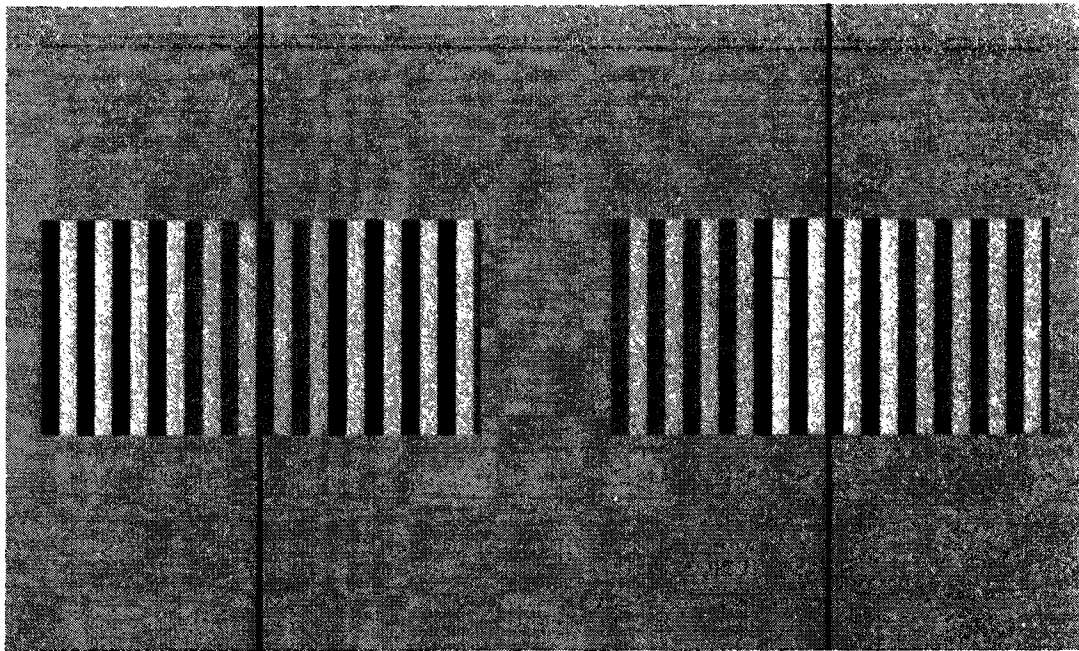
(c)

(d)

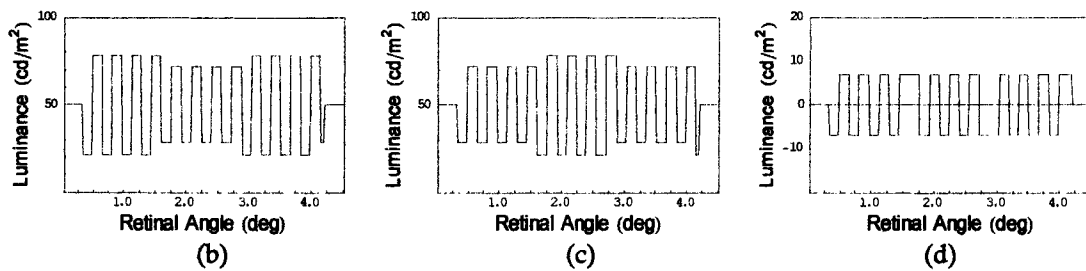


(e)

Figure 29. (a) Experiment 1, condition 1 stereogram layout (square-wave contrast disparity modulation spatial frequency of 0.26 c/deg and square-wave carrier spatial frequency of 3.14 c/deg). To approximate the spatial frequencies from the experiment, view this stereogram from about 85 cm. (b) Luminance plot of left image, (c) Luminance plot of right image, (d) Luminance plot of difference in luminances between left and right image, (e) Fourier plot (adjusted for human contrast sensitivity function, using data for F.W.C. from Blakemore and Campbell, 1969) of difference in luminances between left and right image.



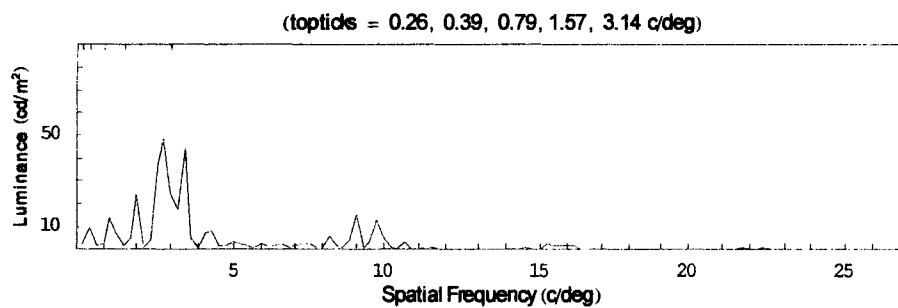
(a)



(b)

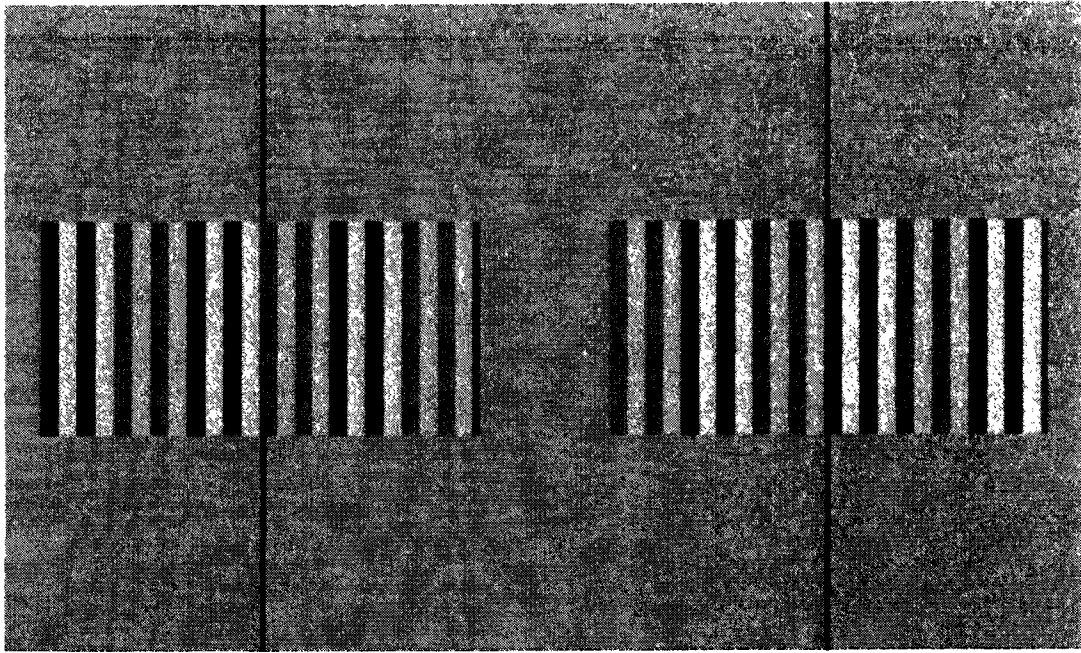
(c)

(d)



(e)

Figure 30. (a) Experiment 1, condition 2 stereogram layout (square-wave contrast disparity modulation spatial frequency of 0.39 c/deg and square-wave carrier spatial frequency of 3.14 c/deg). To approximate the spatial frequencies from the experiment, view this stereogram from about 85 cm. (b) Luminance plot of left image, (c) Luminance plot of right image, (d) Luminance plot of difference in luminances between left and right image, (e) Fourier plot (adjusted for human contrast sensitivity function, using data for F.W.C. from Blakemore and Campbell, 1969) of difference in luminances between left and right image.



(a)

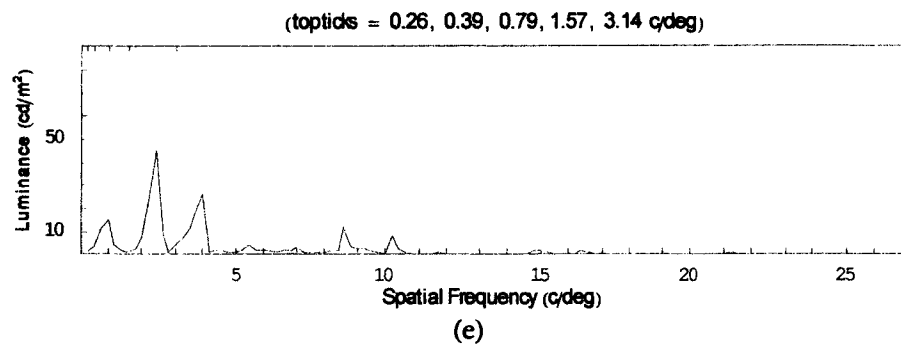
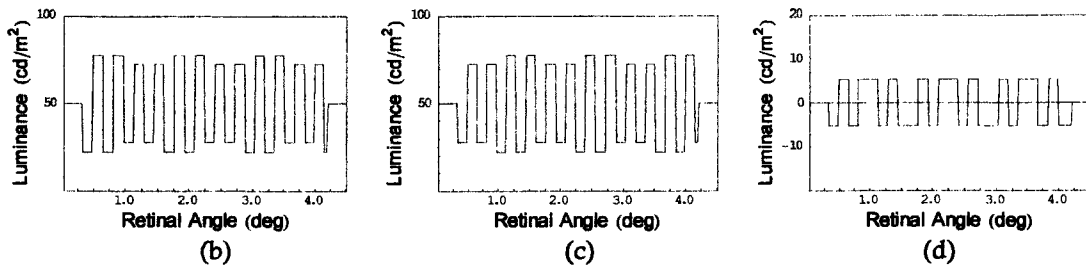
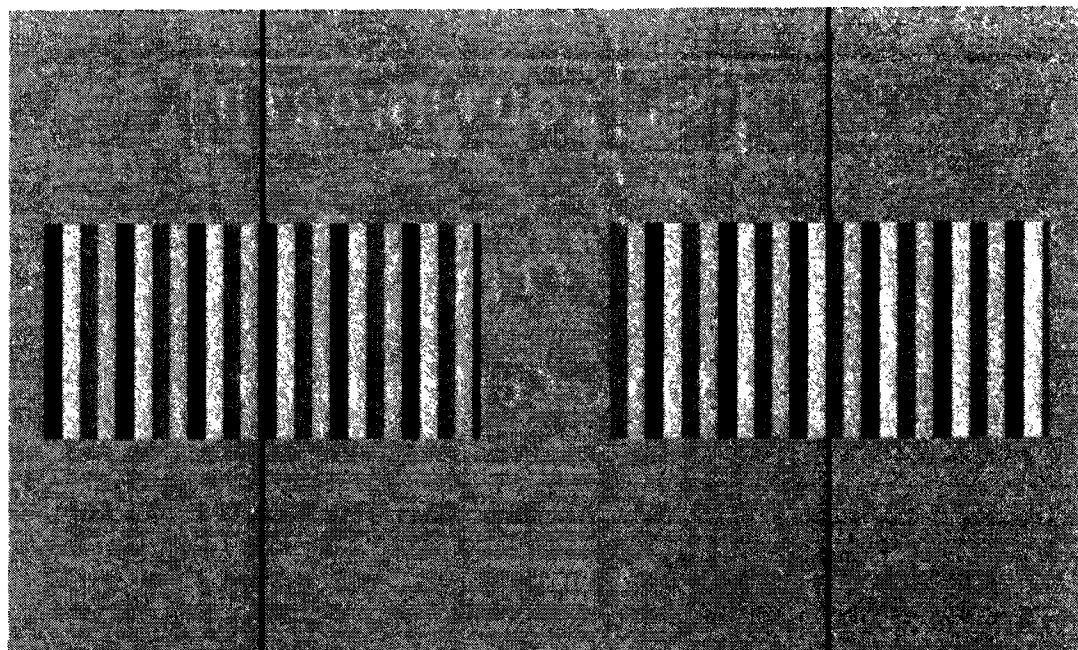
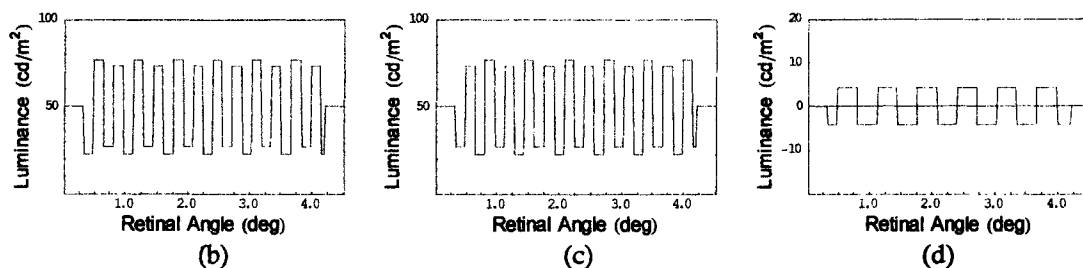


Figure 31. (a) Experiment 1, condition 3 stereogram layout (square-wave contrast disparity modulation spatial frequency of 0.79 c/deg and square-wave carrier spatial frequency of 3.14 c/deg). To approximate the spatial frequencies from the experiment, view this stereogram from about 85 cm. (b) Luminance plot of left image, (c) Luminance plot of right image, (d) Luminance plot of difference in luminances between left and right image, (e) Fourier plot (adjusted for human contrast sensitivity function, using data for F.W.C. from Blakemore and Campbell, 1969) of difference in luminances between left and right image.



(a)

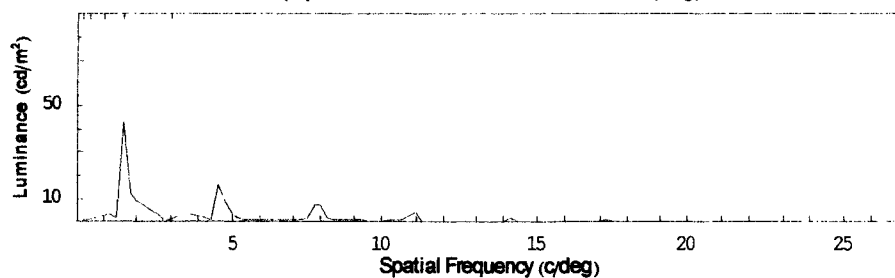


(b)

(c)

(d)

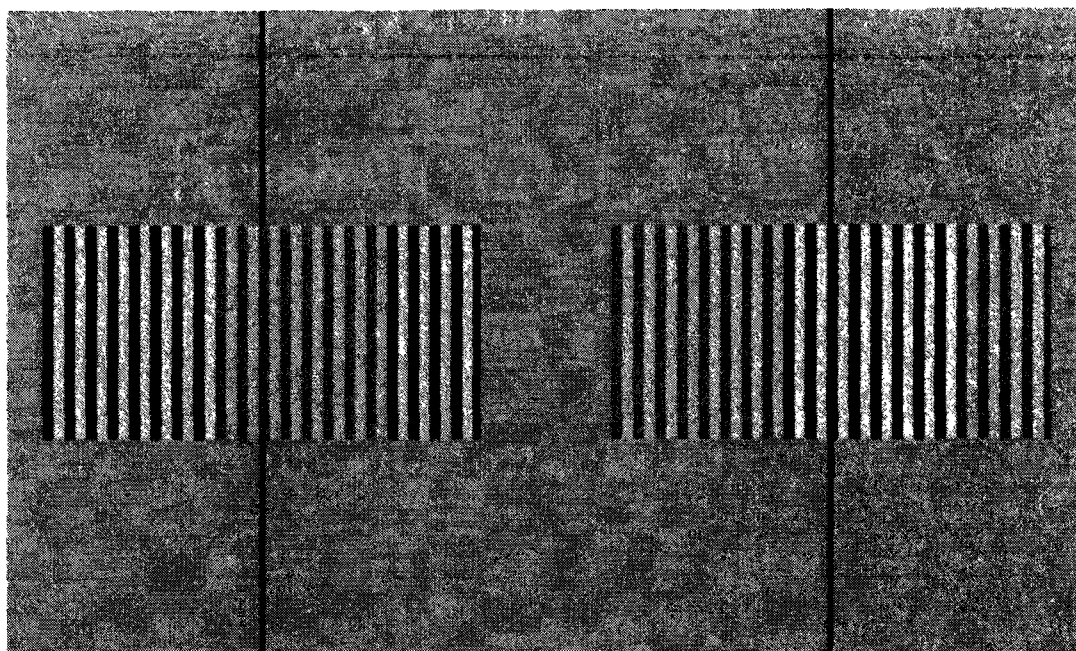
(topticks = 0.26, 0.39, 0.79, 1.57, 3.14 c/deg)



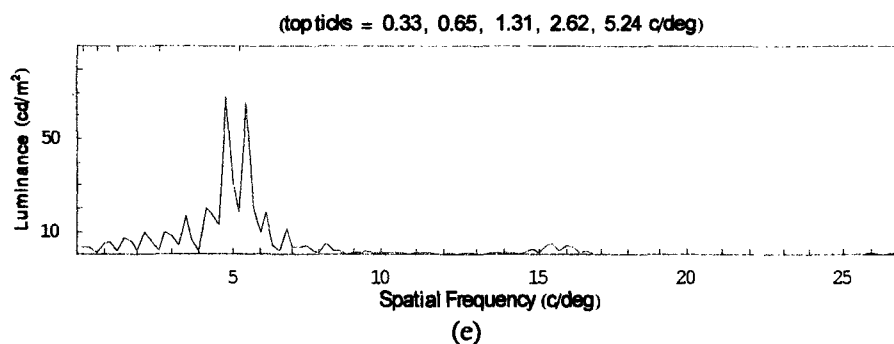
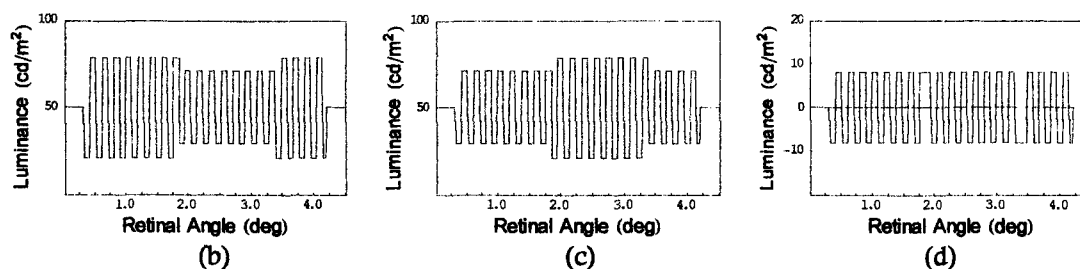
(e)

Figure 32. (a) Experiment 1, condition 4 stereogram layout (square-wave contrast disparity modulation spatial frequency of 1.57 c/deg and square-wave carrier spatial frequency of 3.14 c/deg). To approximate the spatial frequencies from the experiment, view this stereogram from about 85 cm. (b) Luminance plot of left image, (c) Luminance plot of right image, (d) Luminance plot of difference in luminances between left and right image, (e) Fourier plot (adjusted for human contrast sensitivity function, using data for F.W.C. from Blakemore and Campbell, 1969) of difference in luminances between left and right image.

Appendix 2. Exp. 2 Sample Stimuli, Luminance Plots, Fourier's

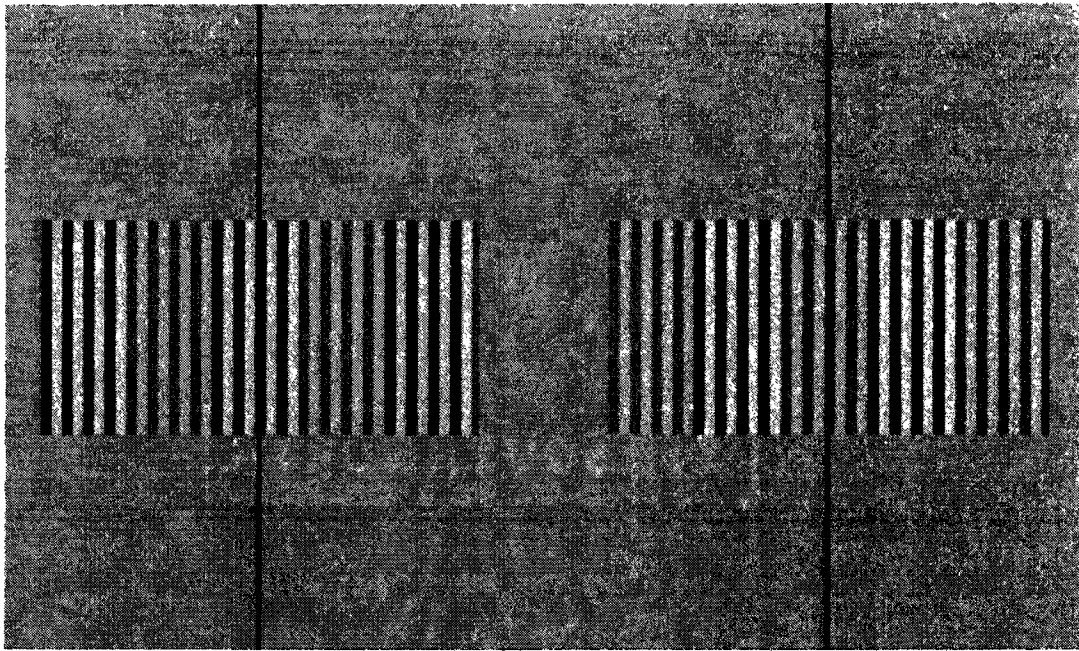


(a)



(e)

Figure 33. (a) Experiment 2, condition 1 stereogram layout (square-wave contrast disparity modulation spatial frequency of 0.33 c/deg and square-wave carrier spatial frequency of 5.24 c/deg). To approximate the spatial frequencies from the experiment, view this stereogram from about 85 cm. (b) Luminance plot of left image, (c) Luminance plot of right image, (d) Luminance plot of difference in luminances between left and right image, (e) Fourier plot (adjusted for human contrast sensitivity function, using data for F.W.C. from Blakemore and Campbell, 1969) of difference in luminances between left and right image.



(a)

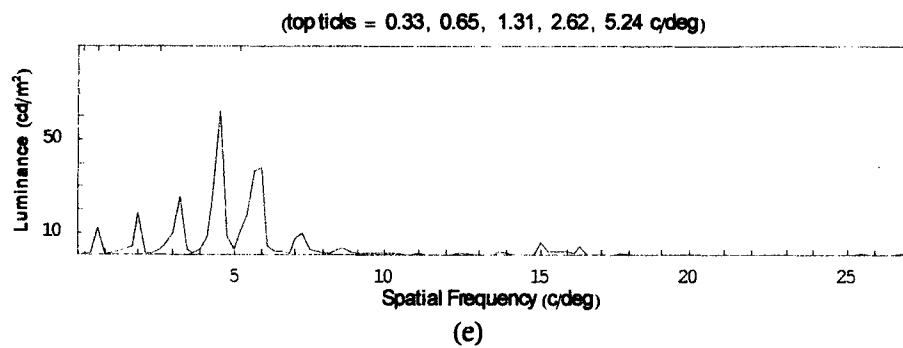
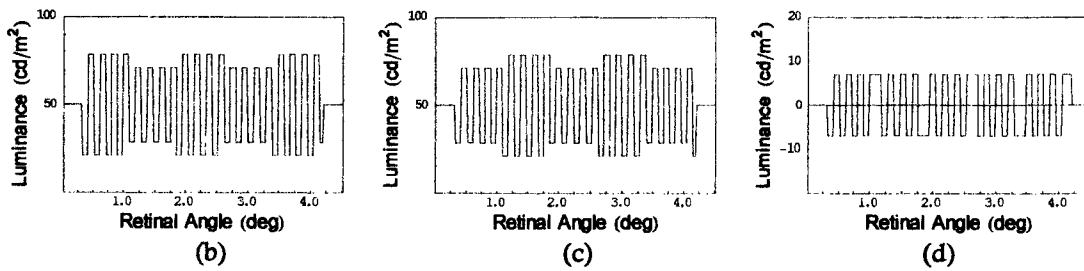
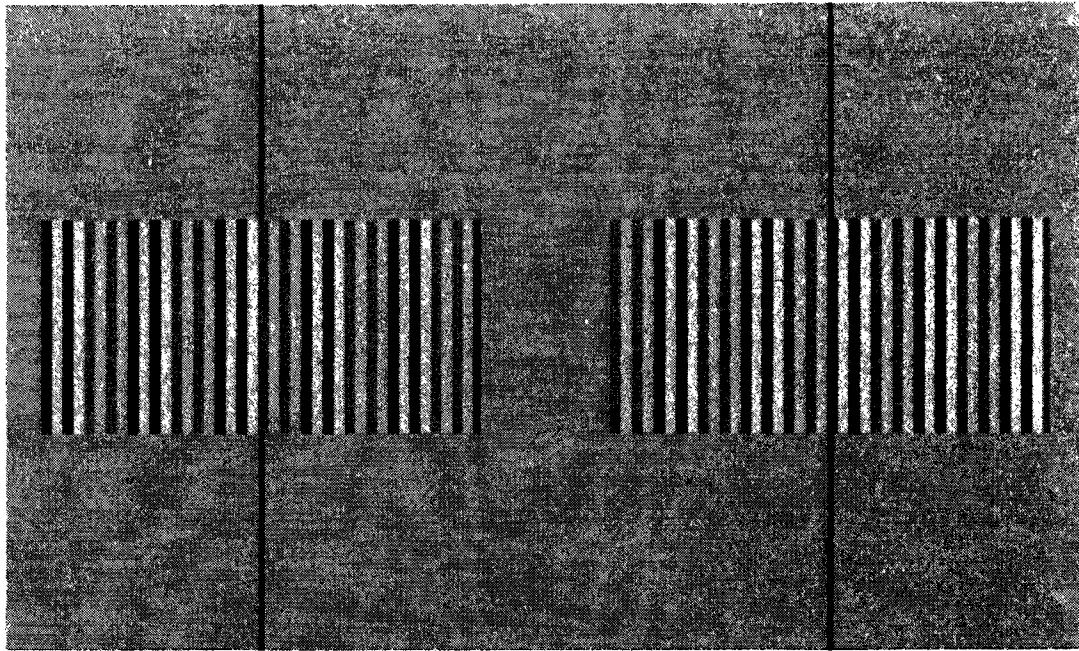
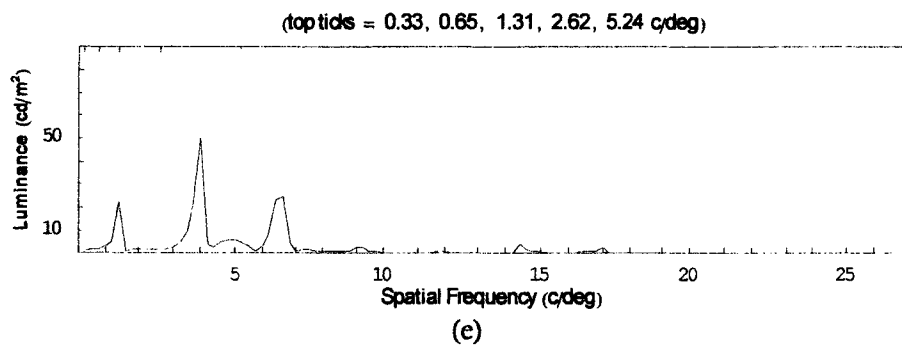
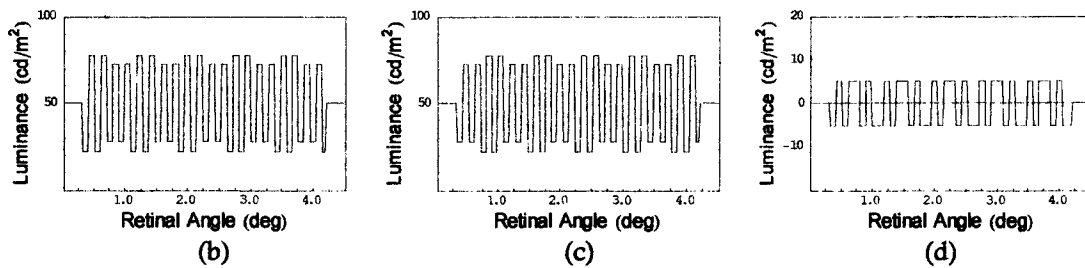


Figure 34. (a) Experiment 2, condition 2 stereogram layout (square-wave contrast disparity modulation spatial frequency of 0.65 c/deg and square-wave carrier spatial frequency of 5.24 c/deg). To approximate the spatial frequencies from the experiment, view this stereogram from about 85 cm. (b) Luminance plot of left image, (c) Luminance plot of right image, (d) Luminance plot of difference in luminances between left and right image, (e) Fourier plot (adjusted for human contrast sensitivity function, using data for F.W.C. from Blakemore and Campbell, 1969) of difference in luminances between left and right image.

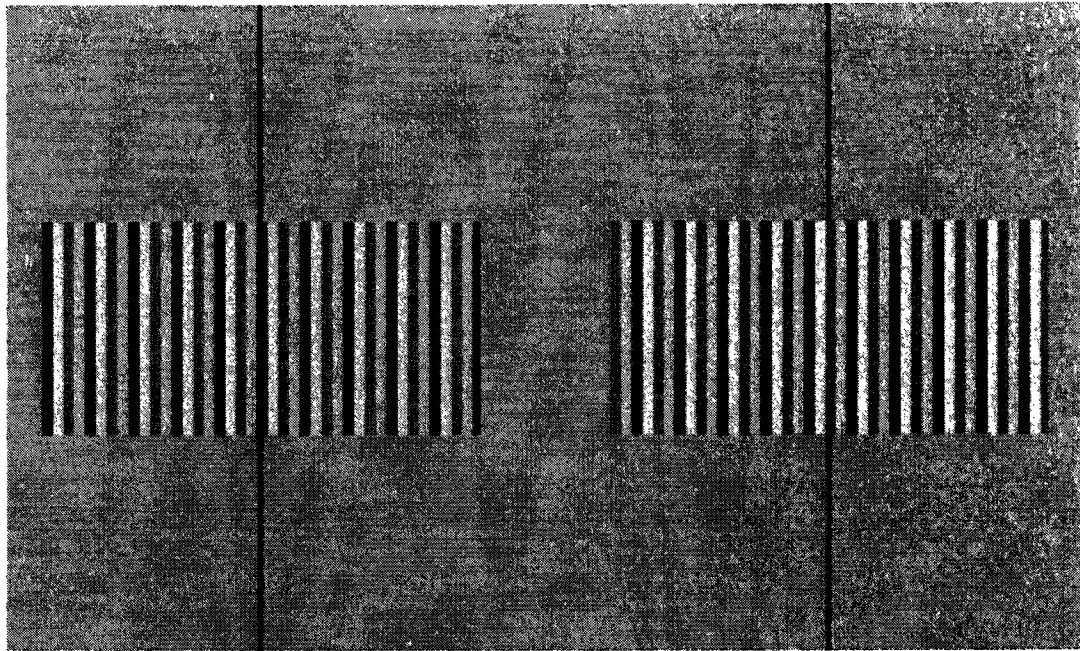


(a)



(e)

Figure 35. (a) Experiment 2, condition 3 stereogram layout (square-wave contrast disparity modulation spatial frequency of 1.31 c/deg and square-wave carrier spatial frequency of 5.24 c/deg). To approximate the spatial frequencies from the experiment, view this stereogram from about 85 cm. (b) Luminance plot of left image, (c) Luminance plot of right image, (d) Luminance plot of difference in luminances between left and right image, (e) Fourier plot (adjusted for human contrast sensitivity function, using data for F.W.C. from Blakemore and Campbell, 1969) of difference in luminances between left and right image.



(a)

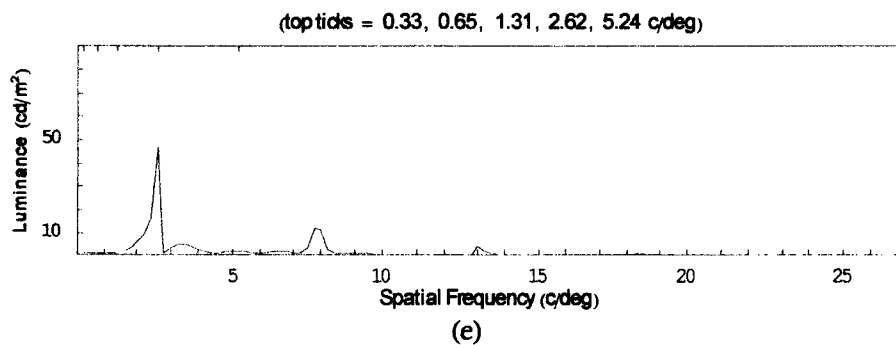
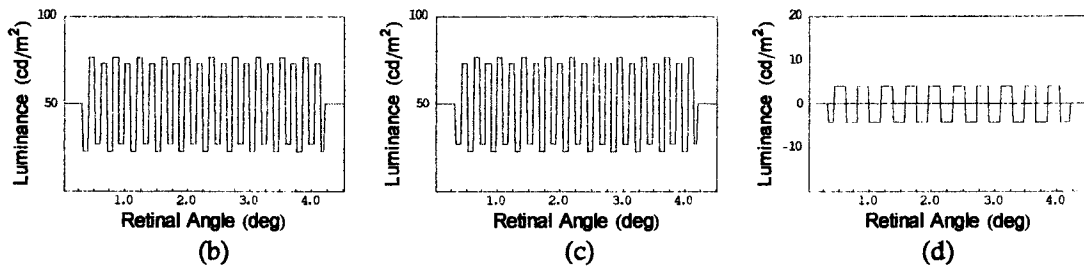
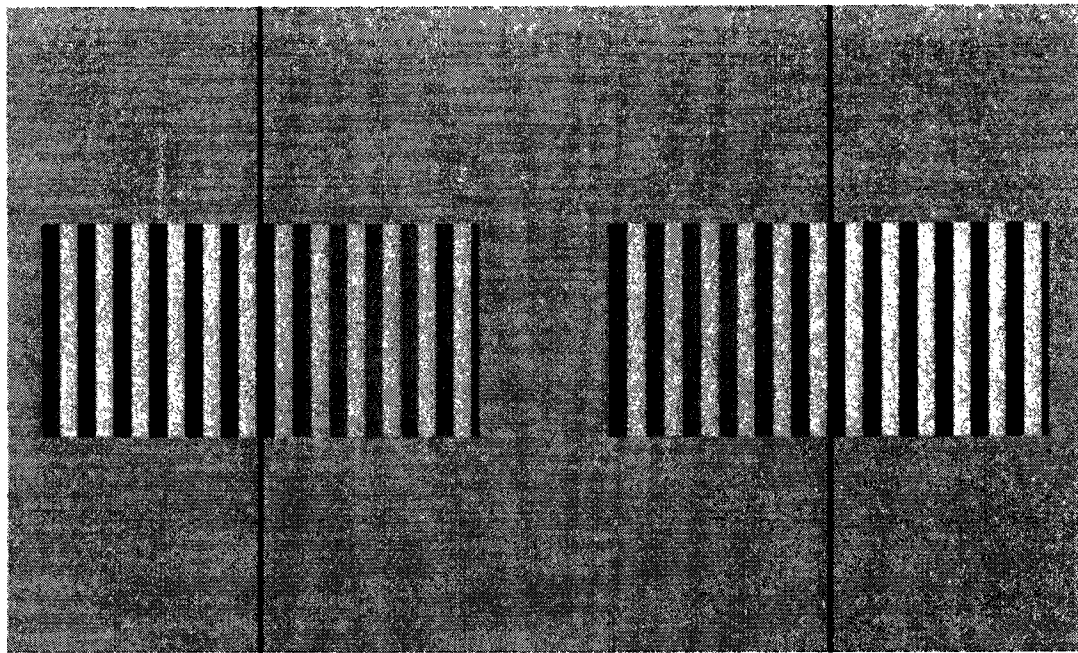
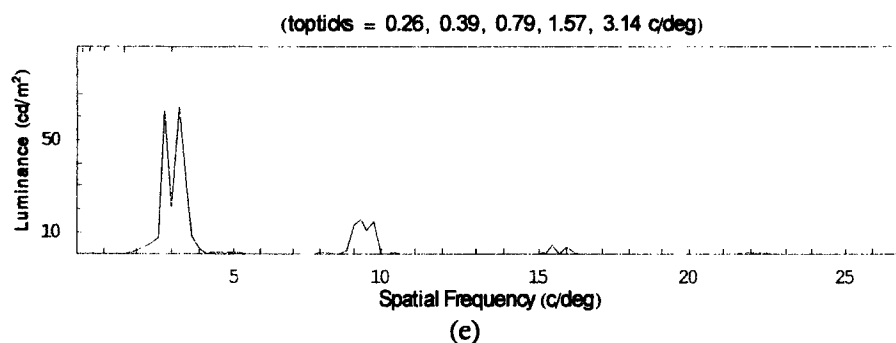
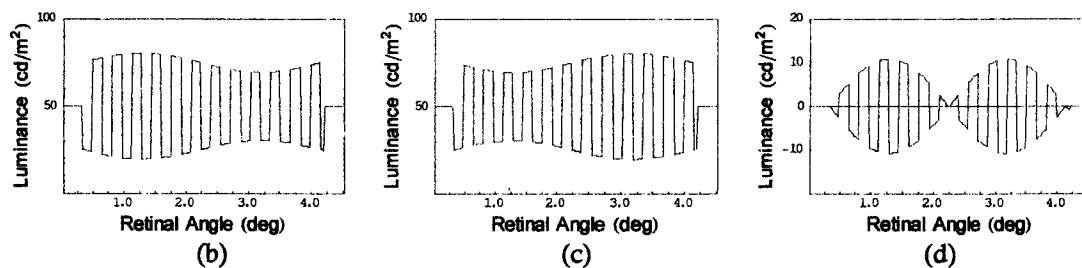


Figure 36. (a) Experiment 2, condition 4 stereogram layout (square-wave contrast disparity modulation spatial frequency of 2.62 c/deg and square-wave carrier spatial frequency of 5.24 c/deg). To approximate the spatial frequencies from the experiment, view this stereogram from about 85 cm. (b) Luminance plot of left image, (c) Luminance plot of right image, (d) Luminance plot of difference in luminances between left and right image, (e) Fourier plot (adjusted for human contrast sensitivity function, using data for F.W.C. from Blakemore and Campbell, 1969) of difference in luminances between left and right image.

Appendix 3. Exp. 3 Sample Stimuli, Luminance Plots, Fourier

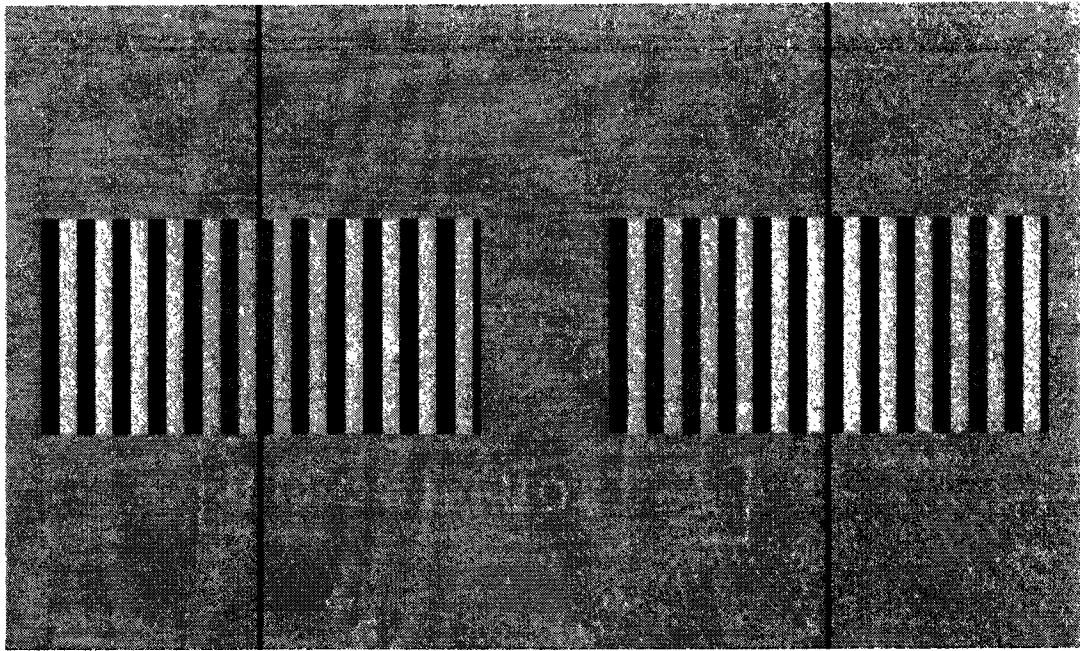


(a)

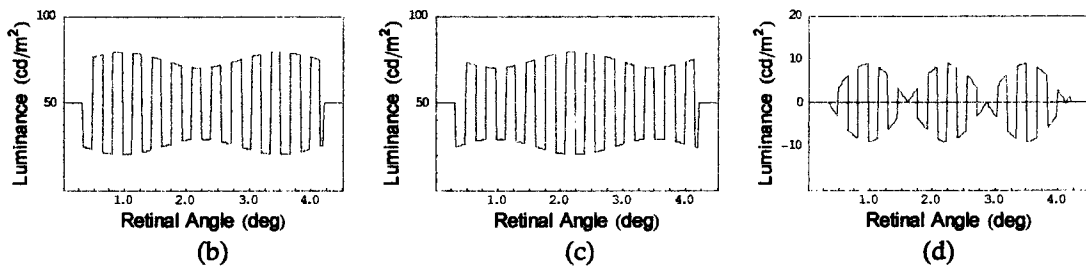


(e)

Figure 37. (a) Experiment 3, condition 1 stereogram layout (sine-wave contrast disparity modulation spatial frequency of 0.26 c/deg and square-wave carrier spatial frequency of 3.14 c/deg). To approximate the spatial frequencies from the experiment, view this stereogram from about 85 cm. (b) Luminance plot of left image, (c) Luminance plot of right image, (d) Luminance plot of difference in luminances between left and right image, (e) Fourier plot (adjusted for human contrast sensitivity function, using data for F.W.C. from Blakemore and Campbell, 1969) of difference in luminances between left and right image.



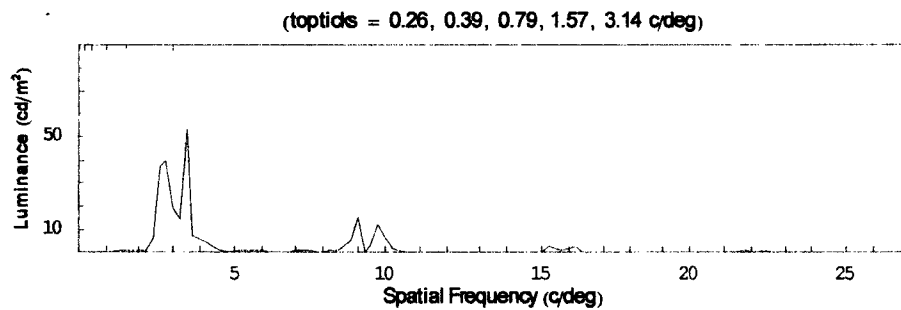
(a)



(b)

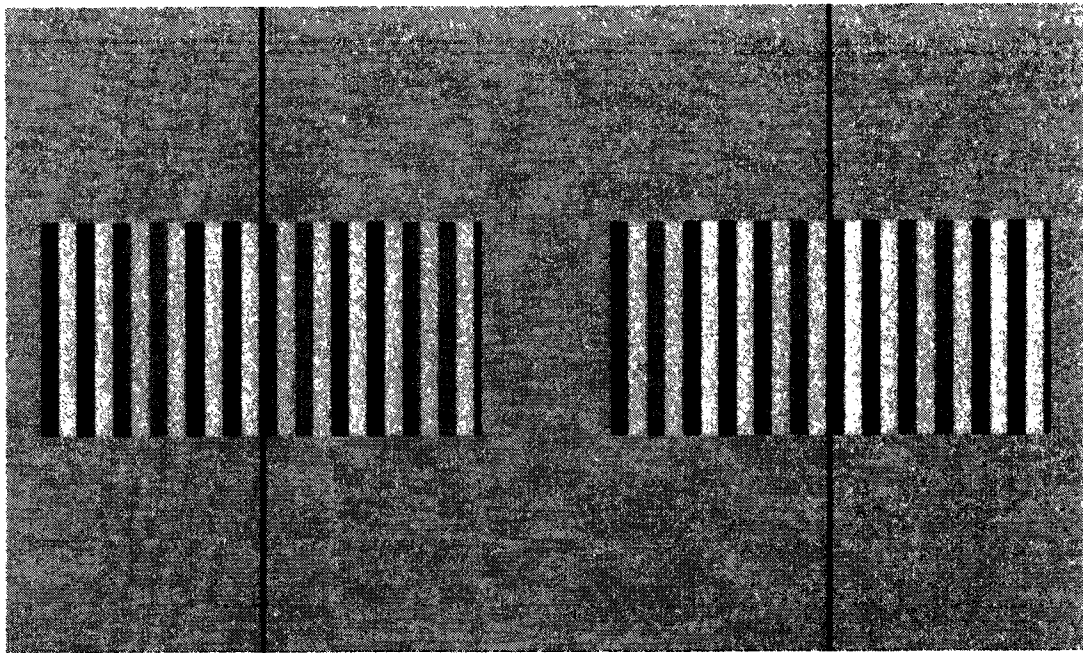
(c)

(d)

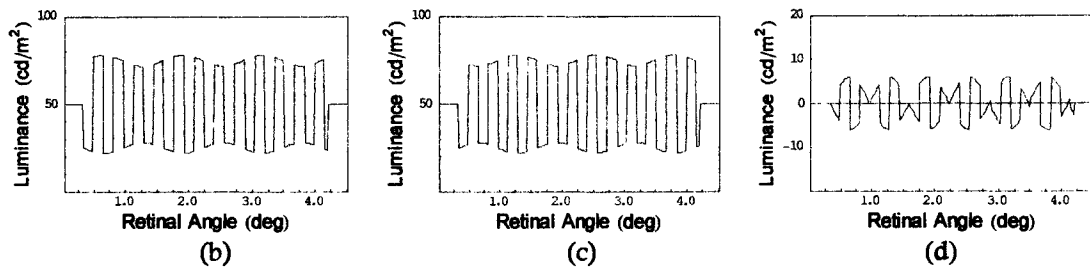


(e)

Figure 38. (a) Experiment 3, condition 2 stereogram layout (sine-wave contrast disparity modulation spatial frequency of 0.39 c/deg and square-wave carrier spatial frequency of 3.14 c/deg). To approximate the spatial frequencies from the experiment, view this stereogram from about 85 cm. (b) Luminance plot of left image, (c) Luminance plot of right image, (d) Luminance plot of difference in luminances between left and right image, (e) Fourier plot (adjusted for human contrast sensitivity function, using data for F.W.C. from Blakemore and Campbell, 1969) of difference in luminances between left and right image.



(a)

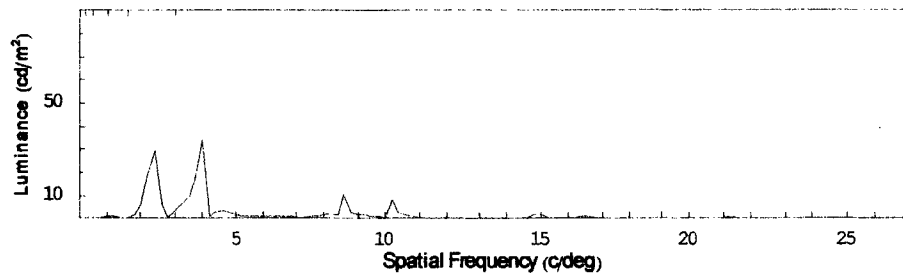


(b)

(c)

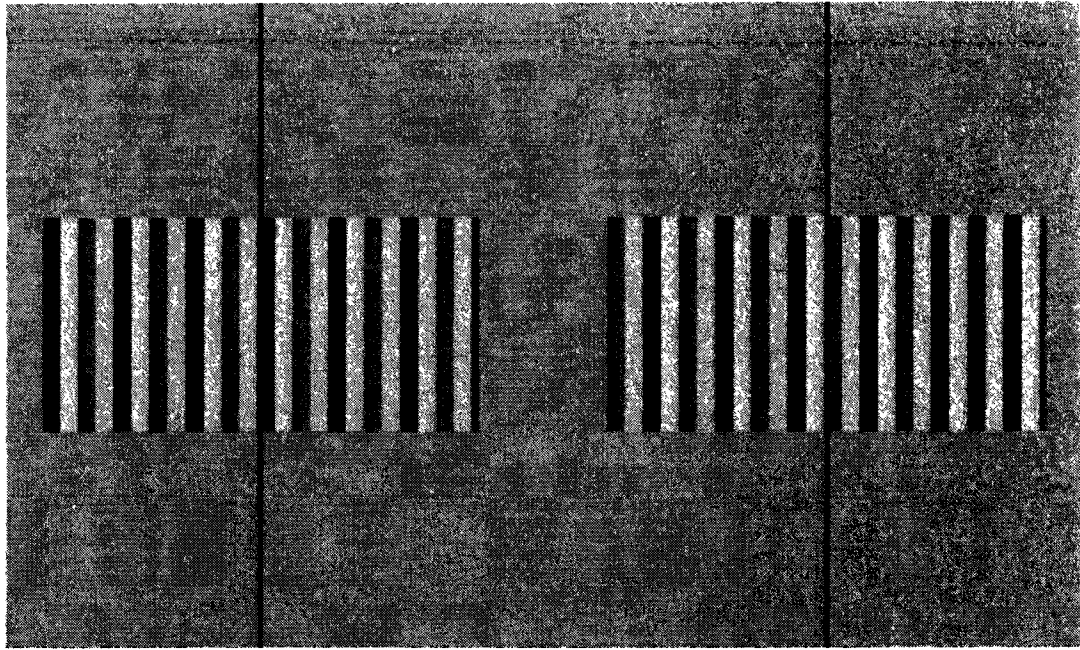
(d)

(topicks = 0.26, 0.39, 0.79, 1.57, 3.14 c/deg)

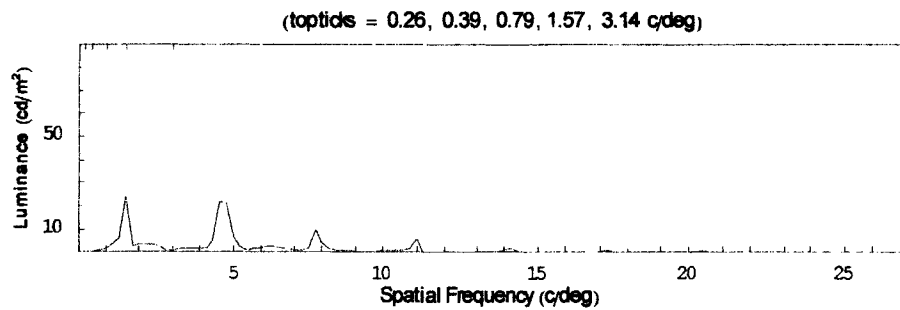
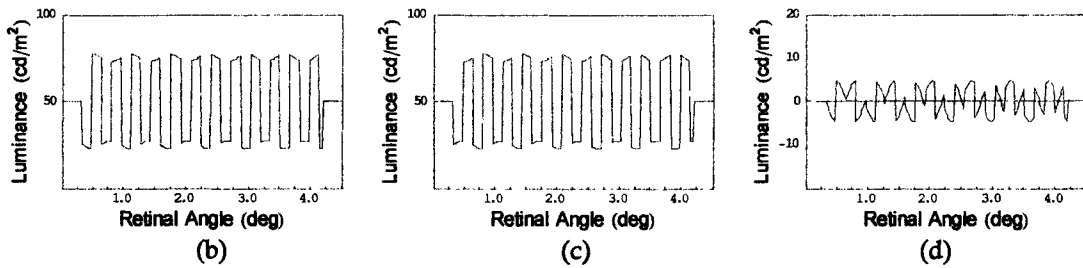


(e)

Figure 39. (a) Experiment 3, condition 3 stereogram layout (sine-wave contrast disparity modulation spatial frequency of 0.79 c/deg and square-wave carrier spatial frequency of 3.14 c/deg). To approximate the spatial frequencies from the experiment, view this stereogram from about 85 cm. (b) Luminance plot of left image, (c) Luminance plot of right image, (d) Luminance plot of difference in luminances between left and right image, (e) Fourier plot (adjusted for human contrast sensitivity function, using data for F.W.C. from Blakemore and Campbell, 1969) of difference in luminances between left and right image.



(a)



(e)

Figure 40. (a) Experiment 3, condition 4 stereogram layout (sine-wave contrast disparity modulation spatial frequency of 1.57 c/deg and square-wave carrier spatial frequency of 3.14 c/deg). To approximate the spatial frequencies from the experiment, view this stereogram from about 85 cm. (b) Luminance plot of left image, (c) Luminance plot of right image, (d) Luminance plot of difference in luminances between left and right image, (e) Fourier plot (adjusted for human contrast sensitivity function, using data for F.W.C. from Blakemore and Campbell, 1969) of difference in luminances between left and right image.

Appendix 4. Exp. 1 Fourier Plots at Threshold

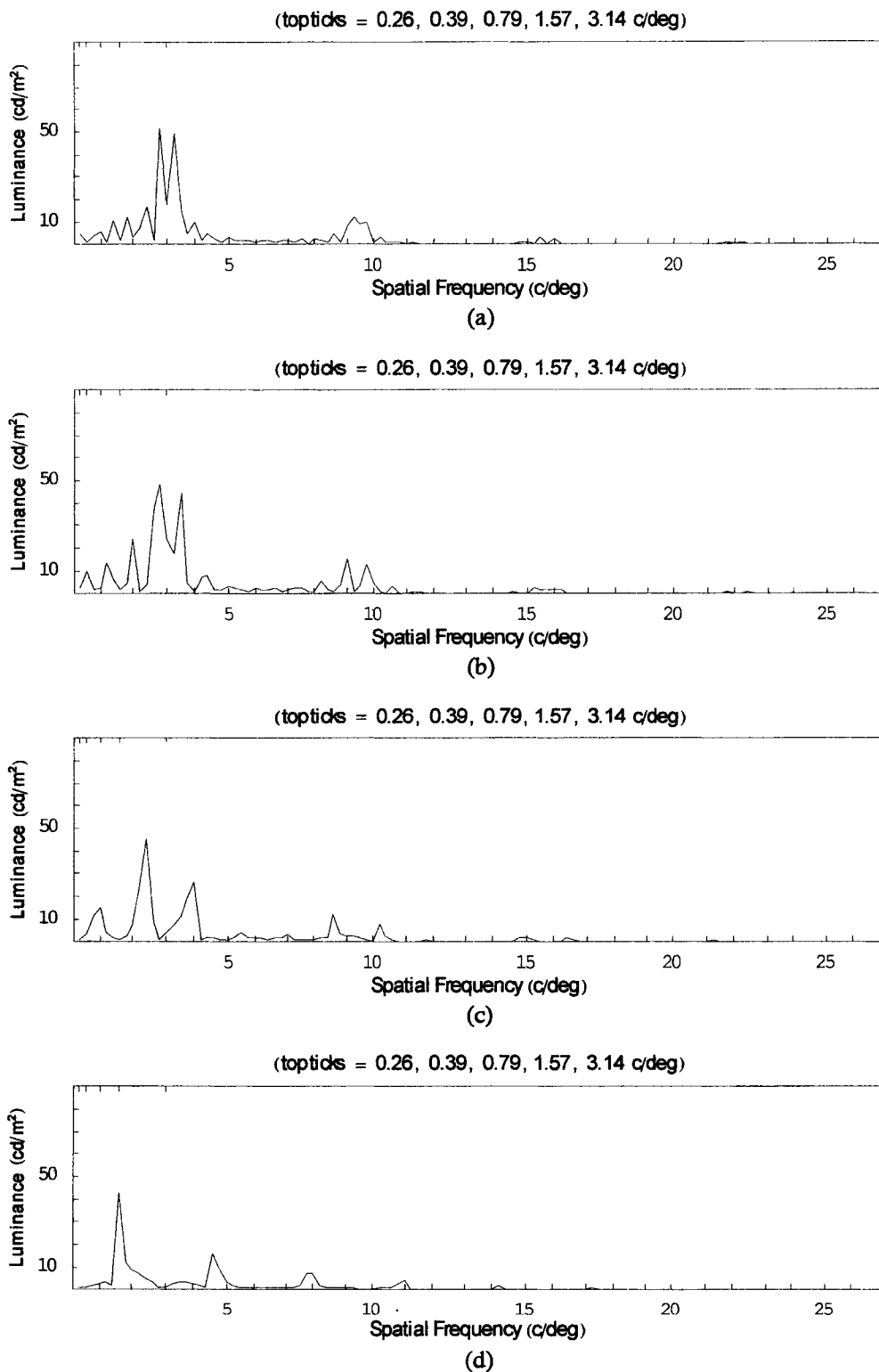


Figure 41. ETF, Experiment 1 (adjusted for human CSF, using data for F.W.C. from Blakemore and Campbell, 1969). Fourier plots of the difference in luminance between the image to one eye and the image to the other eye in a stereo pair for mean threshold stimulus. (a)–(d) represent conditions 1–4 (square-wave modulation spatial frequencies = 0.26 c/deg, 0.39 c/deg, 0.79 c/deg, 1.57 c/deg, respectively).

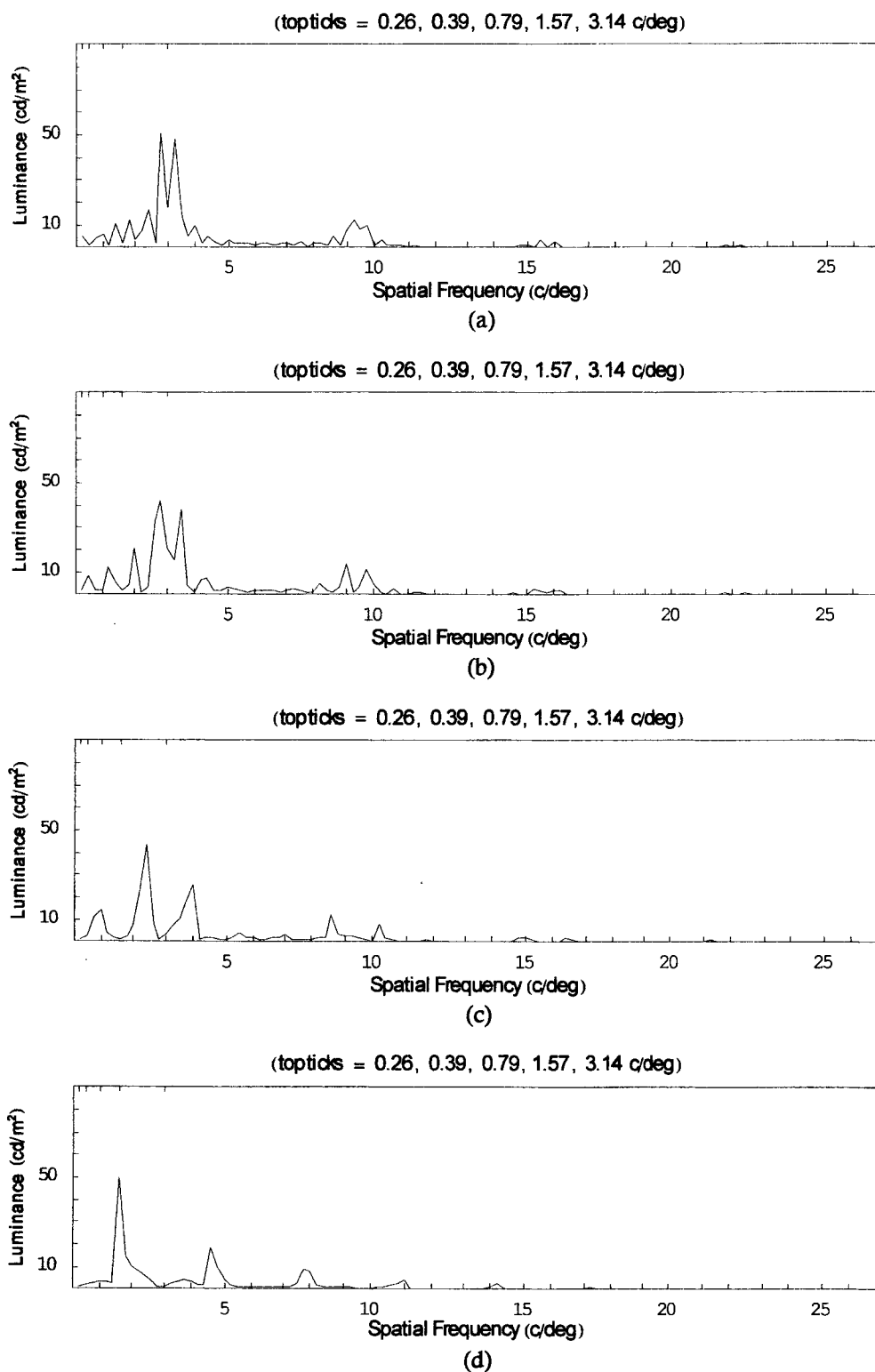


Figure 42. JMS, Experiment 1 (adjusted for human CSF, using data for F.W.C. from Blakemore and Campbell, 1969). Fourier plots of the difference in luminance between the image to one eye and the image to the other eye in a stereo pair for mean threshold stimulus. (a)–(d) represent conditions 1–4 (square-wave modulation spatial frequencies = 0.26 c/deg, 0.39 c/deg, 0.79 c/deg, 1.57 c/deg, respectively).

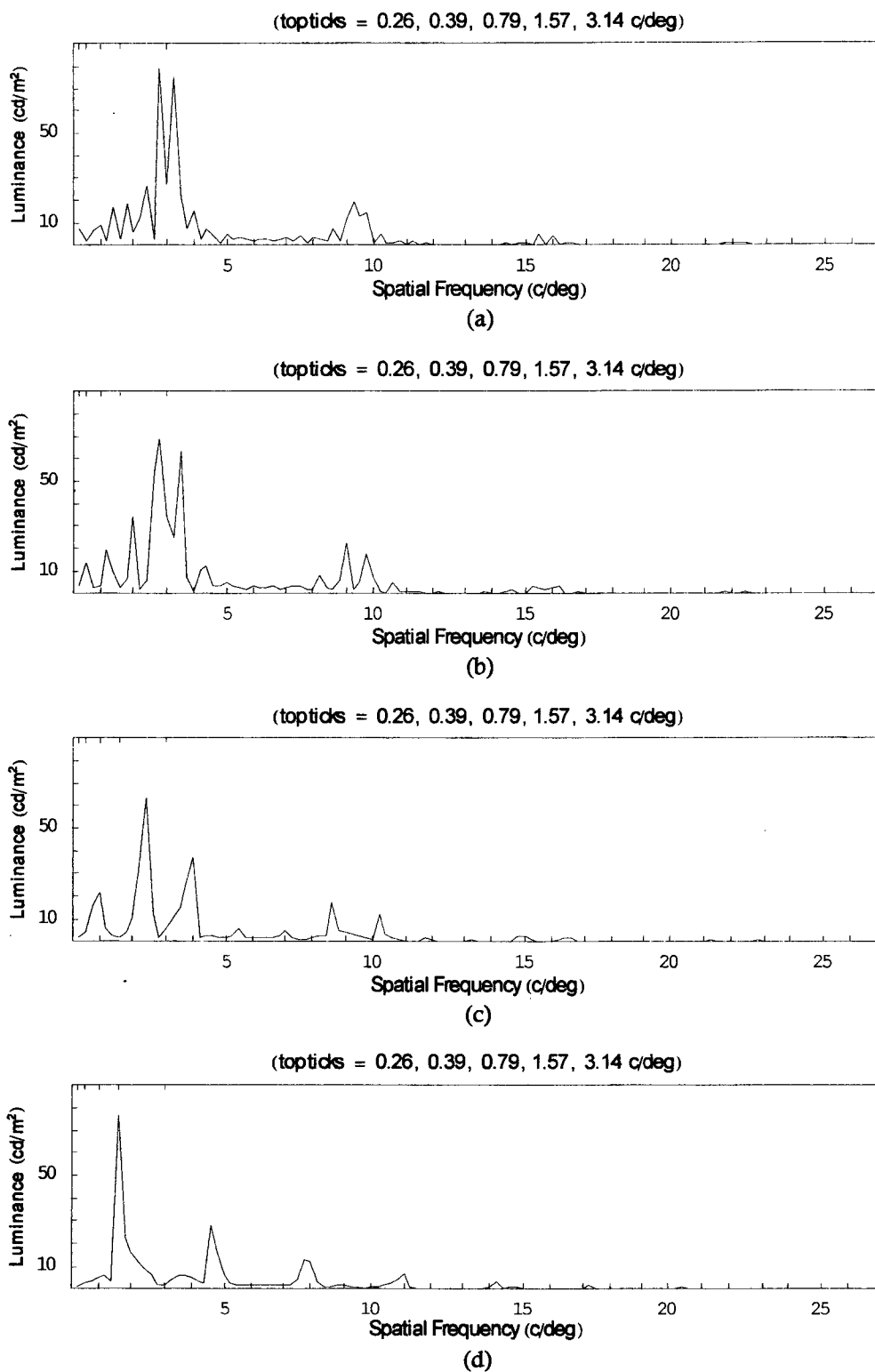


Figure 43. WWS, Experiment 1 (adjusted for human CSF, using data for F.W.C. from Blakemore and Campbell, 1969). Fourier plots of the difference in luminance between the image to one eye and the image to the other eye in a stereo pair for mean threshold stimulus. (a)–(d) represent conditions 1–4 (square-wave modulation spatial frequencies = 0.26 c/deg, 0.39 c/deg, 0.79 c/deg, 1.57 c/deg, respectively).

Appendix 5. Exp. 2 Fourier Plots at Threshold

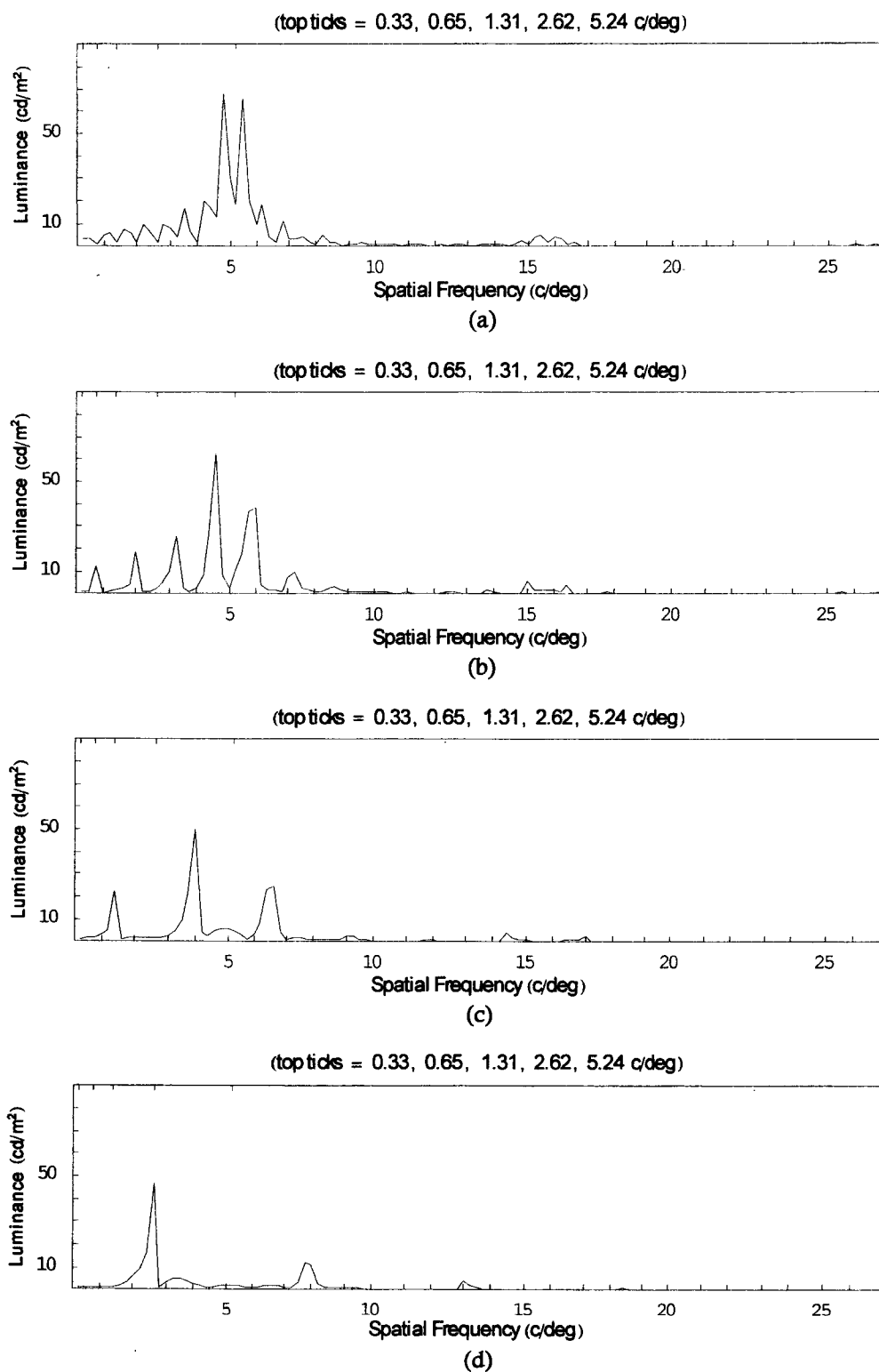


Figure 44. ETF, Experiment 2 (adjusted for human CSF, using data for F.W.C. from Blakemore and Campbell, 1969). Fourier plots of the difference in luminance between the image to one eye and the image to the other eye in a stereo pair for mean threshold stimulus. (a)–(d) represent conditions 1–4 (square-wave modulation spatial frequencies = 0.33 c/deg, 0.65 c/deg, 1.31 c/deg, 2.62 c/deg, respectively).

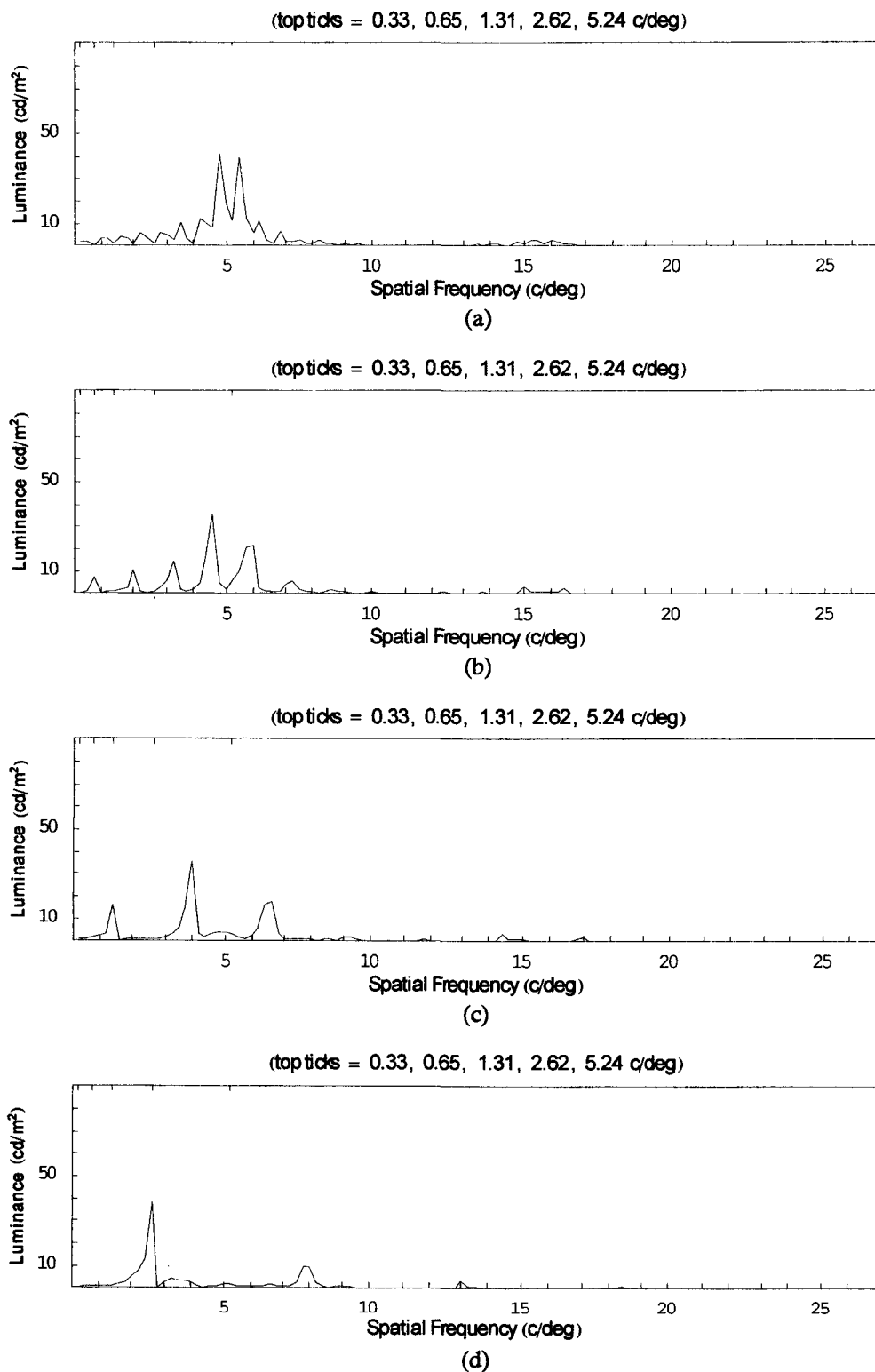


Figure 45. JMS, Experiment 2 (adjusted for human CSF, using data for F.W.C. from Blakemore and Campbell, 1969). Fourier plots of the difference in luminance between the image to one eye and the image to the other eye in a stereo pair for mean threshold stimulus. (a)–(d) represent conditions 1–4 (square-wave modulation spatial frequencies = 0.33 c/deg, 0.65 c/deg, 1.31 c/deg, 2.62 c/deg, respectively).

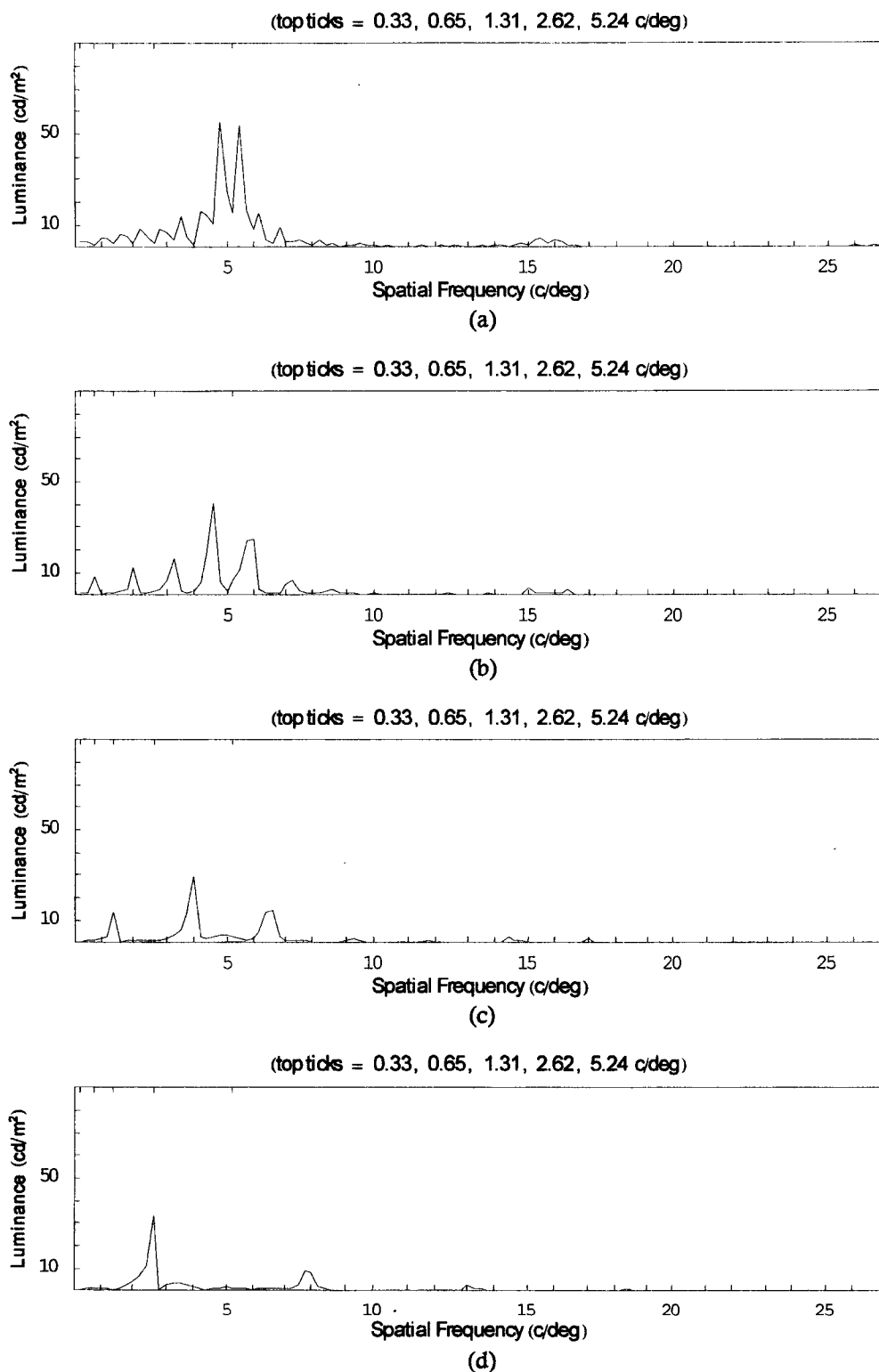


Figure 46. WWS, Experiment 2 (adjusted for human CSF, using data for F.W.C. from Blakemore and Campbell, 1969). Fourier plots of the difference in luminance between the image to one eye and the image to the other eye in a stereo pair for mean threshold stimulus. (a)–(d) represent conditions 1–4 (square-wave modulation spatial frequencies = 0.33 c/deg, 0.65 c/deg, 1.31 c/deg, 2.62 c/deg, respectively).

Appendix 6. Exp. 3 Fourier Plots at Threshold

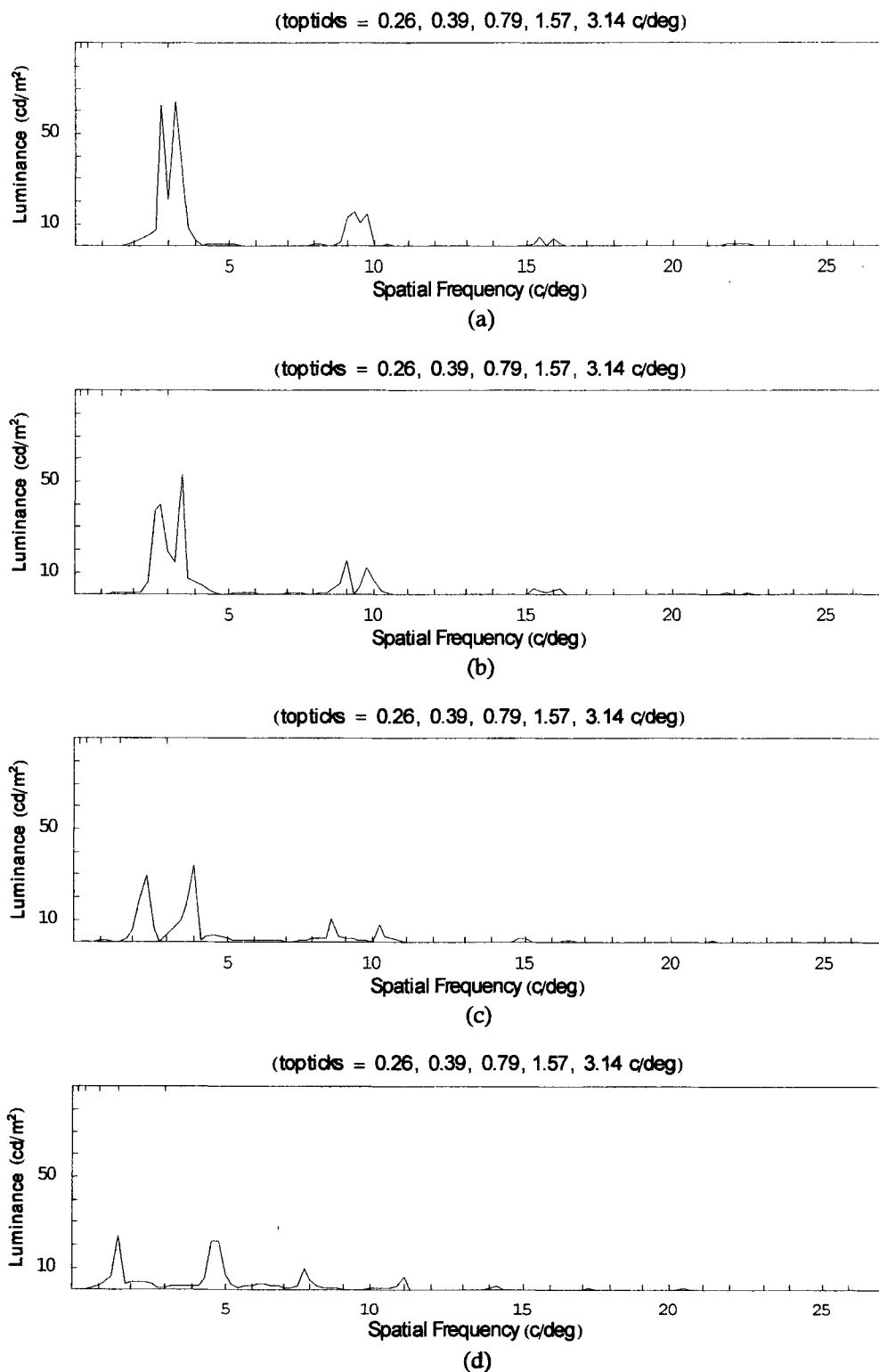


Figure 47. ETF, Experiment 3 (adjusted for human CSF, using data for F.W.C. from Blakemore and Campbell, 1969). Fourier plots of the difference in luminance between the image to one eye and the image to the other eye in a stereo pair for mean threshold stimulus. (a)–(d) represent conditions 1–4 (sine-wave modulation spatial frequencies = 0.26 c/deg, 0.39 c/deg, 0.79 c/deg, 1.57 c/deg, respectively).

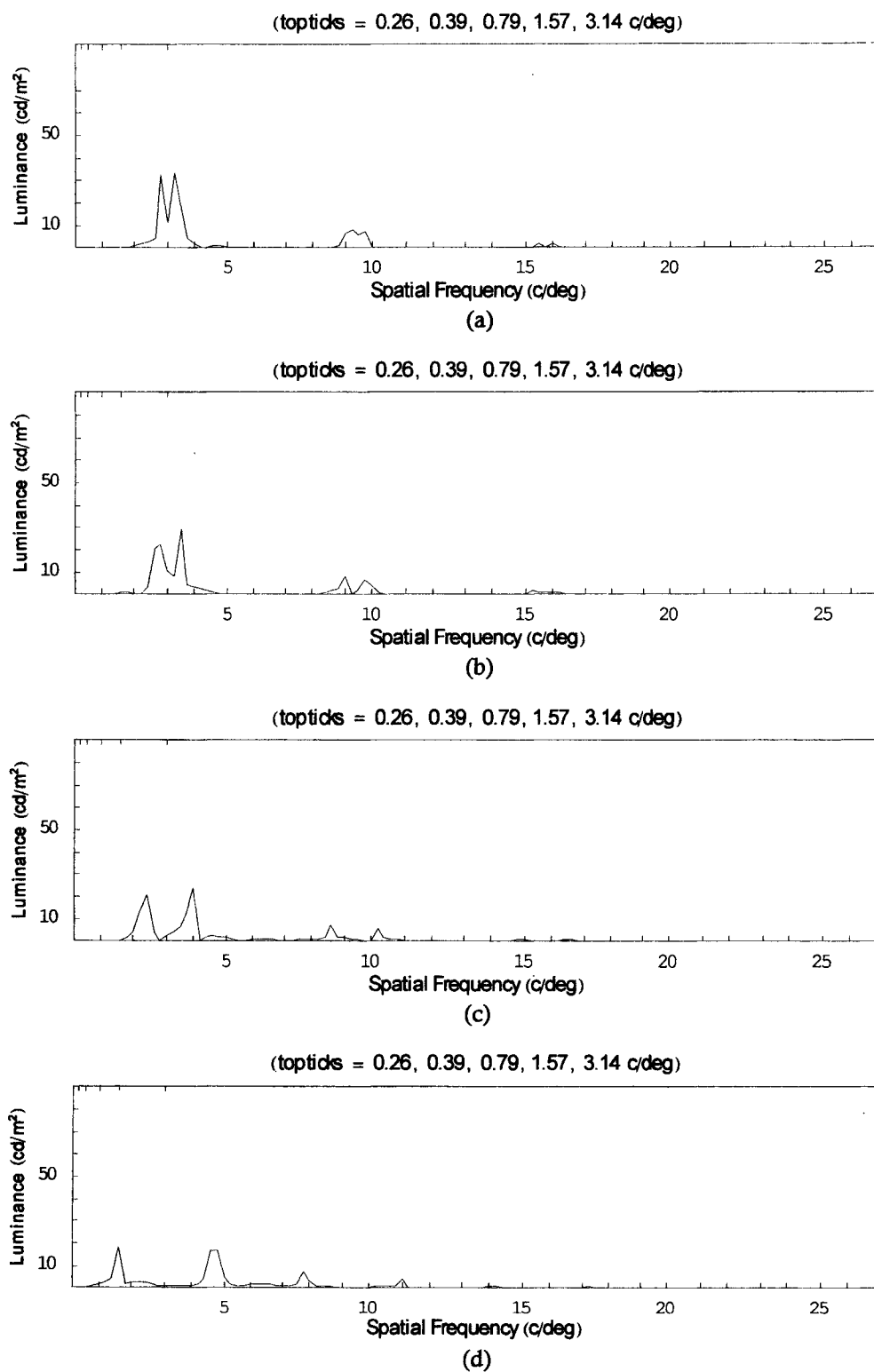


Figure 48. JMS, Experiment 3 (adjusted for human CSF, using data for F.W.C. from Blakemore and Campbell, 1969). Fourier plots of the difference in luminance between the image to one eye and the image to the other eye in a stereo pair for mean threshold stimulus. (a)–(d) represent conditions 1–4 (sine-wave modulation spatial frequencies = 0.26 c/deg, 0.39 c/deg, 0.79 c/deg, 1.57 c/deg, respectively).

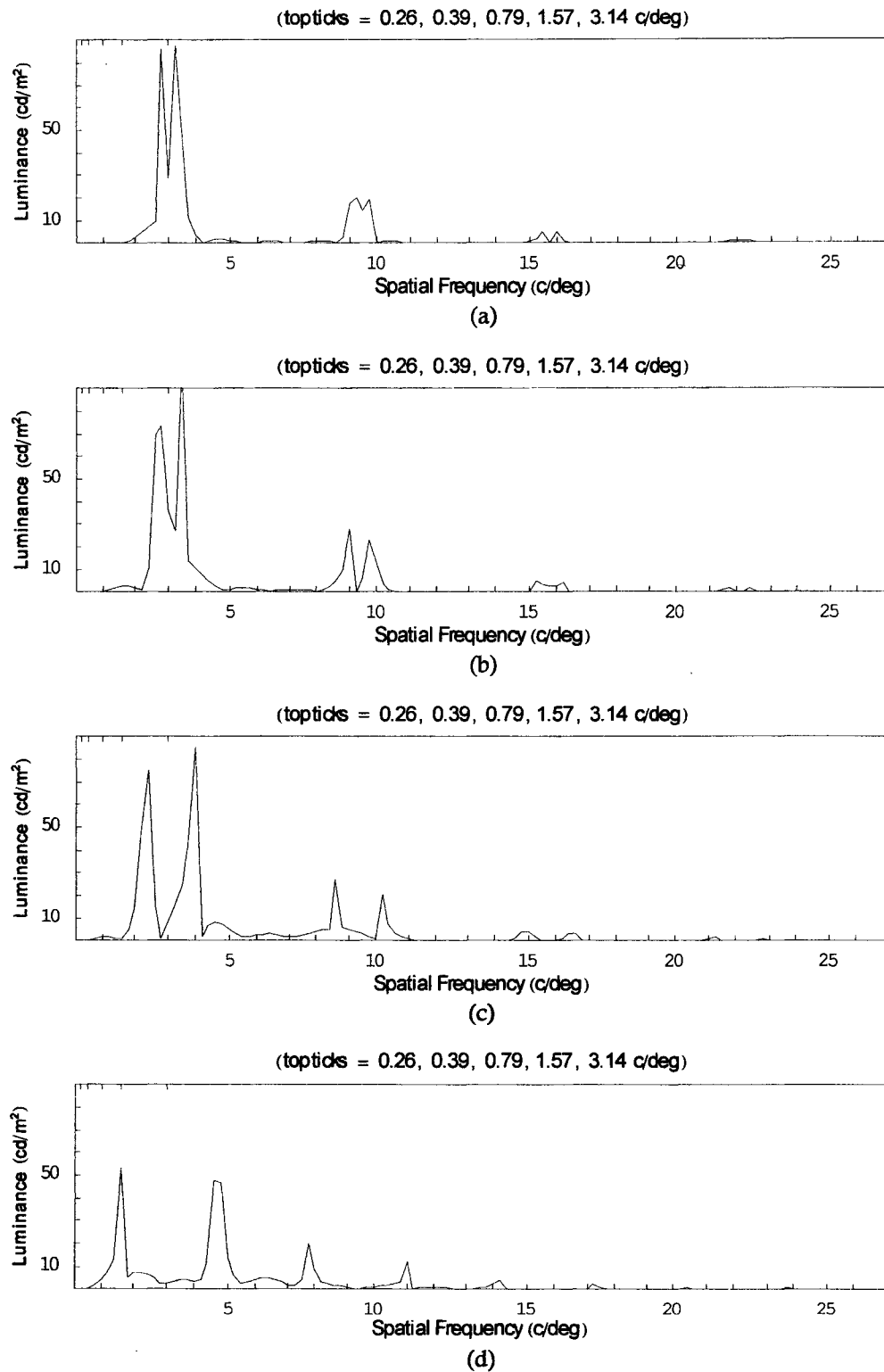
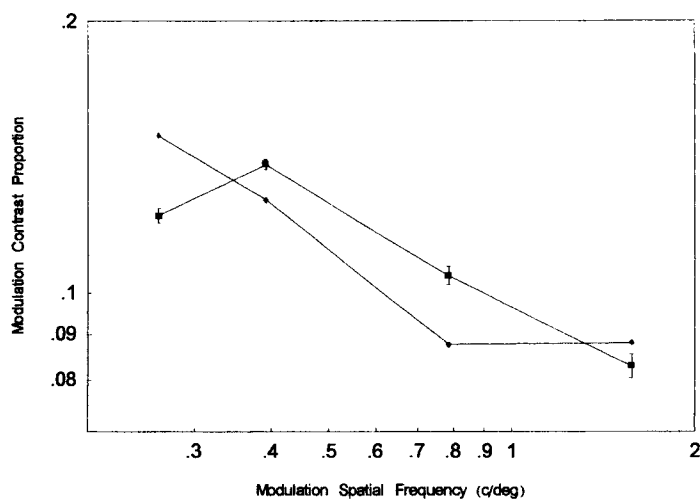
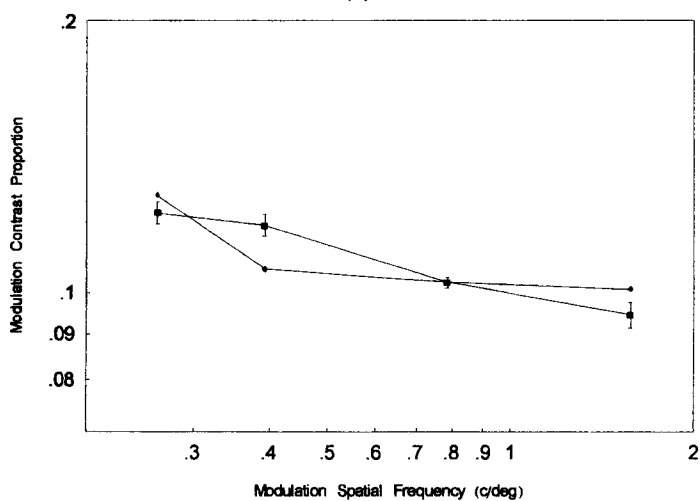


Figure 49. WWS, Experiment 3 (adjusted for human CSF, using data for F.W.C. from Blakemore and Campbell, 1969). Fourier plots of the difference in luminance between the image to one eye and the image to the other eye in a stereo pair for mean threshold stimulus. (a)–(d) represent conditions 1–4 (sine-wave modulation spatial frequencies = 0.26 c/deg, 0.39 c/deg, 0.79 c/deg, 1.57 c/deg, respectively).

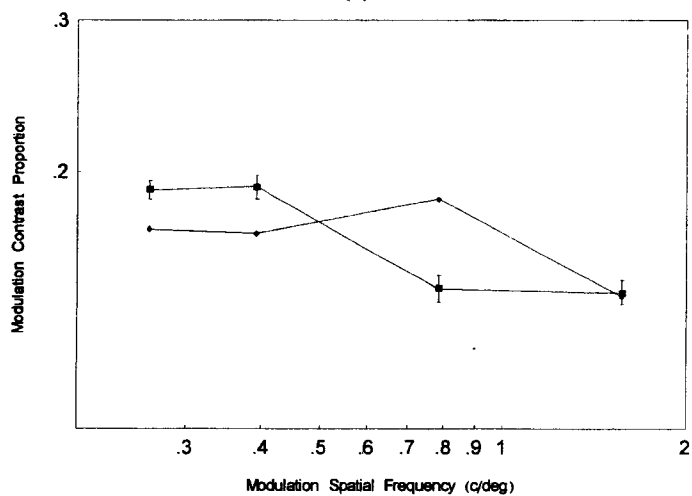
Appendix 7. 1-Parameter Model Results



(a)

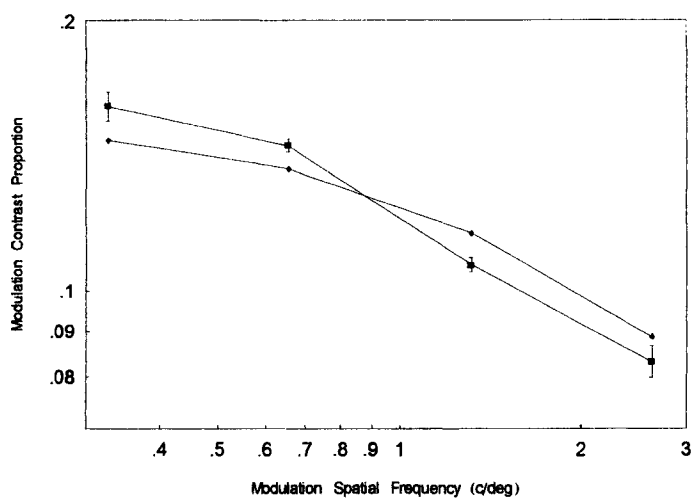


(b)

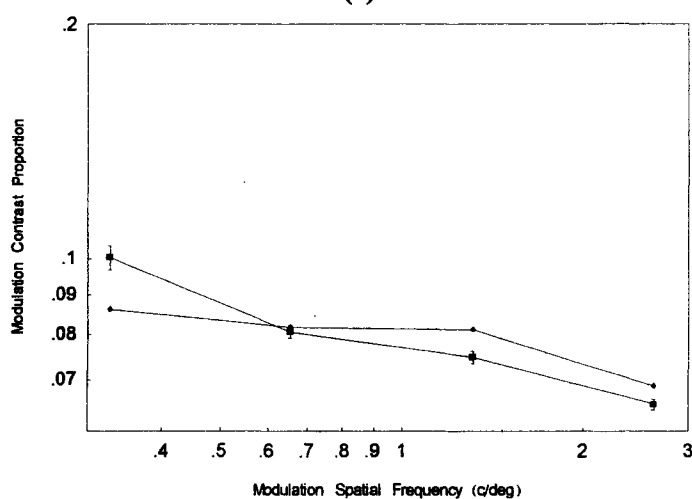


(c)

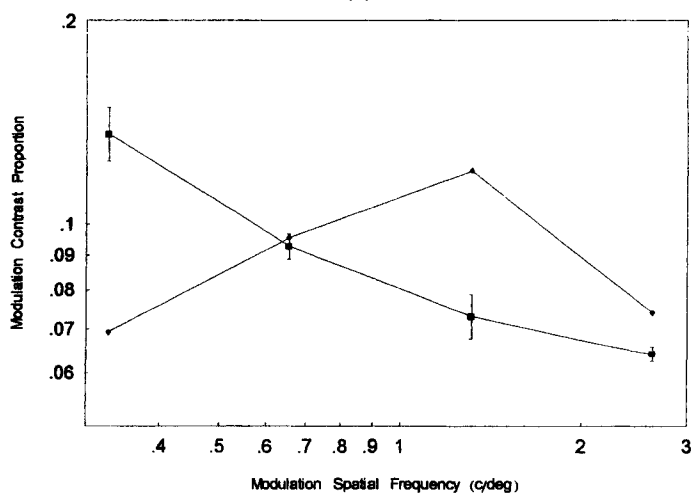
Figure 50. Experiment 1 contrast disparity thresholds and 1-parameter model predictions. (a) ETF thresholds (boxes) and model predictions (diamonds), (b) JMS thresholds (boxes) and predictions (diamonds), (c) WWS thresholds (boxes) and predictions (diamonds). (Experiment 1 square-wave contrast disparity modulation spatial frequencies are 0.26 c/deg, 0.39 c/deg, 0.79 c/deg and 1.57 c/deg. Square-wave carrier spatial frequency is 3.14 c/deg. Error bars are ± 1.483 median absolute deviation/ \sqrt{n} .)



(a)



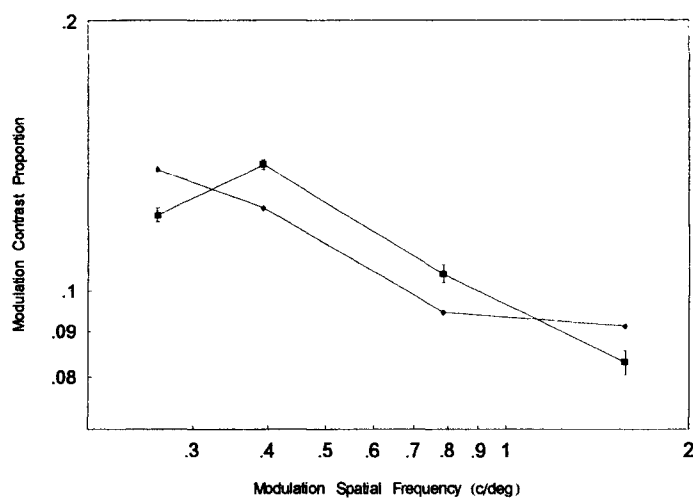
(b)



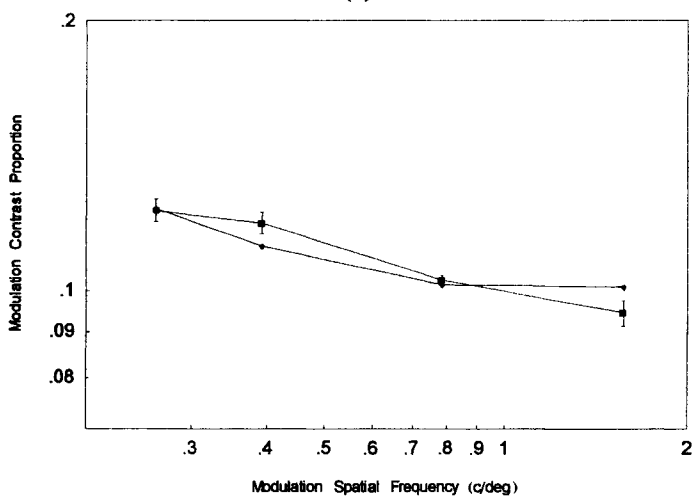
(c)

Figure 51. Experiment 2 contrast disparity thresholds and 1-parameter model predictions. (a) ETF thresholds (boxes) and model predictions (diamonds), (b) JMS thresholds (boxes) and predictions (diamonds), (c) WWS thresholds (boxes) and predictions (diamonds). (Experiment 2 square-wave contrast disparity modulation spatial frequencies are 0.33 c/deg, 0.65 c/deg, 1.31 c/deg and 2.62 c/deg. Square-wave carrier spatial frequency is 5.24 c/deg. Error bars are ± 1.483 median absolute deviation/ \sqrt{n} .)

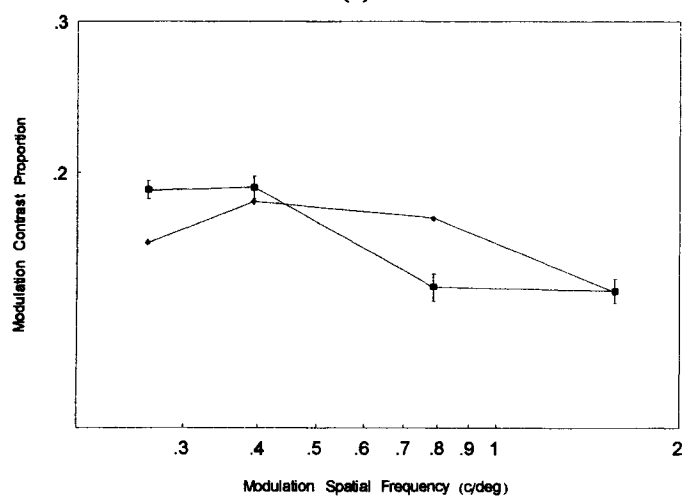
Appendix 8. 2-Parameter Model Results



(a)

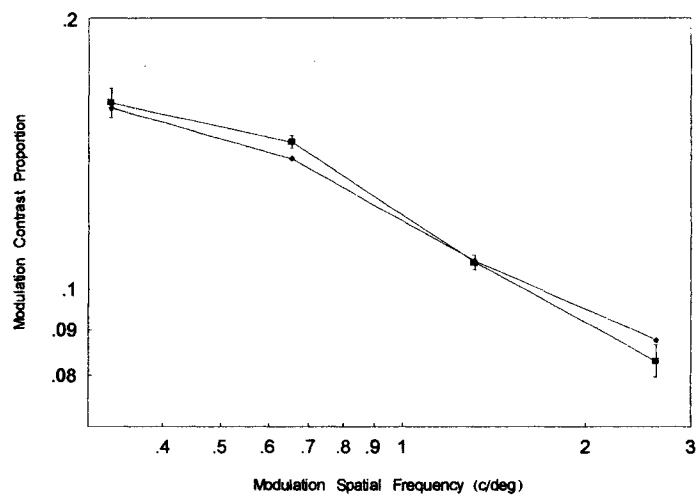


(b)

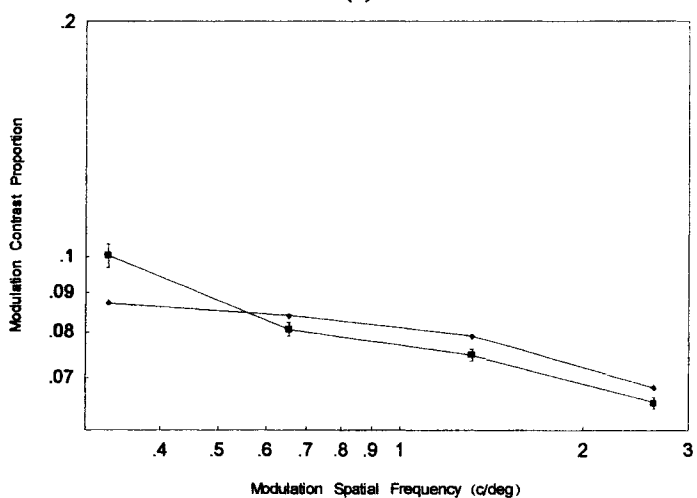


(c)

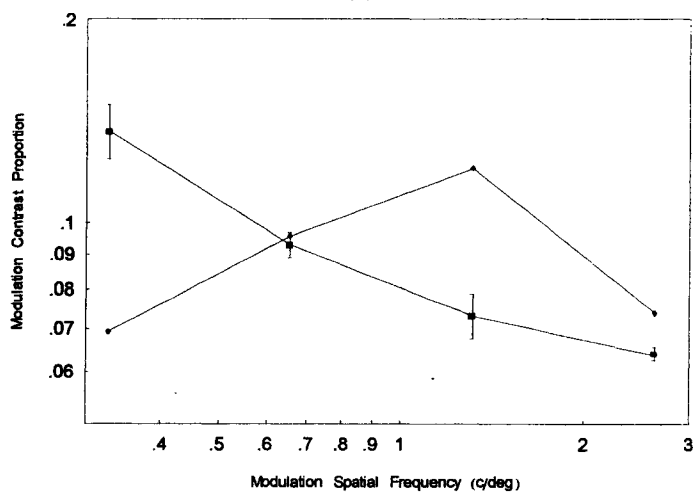
Figure 52. Experiment 1 contrast disparity thresholds and 2-parameter model predictions. (a) ETF thresholds (boxes) and model predictions (diamonds), (b) JMS thresholds (boxes) and predictions (diamonds), (c) WWS thresholds (boxes) and predictions (diamonds). (Experiment 1 square-wave contrast disparity modulation spatial frequencies are 0.26 c/deg, 0.39 c/deg, 0.79 c/deg and 1.57 c/deg. Square-wave carrier spatial frequency is 3.14 c/deg. Error bars are ± 1.483 median absolute deviation/ \sqrt{n} .)



(a)



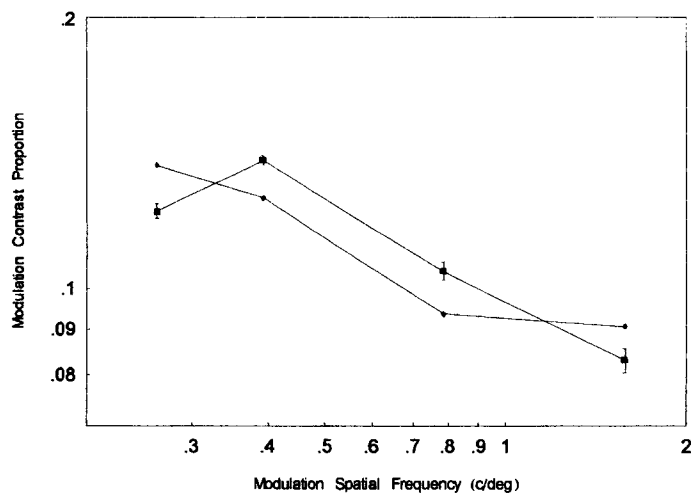
(b)



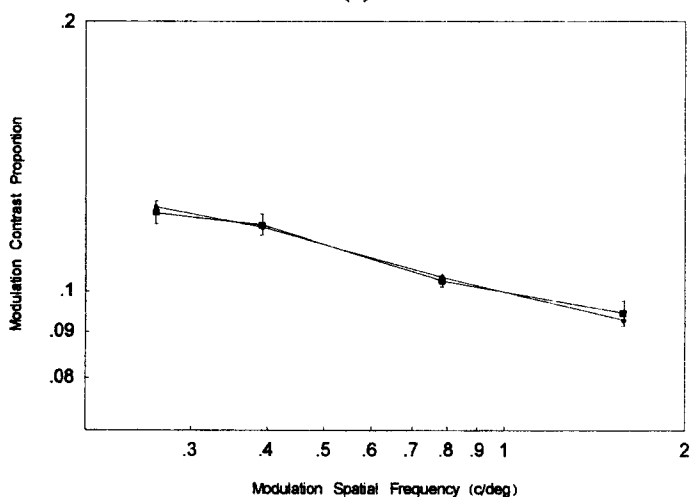
(c)

Figure 53. Experiment 2 contrast disparity thresholds and 2-parameter model predictions. (a) ETF thresholds (boxes) and model predictions (diamonds), (b) JMS thresholds (boxes) and predictions (diamonds), (c) WWS thresholds (boxes) and predictions (diamonds). (Experiment 2 square-wave contrast disparity modulation spatial frequencies are 0.33 c/deg, 0.65 c/deg, 1.31 c/deg and 2.62 c/deg. Square-wave carrier spatial frequency is 5.24 c/deg. Error bars are ± 1.483 median absolute deviation/ \sqrt{n} .)

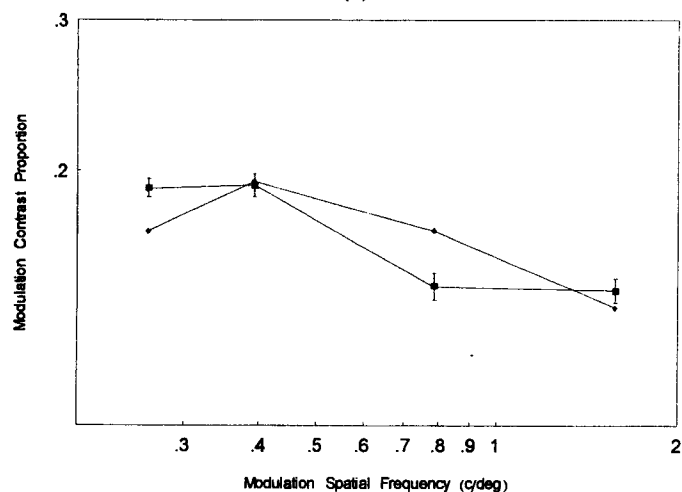
Appendix 9. 3-Parameter Model Results



(a)

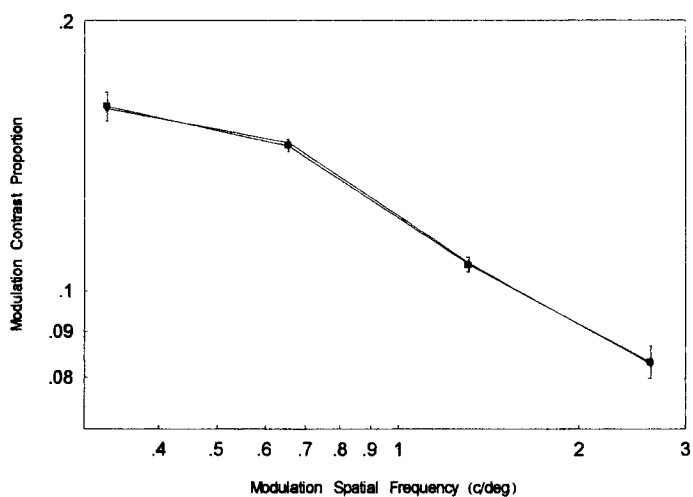


(b)

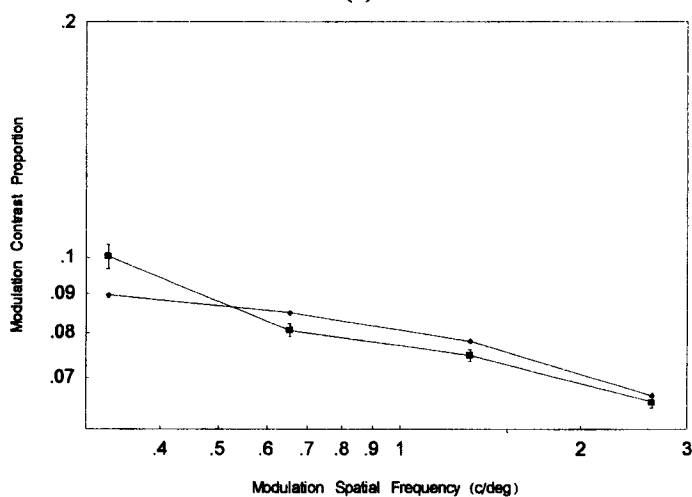


(c)

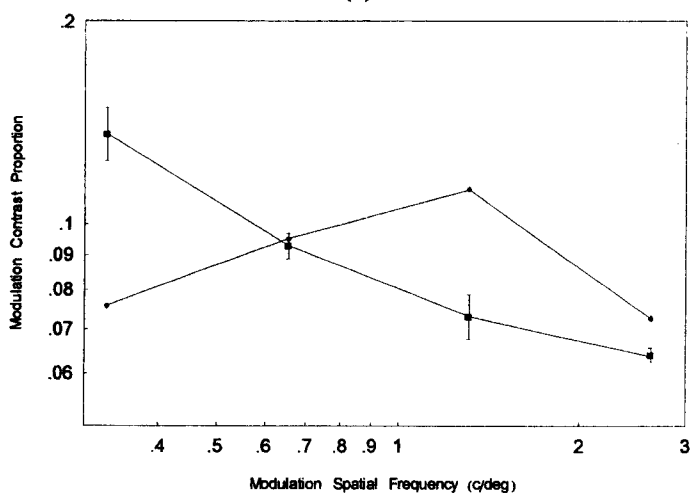
Figure 54. Experiment 1 contrast disparity thresholds and 3-parameter model predictions. (a) ETF thresholds (boxes) and model predictions (diamonds), (b) JMS thresholds (boxes) and predictions (diamonds), (c) WWS thresholds (boxes) and predictions (diamonds). (Experiment 1 square-wave contrast disparity modulation spatial frequencies are 0.26 c/deg, 0.39 c/deg, 0.79 c/deg and 1.57 c/deg. Square-wave carrier spatial frequency is 3.14 c/deg. Error bars are ± 1.483 median absolute deviation/ \sqrt{n} .)



(a)



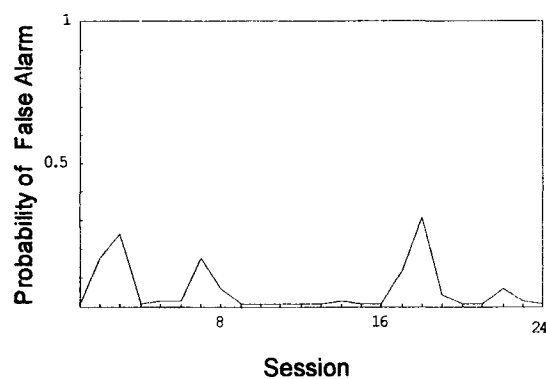
(b)



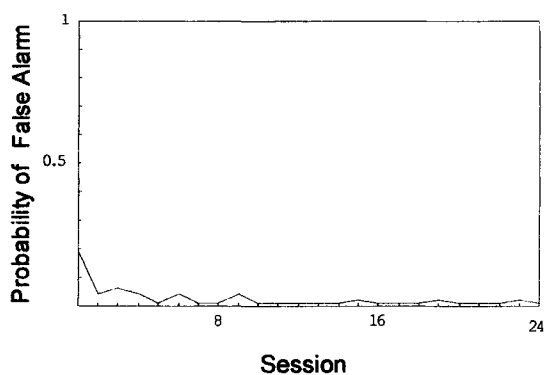
(c)

Figure 55. Experiment 2 contrast disparity thresholds and 3-parameter model predictions. (a) ETF thresholds (boxes) and model predictions (diamonds), (b) JMS thresholds (boxes) and predictions (diamonds), (c) WWS thresholds (boxes) and predictions (diamonds). (Experiment 2 square-wave contrast disparity modulation spatial frequencies are 0.33 c/deg, 0.65 c/deg, 1.31 c/deg and 2.62 c/deg. Square-wave carrier spatial frequency is 5.24 c/deg. Error bars are ± 1.483 median absolute deviation/ \sqrt{n} .)

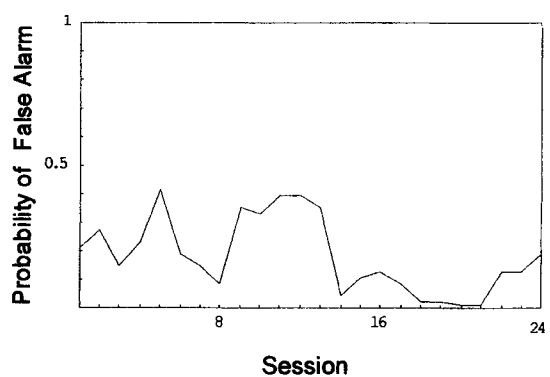
Appendix 10. False Alarm Time Series



(a)



(b)



(c)

Figure 56. Probability of false alarm as a function of experimental session. Experiments 1, 2 and 3 are represented by sessions 1-8, 9-16, and 17-24, respectively. (a) ETF, (b) JMS, (c) WWS

A rule of thumb based on Monte Carlo studies states that in order to be reasonably sure of a probability estimate, \hat{p} , based on n trials, one should ensure that

$$n \min(\hat{p}, 1 - \hat{p}) \geq 10$$

(DeVeaux, Velleman, and Bock, 2005, p. 358). Given that each point in Figure 56 is based on 50 trials, the minimum false alarm rate for which we can be somewhat confident is 0.2.

Relating this rule to threshold plots for Experiments 1-3, no clear pattern emerges across subjects. In the case of WWS, a somewhat plausible argument can be made that criterion changes account for the change in overall levels of plots (mid-range in Experiment 1, lowest in Experiment 2, and highest in Experiment 3).

Appendix 11. Contrast Disparity Modulation Scheme

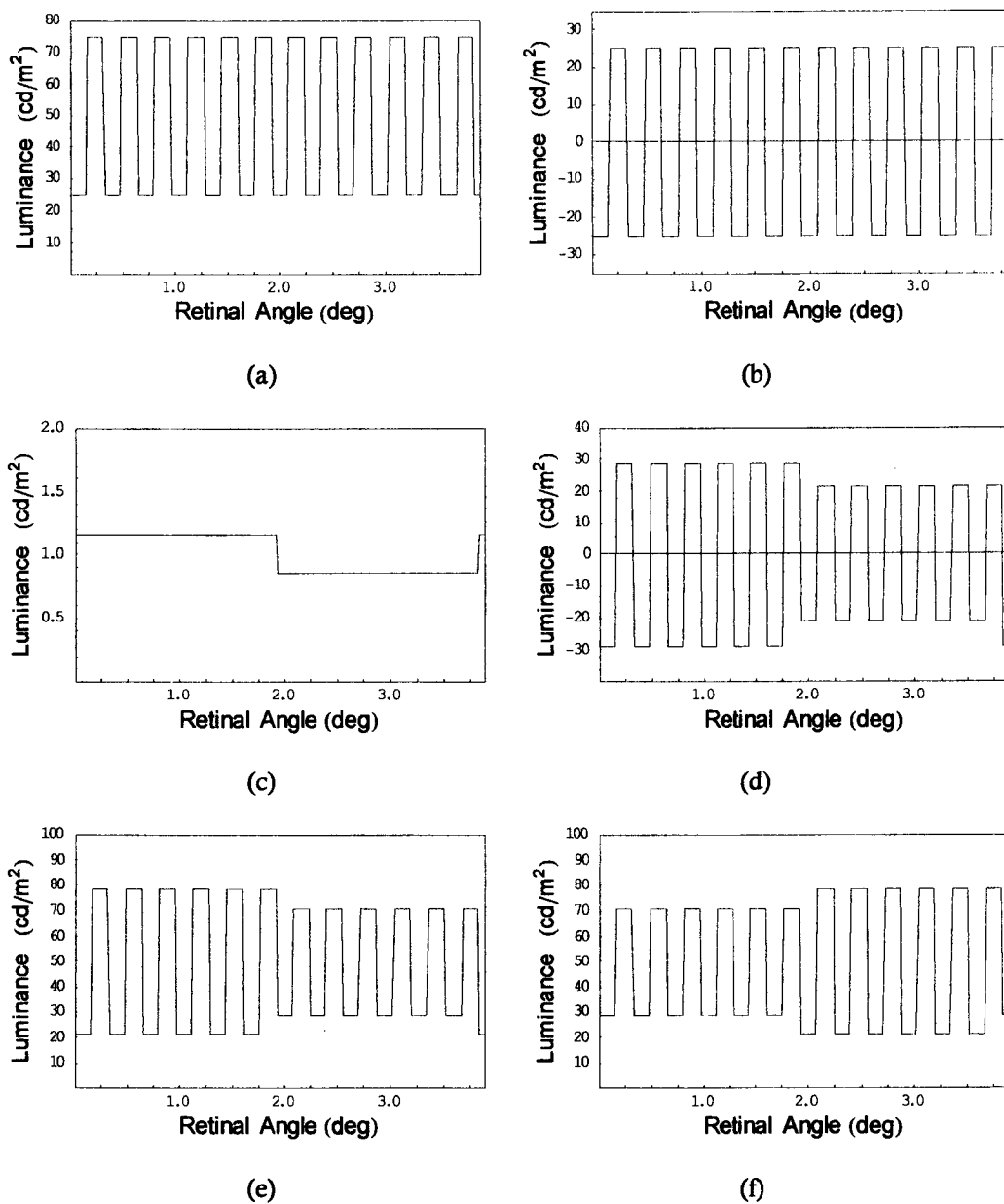


Figure 57. Contrast disparity modulation scheme, illustrated for a modulation contrast proportion of 0.15. (Carrier contrast and mean luminance are 0.5 and 50 cd/m^2 , respectively. Spatial frequencies are those of Experiment 1, condition 1). (a) luminance waveform of the unmodulated carrier, (b) luminance waveform of carrier after shifting to center around the zero level, (c) contrast disparity modulation waveform for a modulation contrast proportion of 0.15, (d) luminance waveform of the modulated carrier (i.e., the product of the unmodulated carrier and the contrast disparity modulation waveform), (e) final luminance waveform of the modulated carrier, after shifting to restore the mean luminance level, (f) corresponding final luminance waveform for the other eye. The resulting contrasts in the higher contrast and lower contrast segments of the final luminance waveforms are 0.575 and 0.425, respectively, which amount to a 15% increase and 15% decrease around the mean contrast of 0.5.

Appendix 12. Monitor Calibration

Cathode ray tube output (luminance) varies non-linearly with input (control voltage). This non-linear transfer function (see Figure 58.) is given by $L = kV^\gamma$, where L is luminance in cd/m^2 , k and γ are system-specific constants, and V is the controlling variable. Proximally, the controlling variable at the CRT is a voltage but, more distally ("upstream"), the controlling variable may be a software value, such as

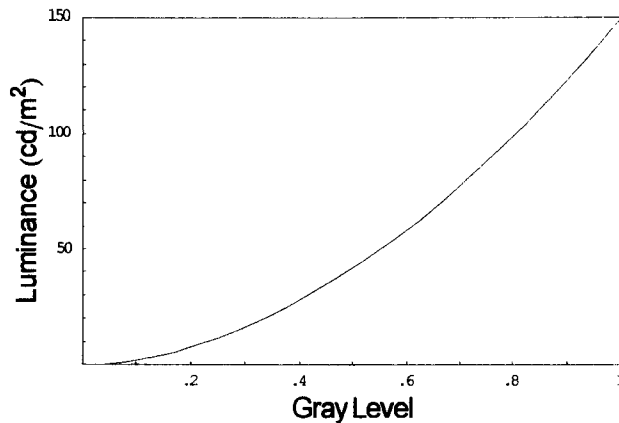


Figure 58. Luminance as a function of GrayLevel for Apple ColorSync Display used in Experiments 1-3. $L = kV^\gamma$, where L is luminance, V is GrayLevel, k is 148.929 and γ is 1.83579.

GrayLevel. Unless some controlling variable in the control stream is adjusted to compensate for the non-linear transfer function, CRT luminances will differ systematically from expectations.

Gamma correction (see Robson, 1999) adjusts a controlling variable to produce a more linear transfer function. Prior to gamma correction, the transfer function of the system of interest must be characterized in terms of input and output. The resulting data are then logged and a least-squares regression is performed to determine k and γ . At runtime, gamma correction is accomplished using $V = (L/k)^{1/\gamma}$, where V is the corrected value of the controlling variable, L is the desired luminance, and k and γ are the system-specific constants. For our experiments, the transfer function for the Apple ColorSync Display was characterized by determining the monitor luminance produced by each GrayLevel value, ranging from 0 to 1, in steps of 0.1. (The display was partitioned into the 9 cells of a 3x3 matrix and the mean monitor luminance at

each GrayLevel was based on 9 measurements, 1 per cell, using a Minolta LS-110 photometer.) After taking the log of the data and doing the least-squares regression, it was found that $k = 148.929$ and $\gamma = 1.83579$.

Using the above values of k and γ , stimulus luminance and contrast values were confirmed over several days using stereograms (similar to those used in Experiment 1) for a full range of contrast modulation values. In all cases, luminances were measured after at least 30 minutes of monitor warm-up time, using a Minolta LS-110 photometer in the laboratory where Experiments 1-3 took place (a darkened room with no other light source, except for a very small amount of light entering under the only door).

Appendix 13. IRB Documentation

UNIVERSITY OF NEW HAMPSHIRE

Office of Sponsored Research
Service Building
51 College Road
Durham, New Hampshire
03824-3585
(603) 862-3564 FAX

LAST NAME	Filley	FIRST NAME	Eugene
DEPT	Psychology Department, Conant Hall	APP'L DATE	1/21/2002
OFF-CAMPUS ADDRESS (if applicable)	Psychology Department, Conant Hall	IRB #	2652
		REVIEW LEVEL	EXP
		DATE OF NOTICE	1/24/2002
PROJECT TITLE	Applying Ideal-Observer Analysis to the Venetian Blind Effect		

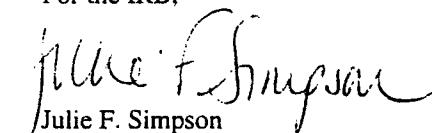
The Institutional Review Board (IRB) for the Protection of Human Subjects in Research reviewed and approved the protocol for your project as Expedited as described in Federal Regulations 45 CFR 46, Subsection 46.110 (b) (1) category 7.

Approval is granted for one year from the approval date above. At the end of the approval period you will be asked to submit a project report with regard to the involvement of human subjects. If your project is still active, you may apply for extension of IRB approval through this office.

The protection of human subjects in your study is an ongoing process for which you hold primary responsibility. In receiving IRB approval for your protocol, you agree to conduct the project in accordance with the ethical principles and guidelines for the protection of human subjects in research, as described in the following three reports: Belmont Report; Title 45, Code of Federal Regulations, Part 46; and UNH's Multiple Project Assurance of Compliance. The full text of these documents is available on the Office of Sponsored Research (OSR) website at http://www.unh.edu/osr/compliance/Regulatory_Compliance.html and by request from OSR.

Changes in your protocol must be submitted to the IRB for review and approval prior to their implementation; you must receive written, unconditional approval from the IRB before implementing them. If you experience any unusual or unanticipated results with regard to the participation of human subjects, report such events to this office within one working day of occurrence. If you have questions or concerns about your project or this approval, please feel free to contact this office at 862-2003. Please refer to the IRB # above in all correspondence related to this project. The IRB wishes you success with your research.

For the IRB,


Julie F. Simpson
Regulatory Compliance Manager

cc: File

William W. Stine, Psychology

UNIVERSITY OF NEW HAMPSHIRE

LAST NAME	Filley	FIRST NAME	Eugene
ADVISOR OR CO-PI	William W. Stine, Psychology	PROJECT APP'L END DATE	1/21/2003
DEPT	Psychology Department, Conant Hall	IRB #	2652
OFF-CAMPUS ADDRESS (if applicable)	Psychology Department, Conant Hall	REVIEW LEVEL	EXP
PROJECT TITLE	Applying Ideal-Observor Analysis to the Venetian Blind Effect	DATE OF NOTICE	11/5/2002

Institutional Review Board Annual Continuing Review Questionnaire

The Institutional Review Board (IRB) is obligated to conduct at least annual reviews of ongoing projects. In order to meet this obligation, the IRB asks you to **answer the following questions and submit a report of findings to-date** (attach) for this project. If the project is **CLOSED**, please submit a final report (copies of abstracts, articles, and/or publications specific to the project are acceptable).

1. Is this project still active (see question #4)? If YES, please read the NOTE below. YES NO
2. Please give date of termination if project has ended. _____
3. Please give proposed date of termination if project is still active, and refer to the NOTE printed below. 1/21/2003
4. At what stage is your research: a) subject recruitment, b) data collection, c) data analysis, d) interpretation, e) other [specify]? [Research projects in stages a - d are considered active, thus you need to request a time extension.] b, c, d
5. How many months have you actually performed the proposed investigation or activity? about 5 months
6. How many subjects have been studied or involved to-date? 3
7. Have you conducted the research in accordance with the procedures reviewed and approved by the IRB? Yes
8. Have any problems emerged or serious unexpected adverse subject experiences been observed? If YES, please describe on a separate sheet. YES NO

Principal Investigator/
Advisor Signature: _____

Eugene Filley

Date: 11/12/2002

PLEASE ATTACH A BLANK COPY EACH INFORMED CONSENT DOCUMENT YOU ARE CURRENTLY USING, and return the completed form and report to the UNH Office of Sponsored Research, 107 Service Building, Durham, NH 03824.

NOTE: IRB approval is granted for a maximum period of one year. Approval for your project ends on the date stated above. If your project will continue beyond this date, you must request a time extension at least two weeks prior to the approval expiration date. To do this, complete and return this form along with a written request for a time extension. If you have any questions, please call Julie Simpson at 862-2003, or Kathleen Stilwell at 862-3536.

CC: William W. Stine, Psychology

UNIVERSITY OF NEW HAMPSHIRE

Office of Sponsored Research
Service Building
51 College Road
Durham, New Hampshire 03824-3585
(603) 862-3564 FAX

LAST NAME	Filley	FIRST NAME	Eugene
DEPT	Psychology Department, Conant Hall	APPROVAL EXPIR. DATE	1/21/2004
OFF-CAMPUS ADDRESS (if applicable)	Psychology Department, Conant Hall	IRB #	2652
		REVIEW LEVEL	EXP
		DATE OF NOTICE	1/10/2003

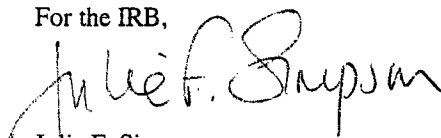
PROJECT TITLE Applying Ideal-Observer Analysis to the Venetian Blind Effect

The Institutional Review Board for the Protection of Human Subjects in Research has reviewed and approved your request for time extension for this protocol. **Approval for this protocol expires on the date indicated above.** At the end of the approval period you will be asked to submit a project report with regard to the involvement of human subjects. If your project is still active, you may apply for extension of IRB approval through this office.

The protection of human subjects in your study is an ongoing process for which you hold primary responsibility. **Changes in your protocol must be submitted to the IRB for review and receive written, unconditional approval prior to implementation.** If you have questions or concerns about your project or this approval, please feel free to contact this office at 862-2003.

Please refer to the IRB # above in all correspondence related to this project. The IRB wishes you success with your research.

For the IRB,



Julie F. Simpson
Regulatory Compliance Manager

cc: File
William W. Stine, Psychology

ORIG APP'L 1/21/2002

UNIVERSITY OF NEW HAMPSHIRE

LAST NAME	Filley	FIRST NAME	Eugene
ADVISOR OR CO-PI	William W. Stine, Psychology	PROJECT APP'L END DATE	1/21/2004
DEPT	Psychology Department, Conant Hall	IRB #	2652
OFF-CAMPUS ADDRESS (if applicable)	Psychology Department Conant Hall	REVIEW LEVEL	EXP
PROJECT TITLE	Applying Ideal-Observer Analysis to the Venetian Blind Effect		
		DATE OF NOTICE	11/17/2003

Institutional Review Board Annual Continuing Review Questionnaire

The Institutional Review Board (IRB) is obligated to conduct at least annual reviews of ongoing projects. In order to meet this obligation, the IRB asks you to **answer the following questions and submit a report of findings to-date** (attach) for this project. If the project is **CLOSED**, please submit a final report (copies of abstracts, articles, and/or publications specific to the project are acceptable).

1. Is this project still active (see question #4)? If YES, please read the NOTE below. YES NO
2. Please give date of termination if project has ended. _____
3. Please give proposed date of termination if project is still active, and refer to the NOTE printed below. 1/21/2005
4. At what stage is your research: a) subject recruitment, b) data collection, c) data analysis, d) interpretation, e) other [specify]? *[Research projects in stages a - d are considered active, thus you need to request a time extension.]* c
5. How many months have you actually performed the proposed investigation or activity? 12 since last review
6. How many subjects have been studied or involved to-date? 3
7. Have you conducted the research in accordance with the procedures reviewed and approved by the IRB? Yes
8. Have any problems emerged or serious unexpected adverse subject experiences been observed? If YES, please describe on a separate sheet. YES NO

Principal Investigator/
Advisor Signature:



Date:

1/20/03

PLEASE ATTACH A BLANK COPY EACH INFORMED CONSENT DOCUMENT YOU ARE CURRENTLY USING, and return the completed form and report to the UNH Office of Sponsored Research, 107 Service Building, Durham, NH 03824.

NOTE: IRB approval is granted for a maximum period of one year. Approval for your project ends on the date stated above. If your project will continue beyond this date, you must request a time extension at least two weeks prior to the approval expiration date. To do this, complete and return this form along with a written request for a time extension. If you have any questions, please call Julie Simpson at 862-2003, or Kathleen Stilwell at 862-3536.

CC: William W. Stine, Psychology



UNIVERSITY of NEW HAMPSHIRE

January 14, 2004

Filley, Eugene
Psychology
Conant Hall

IRB #: 2652

Study: Applying Ideal-Observer Analysis to the Venetian Blind Effect

Review Level: Expedited

Approval Expiration Date: 01/21/2005

The Institutional Review Board for the Protection of Human Subjects in Research (IRB) has reviewed and approved your request for time extension for this study. Approval for this study expires on the date indicated above. At the end of the approval period you will be asked to submit a report with regard to the involvement of human subjects. If your study is still active, you may apply for extension of IRB approval through this office.

Researchers who conduct studies involving human subjects have responsibilities as outlined in the document, *Responsibilities of Directors of Research Studies Involving Human Subjects*. This document is available at <http://www.unh.edu/osr/compliance/IRB.html> or from me.

If you have questions or concerns about your study or this approval, please feel free to contact me at 603-862-2003 or Julie.simpson@unh.edu. Please refer to the IRB # above in all correspondence related to this study. The IRB wishes you success with your research.

For the IRB,

Julie F. Simpson
Regulatory Compliance Manager

cc: File
William W. Stine

**Regulatory Compliance Office, Office of Sponsored Research, Service Building,
51 College Road, Durham, NH 03824-3585 * Fax: 603-862-3564**